DOE F 4600.2
(5/09)
(All Other Editions are Obsolete)

ATTACHMENT 3
U.S. Department of Energy
FEDERAL ASSISTANCE REPORTING CHECKLIST
AND INSTRUCTIONS

1. Identification Number: **DE-FE0002056**	2. Program/Project Title: **Modeling CO2 Sequestration in Saline Aquifer and Depleted Oil Reservoir to Evaluate Regional CO2 Sequestration Potential of Ozark Plateau Aquifer System, South-Central Kansas**
3. Recipient: University of Kansas Center for Research	

4. Reporting Requirements:	Frequency	No. of Copies	Addresses
A. MANAGEMENT REPORTING			
☒ Progress Report	Q	Electronic Version to NETL>	*FITS@NETL.DOE.GOV*
☒ Special Status Report	A		
B. SCIENTIFIC/TECHNICAL REPORTING * (Reports/Products must be submitted with appropriate DOE F 241. The 241 forms are available at https://www.osti.gov/elink)			
Report/Product — Form			
☒ Final Scientific/Technical Report — DOE F 241.3	FG	Electronic Version to E-link>	*http://www.osti.gov/elink-2413*
☒ Conference papers/proceedings/etc.* — DOE F 241.3	A		*http://www.osti.gov/elink-2413*
☐ Software/Manual — DOE F 241.4			*http://www.osti.gov/estsc/241-4pre.jsp*
☒ Other (see special instructions) Topical — DOE F 241.3	A		
** Scientific/technical conferences only*			
C. FINANCIAL REPORTING			
☒ SF-425, Federal Financial Report	Q, FG	Electronic Version To NETL>	*FITS@NETL.DOE.GOV*
D. CLOSEOUT REPORTING			
☐ Patent Certification	FC	Electronic Version To NETL>	*FITS@NETL.DOE.GOV*
☐ Property Certificate	FC		
☐ Other			
E. OTHER REPORTING			
☒ Annual Indirect Cost Proposal	A	Electronic Version To NETL>	*FITS@NETL.DOE.GOV*
☒ Annual Inventory Report of Federally Owned Property, if any	A		
☐ Other			
F. AMERICAN RECOVERY AND REINVESTMENT ACT REPORTING			
☐ Reporting and Registration Requirements			*http://www.federalreporting.gov*

FREQUENCY CODES AND DUE DATES:

A - As required; see attached text for applicability.
FG - Final; within ninety (90) calendar days after the project period ends.
FC - Final - End of Effort.
Q - Quarterly; within thirty (30) calendar days after end of the calendar quarter or portion thereof.
S - Semiannually; within thirty (30) calendar days after end of project year and project half-year.
YF - Yearly; 90 calendar days after the end of project year.
YP - Yearly Property - due 15 days after period ending 9/30.

QUARTERLY PROGRESS REPORT

Award Number: DE-FE0002056

Recipient: University of Kansas Center for Research &

Kansas Geological Survey

1930 Constant Avenue

Lawrence, KS 66047

"Modeling CO2 Sequestration in Saline Aquifer and Depleted Oil Reservoir To Evaluate Regional CO2 Sequestration Potential of Ozark Plateau Aquifer System, South-Central Kansas"

Project Director/Principal Investigator: W. Lynn Watney

Principal Investigator: Jason Rush

Twentieth Quarter Progress Report

Date of Report: 11-23-14

Period Covered by the Report: July 1, 2014 to September 30, 2014

Contributors to this Report: Clyde Redger, George Tsoflias, Dennis Hedke, Paul Gerlach, Eugene Holubnyak, Gene Williams, Martin Dubois, John Victorine, Tiraz Birdie, Jennifer Raney, Mike Killian, Holly Field, Tandis Bidgoli, Mina Fazelalavi, Jason Rush, Lynn Watney

EXECUTIVE SUMMARY

The project “Modeling CO2 Sequestration in Saline Aquifer and Depleted Oil Reservoir to Evaluate Regional CO2 Sequestration Potential of Ozark Plateau Aquifer System, South-Central Kansas” is focused on the Paleozoic-age Ozark Plateau Aquifer System (OPAS) in southern Kansas. OPAS is comprised of the thick and deeply buried Arbuckle Group saline aquifer and the overlying Mississippian carbonates that contain large oil and gas reservoirs. The study is collaboration between the KGS, Geology Departments at Kansas State University and The University of Kansas, BEREXCO, INC., Bittersweet Energy, Inc. Hedke-Saenger Geoscience, Ltd., Improved Hydrocarbon Recovery (IHR), Anadarko, Cimarex, Merit Energy, GloriOil, and Cisco.

The project has three areas of focus, 1) a field-scale study at Wellington Field, Sumner County, Kansas, 2) 25,000 square mile regional study of a 33-county area in southern Kansas, and 3) selection and modeling of a depleting oil field in the Chester/Morrow sandstone play in southwest Kansas to evaluate feasibility for CO2-EOR and sequestration capacity in the underlying Arbuckle saline aquifer. Activities at Wellington Field are carried out through BEREXCO, a subcontractor on the project who is assisting in acquiring seismic, geologic, and engineering data for analysis. Evaluation of Wellington Field will assess miscible CO2-EOR potential in the Mississippian tripolitic chert reservoir and CO2 sequestration potential in the underlying Arbuckle Group saline aquifer. Activities in the regional study are carried out through Bittersweet Energy. They are characterizing the Arbuckle Group (saline) aquifer in southern Kansas to estimate regional CO2 sequestration capacity. Supplemental funding has expanded the project area to all of southwest Kansas referred to as the Western Annex. IHR is managing the Chester/Morrow play for CO2-EOR in the western Annex while Bittersweet will use new core and log data from basement test and over 200 mi2 of donated 3D seismic. IHR is managing the industrial partnership including Anadarko Petroleum Corporation, Cimarex Energy Company, Cisco Energy LLC, Glori Oil Ltd., and Merit Energy Company. Project is also supported by Sunflower Electric Power Corporation.

PROJECT STATUS

Task Name	Planned Start Date	Actual Start Date	Planned Finish Date	Actual Finish Date	% Complete
1.0 Project Management & Planning	12/8/2009	12/08/09	2/7/2014		90%
2.0 Characterize the OPAS (Ozark Plateau Aquifer System)	1/1/2010	01/01/10	9/30/2013		95%
3.0 Initial geomodel of Mississippian Chat & Arbuckle Group - Wellington field	1/1/2010	01/01/10	9/30/2010	09/30/10	100%
4.0 Preparation, Drilling, Data Collection, and Analysis - Well #1	9/15/2010	12/15/10	3/31/2011	08/30/11	100%
5.0 Preparation, Drilling, Data Collection and Analysis - Well #2	1/1/2011	02/20/11	6/30/2011	08/30/11	100%
6.0 Update Geomodels	5/1/2011	05/01/11	9/30/2011	10/31/12	100%
7.0 Evaluate CO2 Sequestration Potential in Arbuckle Group Saline Aquifer	8/1/2011	08/01/11	12/31/2011	10/31/12	100%
8.0 Evaluate CO2 Sequestration Potential in Depleted Wellington field	10/15/2011	10/15/11	7/30/2013	+++	99%
9.0 Characterize leakage pathways - risk assessment area	1/1/2010	01/01/10	6/30/2012	10/31/12	100%
10.0 Risk Assessment related to CO2-EOR and CO2 Sequestration in saline aquifer	6/1/2012	06/01/12	9/30/2013	**	99%
11.0 Produced water and wellbore management plans - Risk assessment area	1/1/2012	01/01/12	7/30/2013		99%
12.0 Regional CO2 sequestration potential in OPAS	8/1/2012	02/01/12	9/30/2013	***	99%

Milestone	Planned Completion Date	Actual Completion Date	Validation
HQ Milestone: Kick-off Meeting Held	3/31/2010	03/31/10	Completed
HQ Milestone: Begin collection of formation information from geologic surveys and private vendors	6/30/2010	01/01/10	Completed
HQ Milestone: Semi-Annual Progress Report on data availability and field contractors	9/30/2010	07/30/10	Submitted to Project manager
HQ Milestone: Establish database links to NATCARB and Regional Partnerships	12/31/2010	12/31/10	Completed
HQ Milestone: Annual Review Meeting attended	3/31/2011	10/05/10	Completed
HQ Milestone: Complete major field activities, such as drilling or seismic surveys at several characterization sites	6/30/2011	Note: This milestone was met collectively by all projects. No one project was held accountable to the milestone.	Completed
HQ Milestone: Semi-Annual Progress Report (i.e. Quarterly Report ending June 30, 2011)	9/30/2011	09/30/11	Completed
HQ Milestone: Yearly Review Meeting of all recipients; opportunities for information exchange and collaboration	12/31/2011	11/15/11	Attended meeting
HQ Milestone: Complete at least one major field activity such as well drilling, 2-D or 3-D seismic survey, or well logging	3/31/2012	08/15/12	Completed 3D seismic Cutter competed
HQ Milestone: Complete at least one major field activity such as well drilling, 2-D or 3-D seismic survey, or well logging	6/30/2012	10/09/12	Completed cutter well reach TD
HQ Milestone: Semi-annual report (i.e. Quarterly Report ending June 30, 2012) on project activities summarizing major milestones and costs for the project 9/30/2012	9/30/2012	09/30/12	Completed
FOA Milestone: Updated Project Management Plan	3/31/2010	03/31/10	
FOA Milestone: Submit Site Characterization Plan	5/28/2010		Completed
FOA Milestone: Notification to Project Manager that reservoir data collection has been initiated	9/15/2010	01/01/10	Completed
FOA Milestone: Notification to Project Manager that subcontractors have been identified for drilling/field service operations	7/30/2010	01/01/10	Completed
FOA Milestone: Notification to Project Manager that field service operations have begun at the project site	7/1/2010	01/01/10	Completed
FOA Milestone: Notification to Project Manager that characterization wells have been drilled	6/3/2011	03/09/11	Completed
FOA Milestone: Notification to Project Manager that well logging has been completed	6/3/2011	03/09/11	Completed
FOA Milestone: Notification to Project Manager that actvities on the lessons learned document on site characterization have been initiated	7/15/2012		Completed
FOA Milestone: Notification to Project Manager that activities to populate database with geologic characterization data has begun	12/31/2010	12/31/10	Completed, email summary
KGS Milestone 1.1: Hire geology consultants for OPAS modeling	3/31/2010	03/31/10	Completed
KGS Milestone 1.2: Acquire/analyze seismic, geologic and engineering data - Wellington field	6/30/2010	06/30/10	Completed, quarterly rpt
KGS Milestone 1.3: Develop initial geomodel for Wellington field	9/30/2010	09/30/10	Completed, email summary
KGS Milestone 1.4: Locate and initiate drilling of Well #1 at Wellington field	12/31/2010	12/25/10	Completed, email summary
KGS Milestone 2.1: Complete Well#1 at Wellington - DST, core, log, case, perforate, test zones	3/31/2011	08/30/11	Completed, email summary
KGS Milestone 2.2: Complete Well#2 at Wellington - Drill, DST, log, case, perforate, test zones	6/30/2011	08/30/11	Completed, email summary
KGS Milestone 2.3: Update Wellington geomodels - Arbuckle & Mississippian	9/30/2011	10/31/12	Completed
KGS Milestone 2.4: Evaluate CO2 Sequestration Potential of Arbuckle Group Saline Aquifer - Wellington field	12/31/2011	10/31/12	Completed
KGS Milestone 3.1: CO2 sequestration & EOR potential - Wellington field	3/31/2012		99% complete***-emalil summary to come**
KGS Milestone 3.2: Characterize leakage pathways - Risk assessment area	6/30/2012	10/31/12	Completed
KGS Milestone 3.3: Risk assessment related to CO2-EOR and CO2-sequestration	9/30/2012		Completed - **email summary to come****
KGS Milestone 3.4: Regional CO2 Sequestration Potential in OPAS - 17 Counties	12/7/2012		99.9% complete*** -**email summary to come**

TASK SUMMARY IN PREPARATION FOR COMPLETION OF THE PROJECT

This quarterly report is the last, prior to submitting the final report. All of the tasks and subtasks are listed herein with dialog inserted into sections pertaining to significant activities conducted in this last quarter.

Task 1: Program Management and Reporting (PMP)

Task 2. Characterize the OPAS

Subtask 2.1. Acquire geologic, seismic and engineering data
Subtask 2.2. Develop regional correlation framework and integrated geomodel

Type logs were checked for completeness for both digitizing and for stratigraphic correlations over the course of several months. In the process the "type logs" java applet was used to review the wells and to make modifications to the well database. Comments about the experience and recommendations resulted leading to minor modifications to improve the user's experience were made by Holly Field as noted below. This is important in the future to encourage expansion of type logs database both in number of wells and in additional detail in stratigraphic correlations.

Modifications include --

1. Java menu screen has an option to close or "x" out in the upper right hand corner. Closing the window was modified to allow Java to continue running in the background. This prevents the user from having to sign in to the Applet upon each new correlation saving time.
2. In the Applet correlations, it is possible to deselect Tracks on display so that the horizontal distance between the well displays can be shortened. Initially, unselecting the display of the lithologies also removed yellow lines of the "tops". This has now been corrected so that the tops remain visible after a deselection. This is important to maintain the visibility of the tops for continuity of workflow.
3. A webpage was created that chooses CO_2 wells within a county that include a specific top. This allows the user to quickly view wells in a list which gives information on a specific horizon within an area. The URL for this function is http://chasm.kgs.ku.edu/ords/iqstrat.doe_co2_summary_pkg.build_web_page?sCounty=harper&sTops=arbuckle which can be changed to other counties and tops by replacing the county for formation names in question.
4. A request was made to show rejected tops on the Java applet in a differing color from the standard yellow. Also, there is a need to show where a person wanted to place the new or changed top location. John Victorine (programmer) advised that making these changes in the Java correlation displays would likely cause the tops to become clustered or visually convoluted. However, to facilitate the need for clarity on both agreements and recommendations of change from the different applet users, John created charts that

automatically update so that the progress of well changes can be understood without compromising the visual utility of the correlations tool. An example of a chart that shows the horizons and the Source owners for the Cutter KGS 1 well can be found at http://chasm.kgs.ku.edu/ords/iqstrat.type_log_summary_pkg.build_web_page?sKID=1044138961**.**

5. In addition, the number of horizons accepted or rejected for each well within a county is included in the county summary page. For example, Cutter KGS 1 chart reject and accept summaries can be found within the Summary Page for Stevens County. Selecting the number within the reject or accept columns will bring the user to the link above.

Comments were also provided for the future of the Type Logs Applet program.

1. Find a way to make accepting tops less time-consuming. Currently, to accept tops within a well, each top that the user agrees with must be clicked on and accepted. It would be an advantage to be able to select multiple tops on the visual display at once and to then click accepts. A 6,000 ft well may take 15 minutes to accept horizons alone.
2. Furthermore, it is useful to see many wells at once within a correlation, as opposed to being limited currently to two wells. While designing multiple-well correlations was not within the scope of the Type Logs Applet the adaptation to multiple wells is possible since the CO_2 Project General Cross Section Map Applet can utilize data from up to four wells. The use of additional wells in the cross section multiple wells would prevent the need to go back-and-forth between wells, correlating two wells at a time. A geologist that is accustomed to viewing paper logs may find this methodology tedious or more time-consuming if the working cross sections are limited to two wells.
3. Accommodation of short notes linked the horizons that are correlated would help to convey the concept or key element of the correlation.

Subtask 2.3. Subsurface fluid chemistry and flow regime analysis.
Subtask 2.4. Gather and interpret KGS's gravity and magnetic data
Subtask 2.5. Remote sensing analysis for lineaments

Task 3. Geomodel of Mississippian Chat & Arbuckle Group - Wellington field.

Subtask 3.1. Collect geologic & engineering data
Subtask 3.2. Collect 3D seismic data
Subtask 3.3. Process 3D seismic data
Subtask 3.4. Collect gravity and magnetic data
Subtask 3.5. Interpret seismic, gravimetric, and magnetic data
Subtask 3.6. Initial geomodel - Wellington

Task 4: Preparation, Drilling, Data Collection and Analysis – Test Borehole #1

Subtask4.1. Locate Test Borehole #1
Subtask 4.2. Permitting for Test Borehole #1
Subtask 4.3. Drill, retrieve core, and run DST – Test Borehole #1
Subtask 4.4. Openhole Wireline Logging – Test Borehole #1
Subtask 4.5. Wellbore Completion – Test Borehole #1
Subtask 4.6. Analyze wireline log - Test Borehole #1
Subtask 4.7. Test and sample fluids (water) from select intervals – Test Borehole #1
Subtask 4.8. Analyze Arbuckle core from Test Borehole #1
Subtask 4.9. Analyze Mississippian core from Test Borehole #1
Subtask 4.10. PVT analysis of oil and water from Mississippian chat reservoir
Subtask 4.11. Analyze water samples from Test Borehole #1
Subtask 4.12. Microbiological studies on produced water
Subtask 4.13. Correlate log and core properties
Subtask 4.14. Examine diagenetic history of fracture fill

Task 5. Preparation, Drilling, Data Collection, and Analysis - Test Borehole #2

Subtask 5.1. Locate Test Borehole #2
SubTask 5.2. Permitting for Test Borehole #2
Subtask 5.3. Drill, and run DST – Test Borehole #2
Subtask 5.4. Openhole wireline logging - Test Borehole #2
Subtask 5.5. Complete well and perforate selectively to test and sample fluids – Test Borehole #2
Subtask 5.6. Analyze wireline log – Test Borehole #2

Task 6. Update Geomodels

Subtask 6.1. Hydrogeologic studies
Subtask 6.2. 2D shear wave survey
Subtask 6.3. Process & interpret 2D shear
Subtask 6.4. Revise 3D seismic interpretation
Subtask 6.5. Update geomodel - Arbuckle & Miss

Task 7. Evaluate CO2 Sequestration Potential in Arbuckle Group Saline Aquifer - Wellington field

Subtask 7.1. CO2 sequestration potential
Subtask 7.2. Long-term effectiveness of cap rock
Subtask 7.3. CO2 sequestered in brine
Subtask 7.4. CO2 sequestered as residual gas
Subtask 7.5. CO2 sequestered by mineralization
Subtask 7.6. Field management - max CO_2 entrapment
Subtask 7.7. Monte Carlo - total CO_2 sequestration capacity

Task 8. Evaluate CO2 Sequestration Potential by CO2-EOR in Depleted Wellington field

Subtask 8.1. CO2-EOR potential
Subtask 8.2. Long-term effectiveness of cap rock
Subtask 8.3. CO2 sequestered in brine and residual gas
Subtask 8.4. CO2 sequestered by mineralization
Subtask 8.5. Field management - optimize CO2-EOR
Subtask 8.6. Monte Carlo - total CO2 sequestration capacity

Task 9. Characterize leakage pathways - Risk assessment area

Subtask 9.1. Collect reservoir characterization data - external sources
Subtask 9.2. Map fracture-fault network
Subtask 9.3. Verify seal continuity and integrity
Subtask 9.4. Inventory well status
Subtask 9.5. Gather expert advice on well integrity

Affirming possible and previously unrecognized faults has been made easier with the increase in seismic activity in south-central Kanas. The DOE-CO2 mapper has is updated to include the earthquake events since 2011 that are focused around the Mississippian Lime horizontal drilling play. Large volumes of brine are disposed in and around this play extending from north-central Oklahoma into Kansas. Increased seismicity has followed this trend.

The increased in both cumulative brine disposal with some injection wells permitted at high rates (20,000 to 40,000 bbls/day) but lacking daily injection rates and pressures is problematic to understanding or modeling the role of injection and the seismicity or, important to this project, of considering the circumstances in the context of CO2 disposal that has been evaluated in this area. Accordingly, we have elevated the risk of injection of large volumes of fluids pending ongoing analysis outside of this funded program. The fact that the extensive subsurface and surface lineament database exists for the area will be critical to further assessment that will included geomodeling and simulation.

Tandis S. Bidgoli, W. Lynn Watney, Paul Gerlach, and Minh C. Nguyen presented a paper at the 2014 Annual Meeting of the Geological Society of America, titled, "Episodic reactivation of critically-stressed basement faults in southern Kansas: Implications for waste-water disposal and long-term storage of CO_2**".** The paper echoes the concern as the KGS team works with state regulators and chairs a task force on induced seismicity. The paper also lays out an approach to utilizing the data, much of it derived from the regional DOE funded study evaluate seismicity in the context of the geology as described in the abstract -

> *Kansas resides within the stable craton, a characterization that contrasts it with tectonically active portions of the U.S. However, the Proterozoic basement beneath Kansas contains a number of well-defined discontinuities or lineaments, many of which are faults with large offsets that show evidence of reactivation within shallower stratigraphy. Although the role of these faults within the current*

stress regime is not clear, a growing number of researchers argue that the midcontinent crust is critically-stressed and that injecting large volumes of fluid (waste-water or CO_2) poses a high risk for induced seismicity and fluid leakage. The recent uptick in the frequency and size of earthquakes in the southern part of the state has elevated these concerns, but poor knowledge of subsurface faults and their relationship with regional stresses are major obstacles to evaluating the cause of the seismicity and to developing possible mitigating strategies. To address these issues on a broad scale, we use a dense sampling of stratigraphic tops, determined from publically-available well-log data, to construct structure contour maps of 18 regional stratigraphic surfaces. We use a range of surface analysis techniques (e.g., slope, curvature, and residual analysis) combined with thickness variations, determined from isopach maps, to identify potential faults. To evaluate the consistency of the mapped faults, we will compare them to documented surface lineaments and discontinuities determined from analysis of state-wide potential field data. To identify the faults most favorably oriented with respect to in situ stresses and thus, those with the highest potential for reactivation, we will analyze borehole breakouts, drilling-induced fractures, and drilling-enhanced fractures from available well logs (e.g., 4-arm caliper and image logs), which will provide the orientations of the minimum and maximum horizontal stresses. The resulting fault map will identify high and low risk subsurface faults, and ideally provide regional stakeholders some context for recent and future seismic events.

What had been originally mapped as actual and possible faults is a baseline from which additional information will be gathered in the affected area. Data now includes daily injection from selected injection wells and potential opportunities to examine 3D seismic volumes and obtain dynamic and static pressures of the Arbuckle. If it is found that injection is responsible for the earthquake activity, solutions might include limiting rates of injection established by injectivity tests. This is precisely the approach that we have taken with the CO2 storage assessment. The Arbuckle is treated as a reservoir with flow units and baffles, faults and fractures. Flow units are characterized by kv, kh, phi, reservoir quality index, and capillary pressure. These flow units change in thickness and reservoir properties, pinchout, or simply reach permeability barriers, particularly as demonstrated by the regional assessment (**Figure 1**). All simulations, whether for an oil reservoir or the Arbuckle aquifer, utilize conservative injection pressures that are well below the fracture gradient that commonly serves as the recommended rule of thumb pressure maximum. Careful design will be necessary for commercial CO2 injection no matter where the injection is planned.

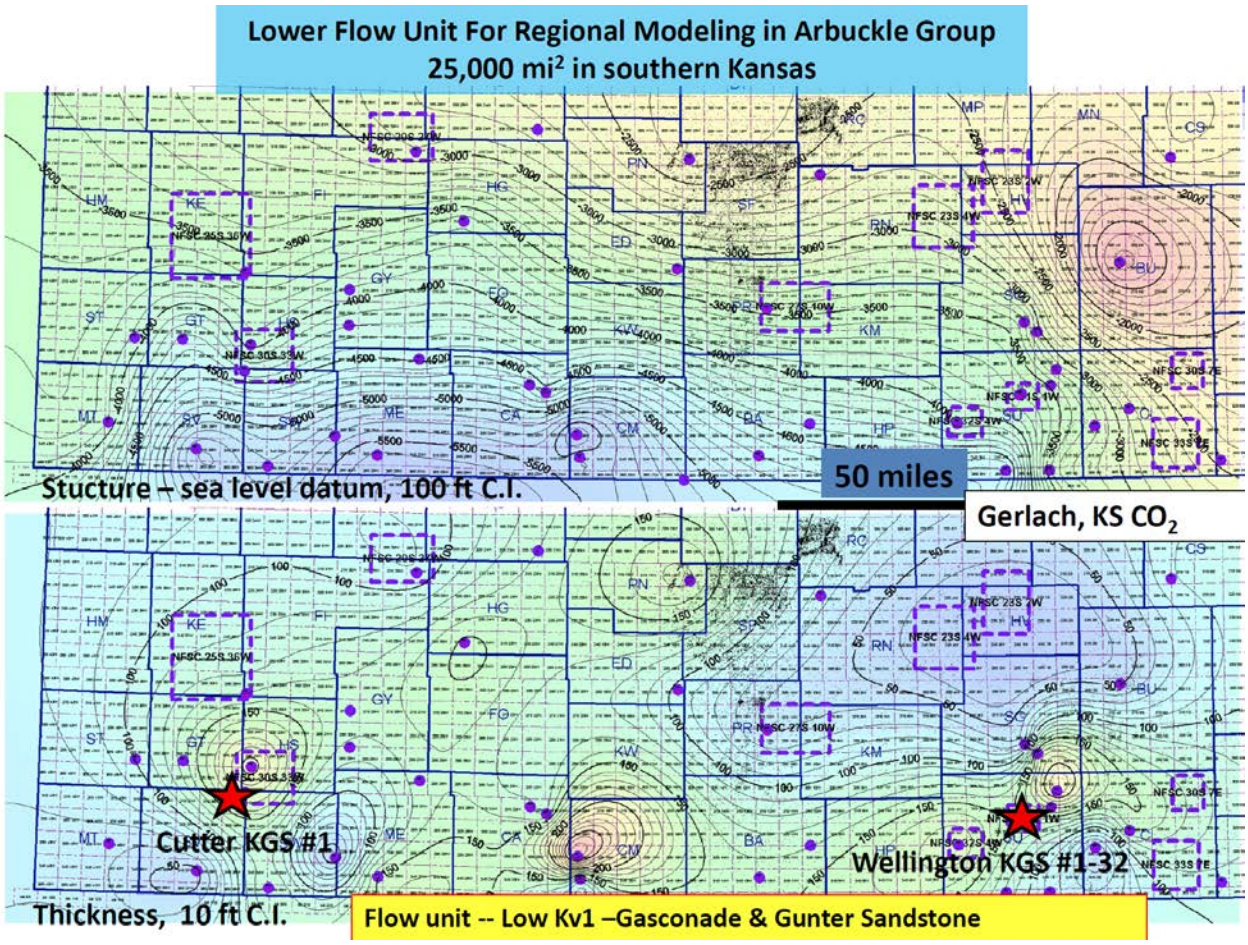

Figure 1. Variability in structure and thickness of a lower flow unit in the Arbuckle in southern Kansas shown to emphasis the fact that the flow units are mappable, and have sufficient control on a regional scale to infer properties for a successful regional simulation and assessment of injectivity and storage.

The regional simulation of the MegaModel for southern Kansas resulted in a regional pressure buildup indicating that with the variable flow unit properties that the system is not fully open when it comes to regional scale CO2 disposal conducted in a 50 year timeframe. However, on the long term the system is open. This indicates that pressures and fluid levels of the Arbuckle will need to be closely monitored and modeled, much like any other aquifer that is used by humans.

The adaptation to the MegaModel to brine injection can be easily done including setting a maximum pore pressure (maybe spatially variable based on fluid levels and overburden above which possible leakage would occur, i.e., fracture-based flow. Leakage could be entered into the model as trends/anisotropy based on actual lineaments of suspected faults or better yet, faults obtained from 3D seismic.

Models and analysis of well tests would 1) evaluate if we have a cumulative increase in pressure and where, 2) define areas with more compartmentalized or directed flow; 3) predict interaction

of pressure in areas with critical faults; 4) provide high-low injection outcomes scenarios; 5) run optimization scenarios to evaluate stabilization/sustainable rates and pressures of disposal to offer management solutions to regulators.

The following is an example of an earthquake swarm coupled with the use of the DOE sponsored Kansas CO2 Interactive Mapper -- **http://maps.kgs.ku.edu/co2/ (Figures 2-12)**.

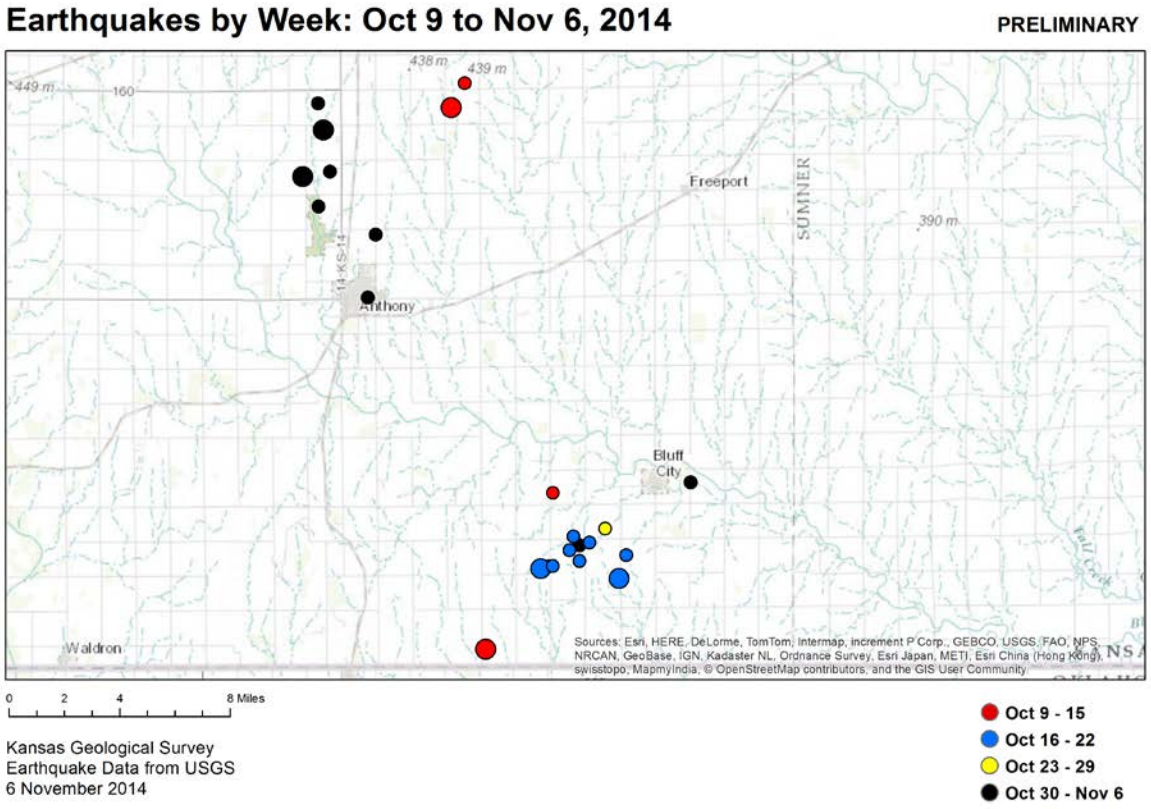

Figure 2. Two earthquake swarms including a 4.3 SE of Anthony in south-central Kansas in Harper County adjacent to Sumner County.

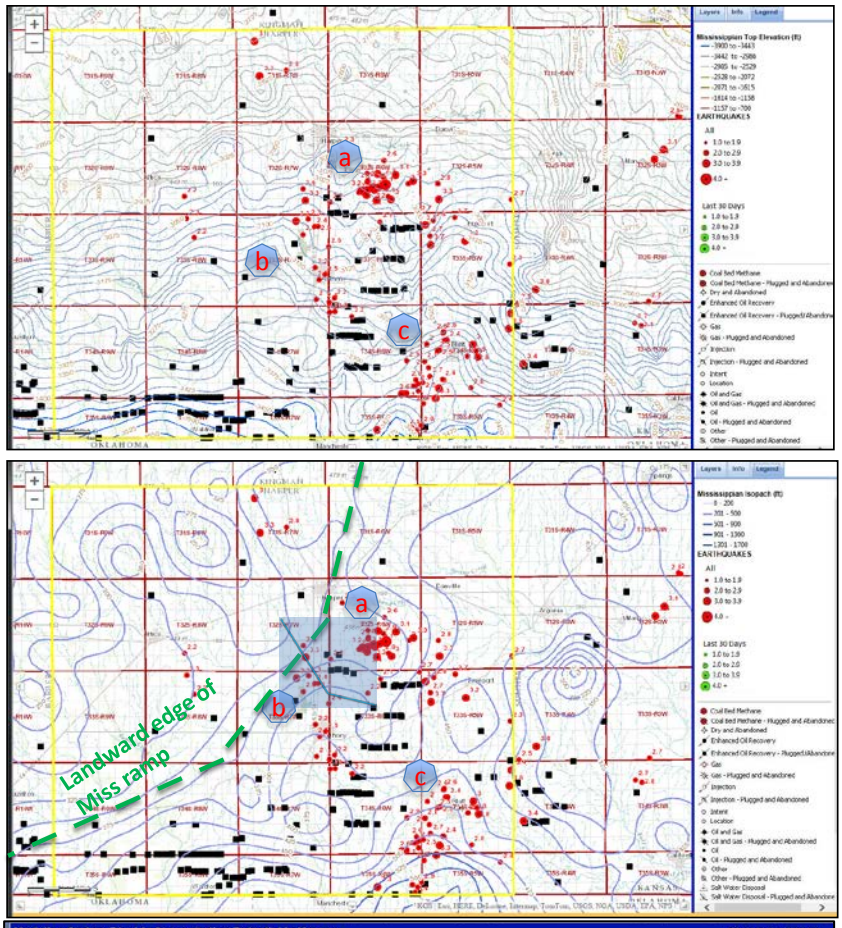

See cross section next page

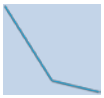

Figure 3. (top) Elevation and isopach of the Mississippian in the area of earthquake clusters (labeled a, b, and c) in Harper County (yellow outline) and western edge of Sumner County. Horizontal wells are black squares and red dots are recent earthquakes, each labeled with their magnitude as determined by USGS. Injection wells are not shown. Mississippian strata thicken along an arch (green dashes) delimiting a thick ramp deposit that is the object of the horizontal drilling and high volume brine extraction. Cluster "a" is a location where the Mississippian is thin, where the landward edge of the ramp extends to the SE. Based on work in this study, the thinning is likely due to small faulting during and post Mississippian deposition, a time when flexure faulting was tectonically active. A cross section in the light blue outline extends across the

Mississippian ramp to illustrate the thickening (Figure 4). (Bottom) Close-up of the Mississippian thinning that locally extend the edge of the ramp.

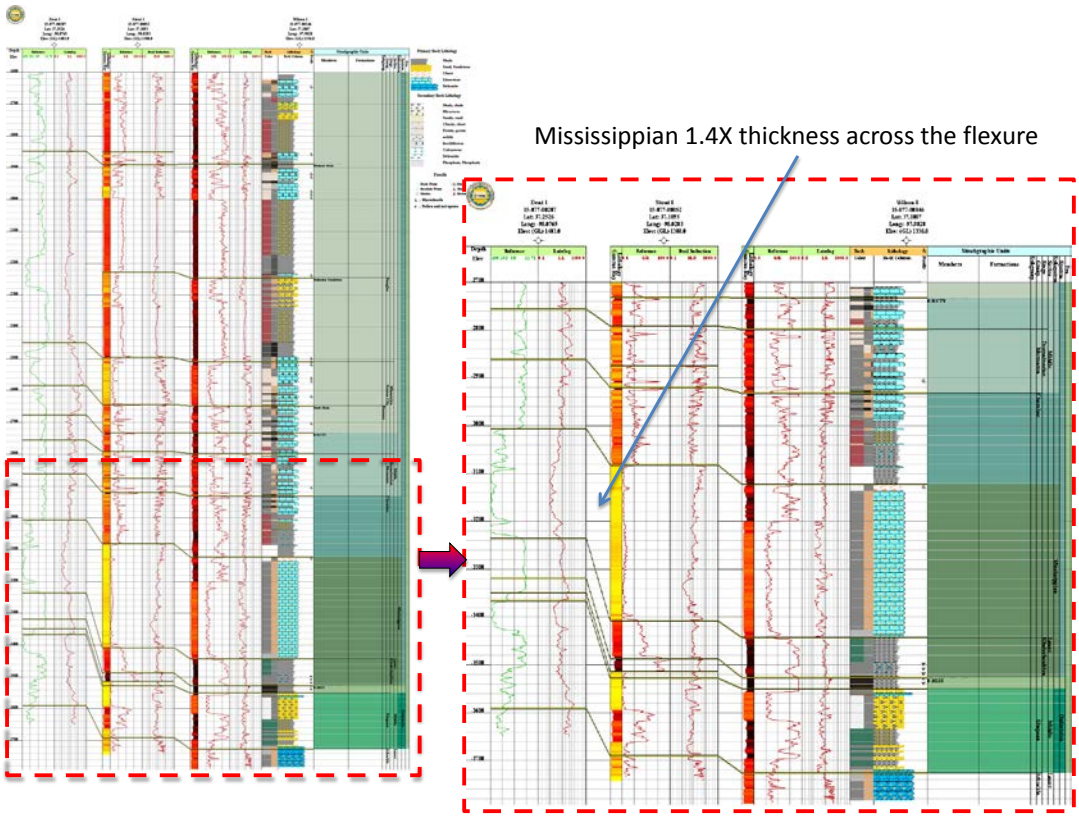

Figure 4. NW-SE structural cross section crossing the inner Mississippian ramp where the Mississippian strata thickens.

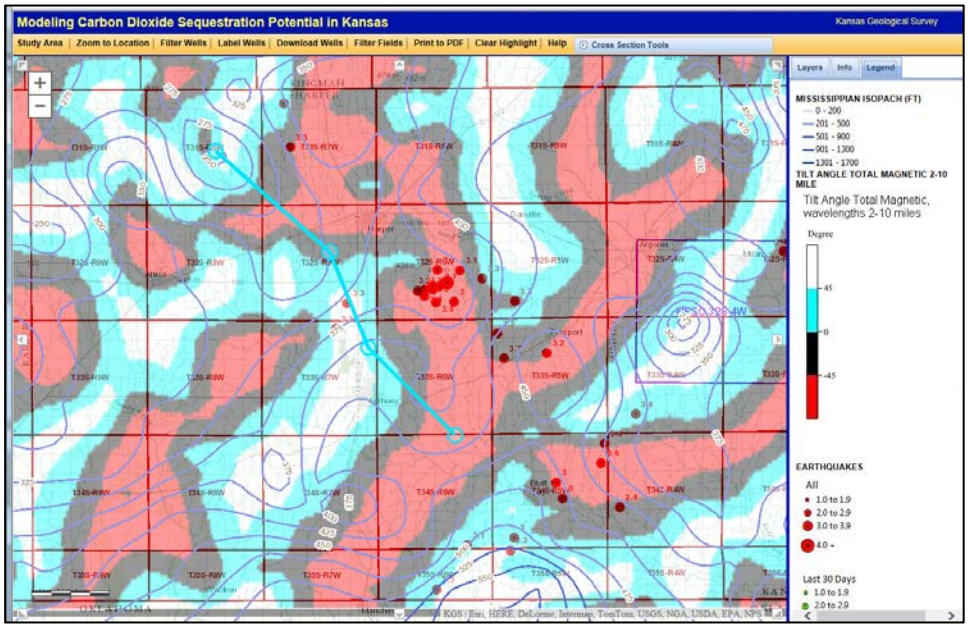

Figure 5. Mississippian isopach superposed on the tilt angle map to the 2-10 mile filter of the total magnetic field. Mississippian ramp parallels the dominant NE-trend. The area is underlain by the Midcontinent Rift. The magnetic negative tilt (red) are likely grabens filled with sediment and the magnetic tilt positives are suggesting either mafic intrusives or beds of extrusive basic volcanics that are steeply dipping in the rift fill. The associations of

potential field and basement rift lithologies have been confirmed in northern Kansas. Note cross section index line. Cross section shown in Figure 6.

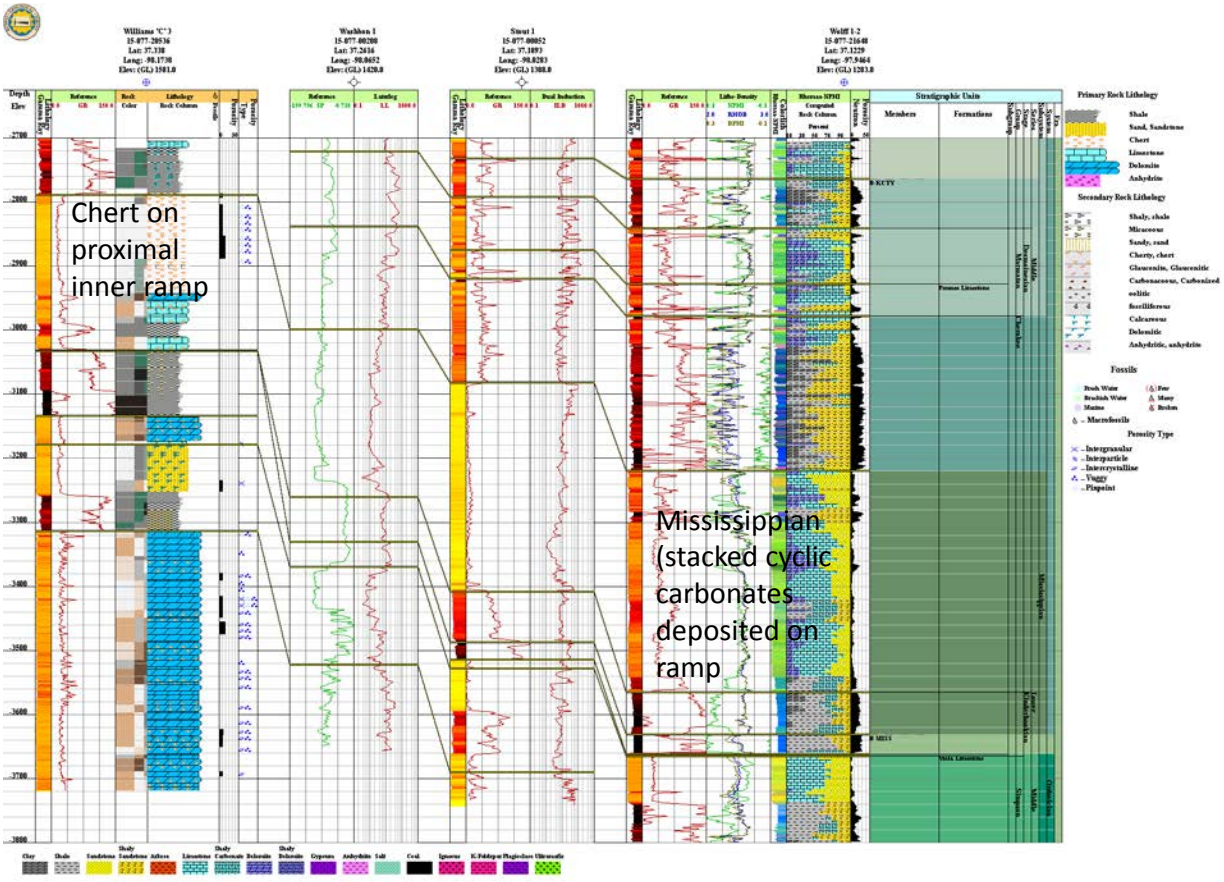

Figure 6. NW-SE structural cross section from proximal to more distal ramp focused on the Mississippian strata. Higher gamma ray intervals (shaly and organic-bearing) in lower portion of the Mississippian and underlying Chattanooga Shale are the likely "unconventional" targets of the horizontal wells drilled in this area from which large volume of brine are also recovered. Note the major changes in lithofacies and thickness. Related work has indicated that concurrent deformation/faulting across the ramp led to a progradational facies succession along the shelf margin. Earthquake clusters are nearby. The role of the suspected faults in the earthquake activity via reactivation appears to be highly likely.

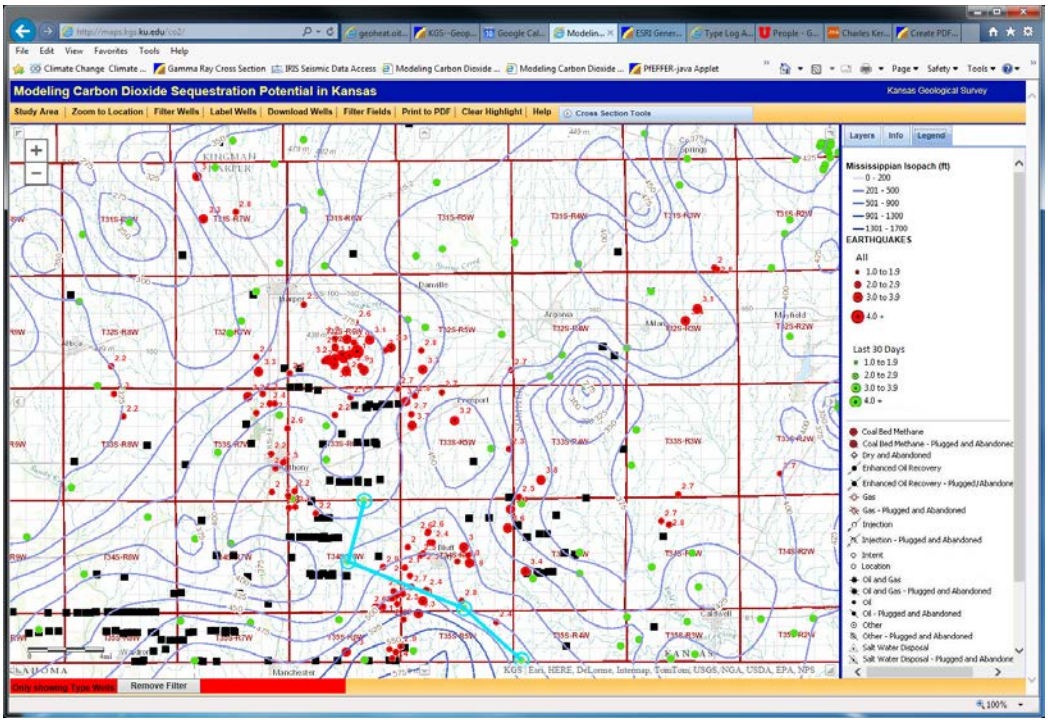

Figure 7. Mississippian isopach again with another cross section located farther south near the Oklahoma border crossing the southern earthquake cluster.

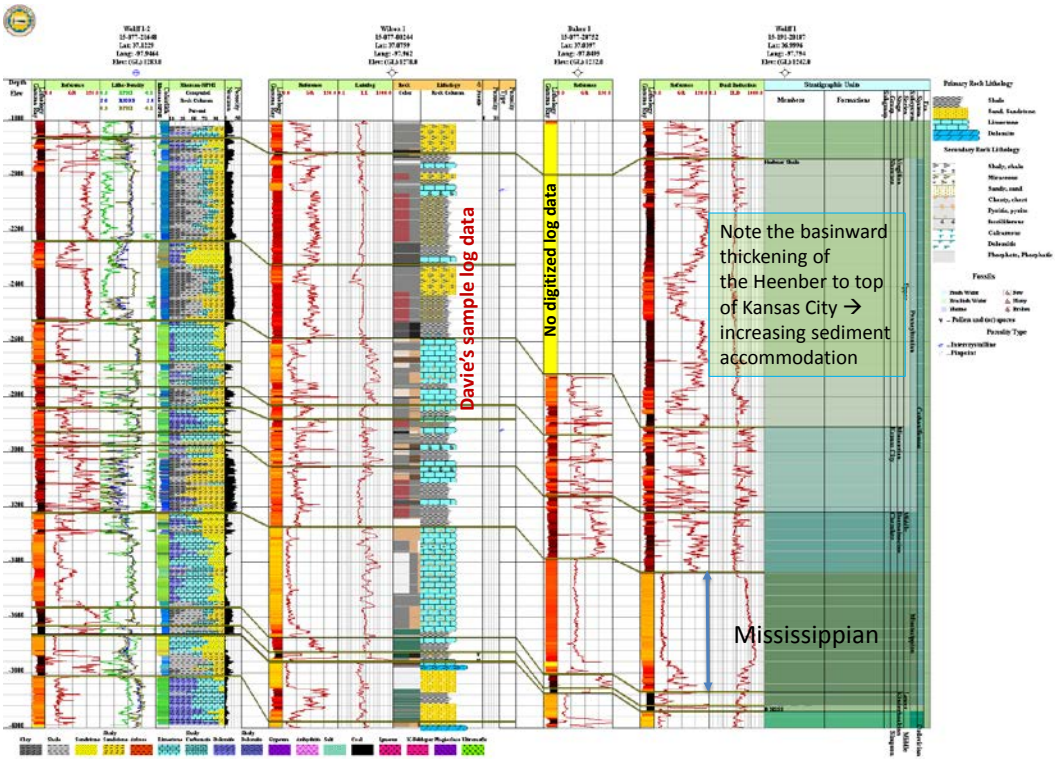

Figure 8. NW-SE structural cross section showing stratigraphic changes continue across the ramp affecting Pennsylvanian age siliciclastics.

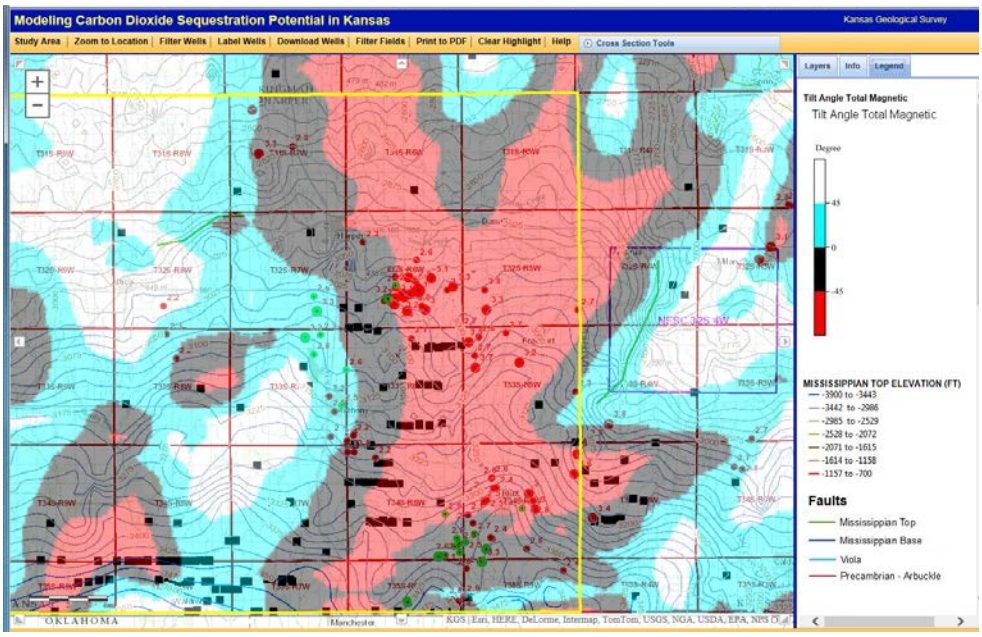

Figure 9. Tilt angle of the total magnetic field without the 2-10 mile filter shown in Figure 5. Horizontal wells and earthquakes are in the tilt angle magnetic low, believed to be comprised of rift-fill sediment. Edge of the sediment fill (inferred rift margin in this area) closely corresponds with the location of the ramp margin on the west and enhanced structural flexure trending more W-E on the south, also the location of an earthquake cluster and more horizontal wells.

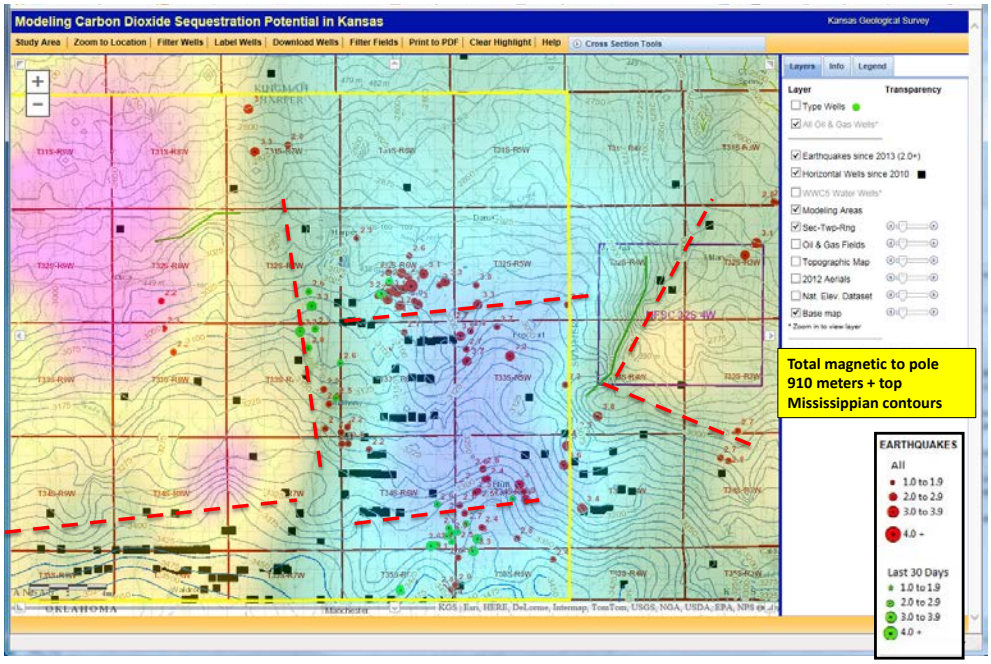

Figure 10. Total magnetic reduce to pole overlain with Mississippian structural contours nicely constrains the Mississippian Lime Play and the locus of earthquake activity. The complexity in understanding which faults move also depends on the stress direction, differential horizontal stress, and the orientation, length, and damage zone of the faults.

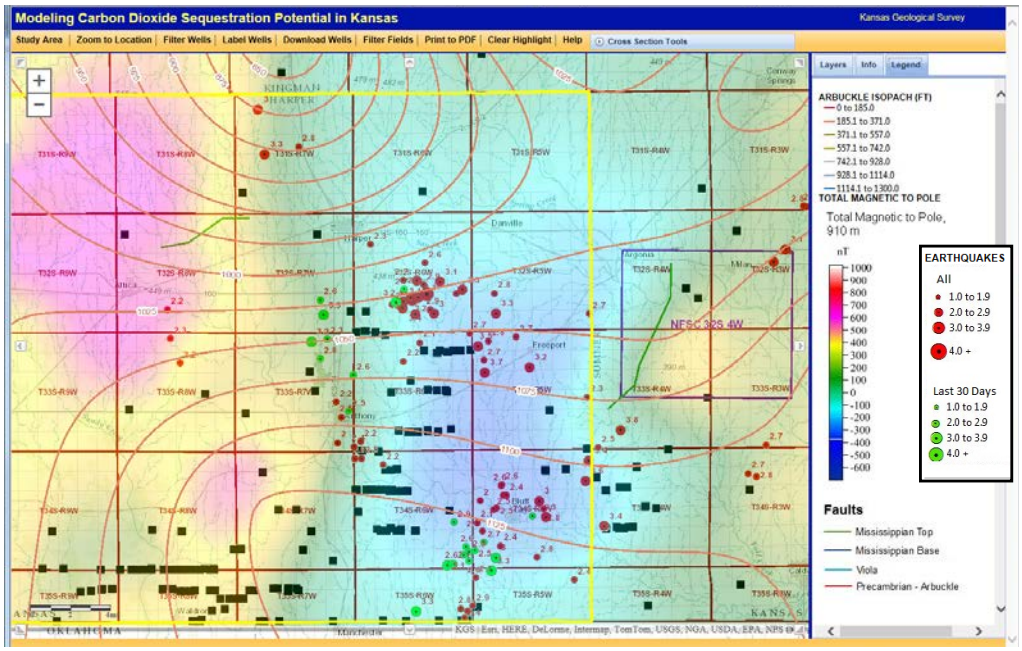

Figure 11. Same magnetic map as in Figure 10, but with an overlay of the Arbuckle isopach map. A notable north to south thickening of the Arbuckle is noted at the site of the northern earthquake cluster. The change is also along a west-east lineament shown in Figure 10. Maximum thickness on the south is confined to the magnetic low corresponding with the underlying rift system. This is not unexpected with a reactivating fault system.

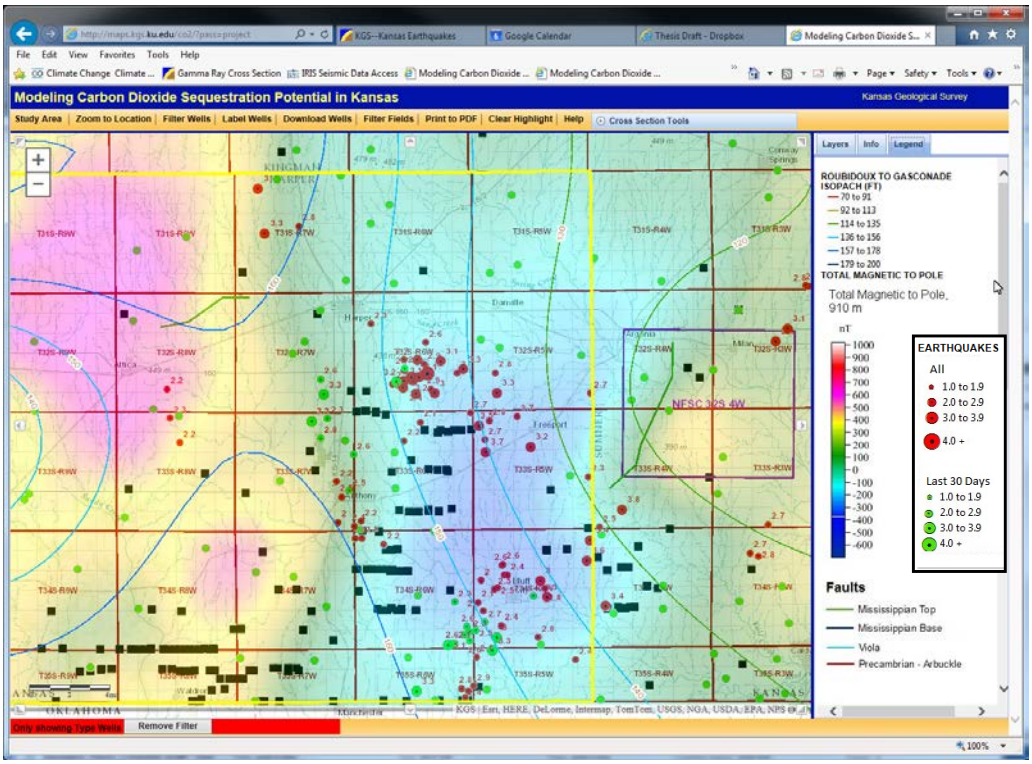

Figure 12. Isopach of the Gasconade interval in the Arbuckle, the highly permeable portion in the lower Arbuckle thickens to the west across the magnetic low, possibly coincidence or

changes in sediment accommodation due to differential subsidence linked to the heterogeneity imposed by the underlying basement rift.

Task 10: Risk Assessment Related to CO_2-EOR in Mississippian Chat Reservoir and CO_2 Sequestration in Arbuckle Aquifers

Subtask 10.1. Model CO_2 plume for 100, 1000, and 5000 yrs after injection stops
Subtask 10.2. Model plume attenuation during and after injection
Subtask 10.3. Model effects of natural aquifer flow on CO_2 plume
Subtask 10.4. Estimate time frame for free phase CO_2 to become negligible
Subtask 10.5. Model effectiveness of cap rocks to contain leakage
Subtask 10.6. Leakage modeling through abandoned wells
Subtask 10.7. Model worst-case CO_2 leakage scenario
Subtask 10.8. Estimate surface environmental effects due to leakage

Leakage and risk have also been addressed by comparing pressures and fluid levels in the Arbuckle with the overlying freshwater aquifers. The distance separating the Arbuckle and from the shallower zones that increase to the west through Kansas and the near constancy of potentiometric surface of the Arbuckle saline aquifer provide a cushion for injection in the Arbuckle. A simplified north-south cross section scaled in feet shows the separation in feet from the shallow freshwater aquifer package (blue) and the Arbuckle (gray) (**Figure 13**).

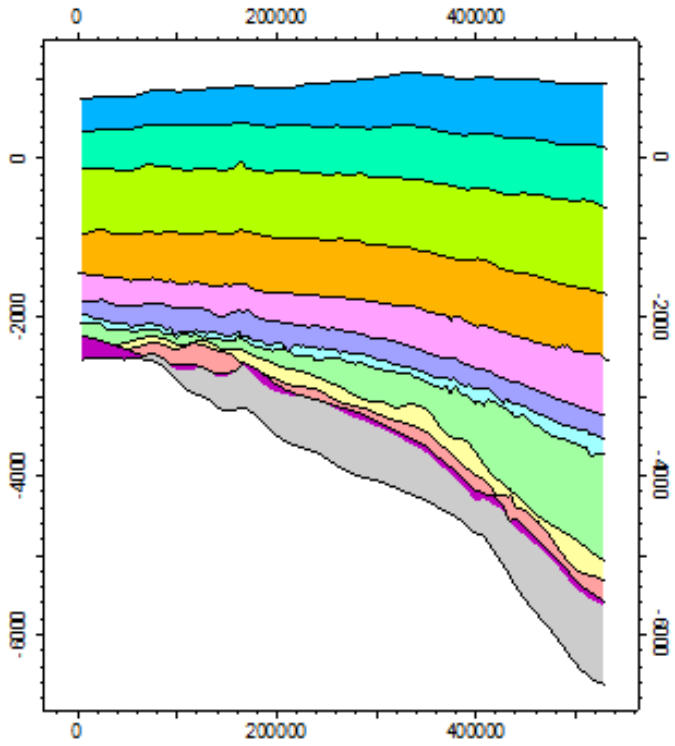

Figure 13. North to south structural cross section illustrating distance between base of near surface aquifers (blue) and the top of the Arbuckle (gray). Scale is in feet.

The confining layers between the shallow freshwater aquifers and the Arbuckle are many and are thick and are comprised of both shales and evaporites (**Figure 14, illustrating the Wellington KGS #1-32**).

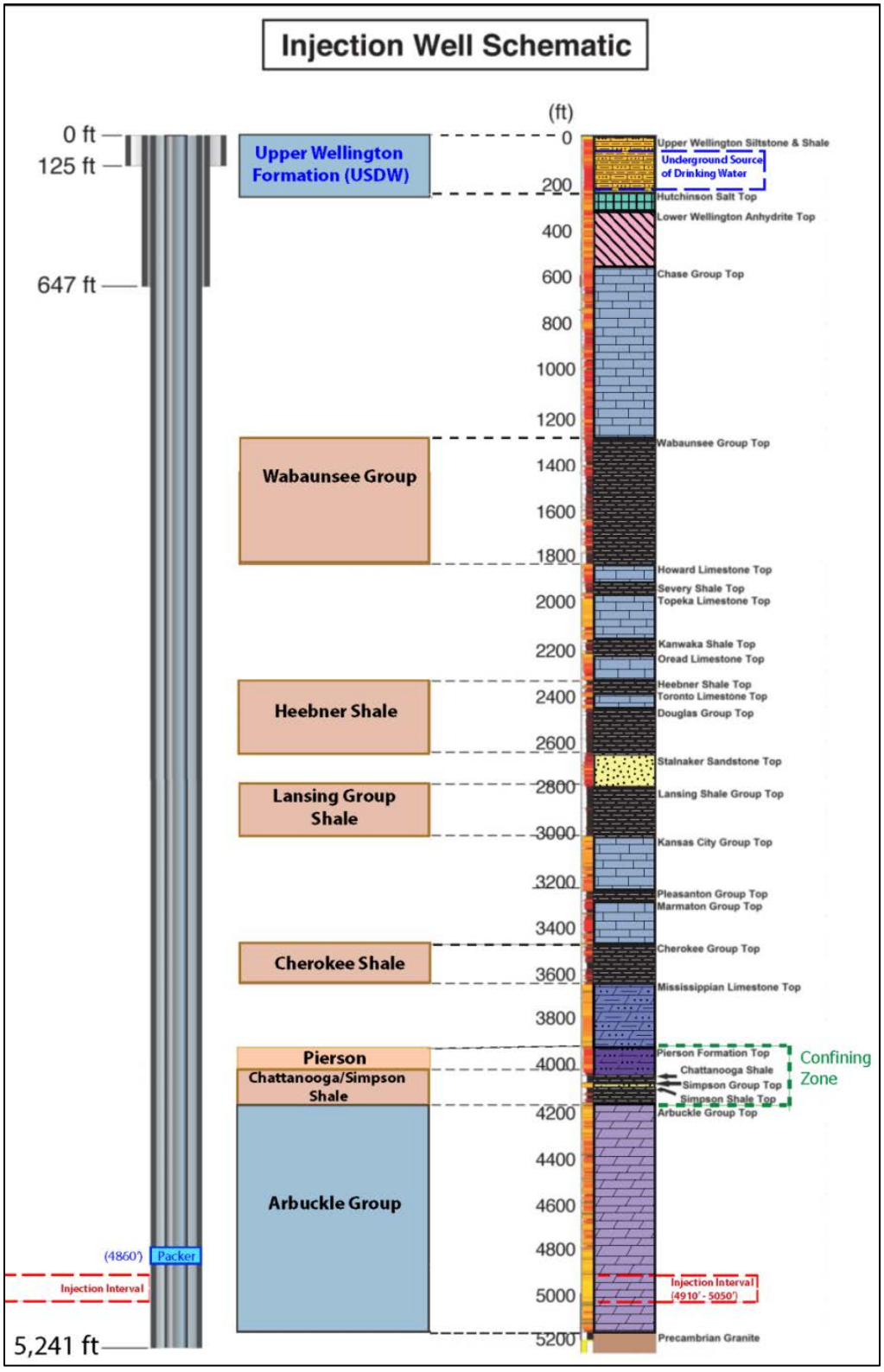

Figure 14. Large degree of hydraulic confinement between Arbuckle and freshwater aquifers. The intervals show no hydraulic connection in central and western Kansas encompassing the area of the regional CO2 assessment.

The following figures illustrate the basic hydrologic framework of the shallow aquifers and the Arbuckle and comparisons between (**Figures 15-25).**

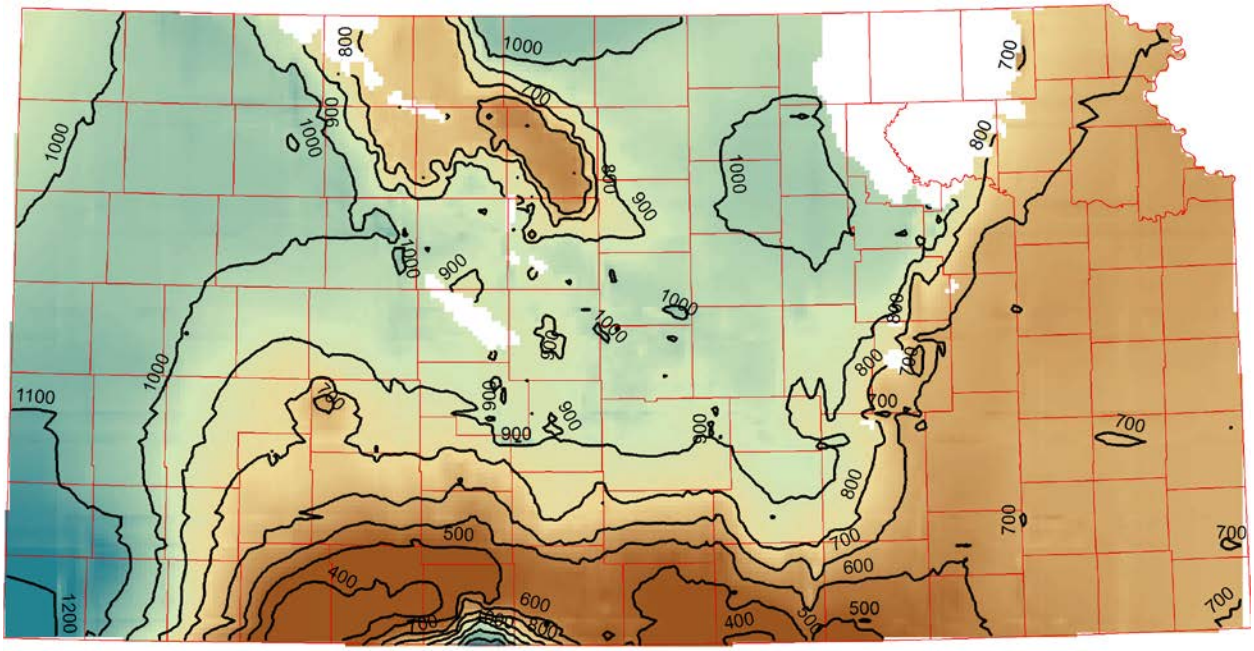

Figure 15. *In situ* groundwater levels for the Arbuckle (ft, msl). In-situ water levels are lower by about 600 ft in SW Kansas due to heavier brines.

Salinity is high in the brines within the Arbuckle in southern Kansas, exceeding 100,000 TDS (Figure 16). The higher brine concentrations closely follow depth of the Arbuckle.

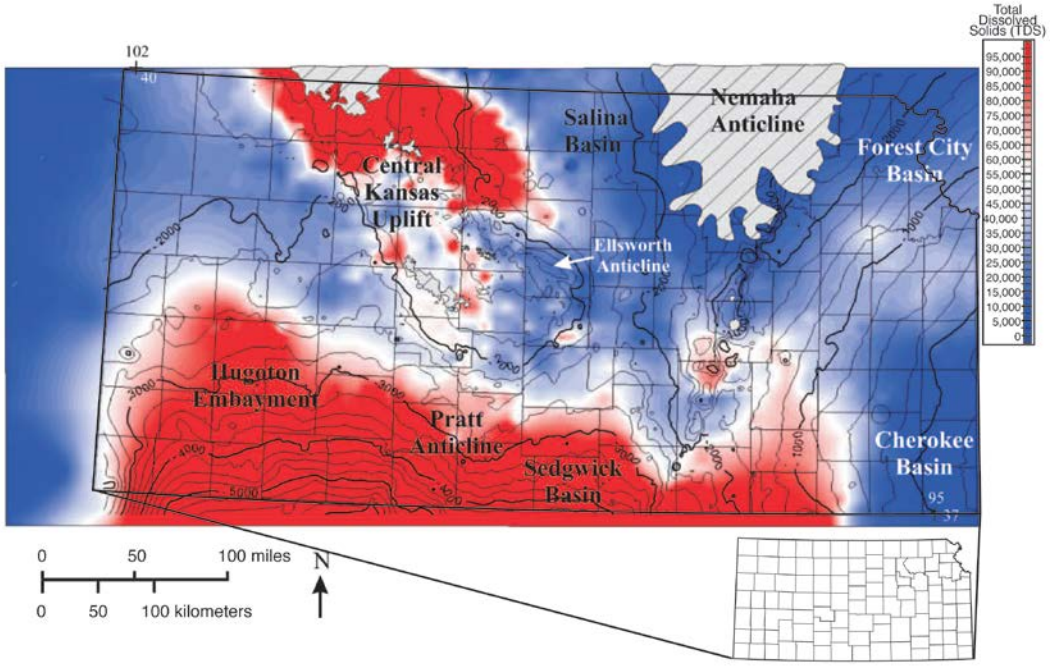

Figure 16. Total Dissolved Solids > 100,000 ppm in SW Kansas.

The equivalent freshwater head of the Arbuckle (Figure 17) removes the effects of the variable salinity the brine and shows very low gradient elevation sloping from west to east. The steepest gradient is there the Arbuckle crosses is and partly truncated by the Nemaha Uplift running NE-ward through the eastern half of Kansas.

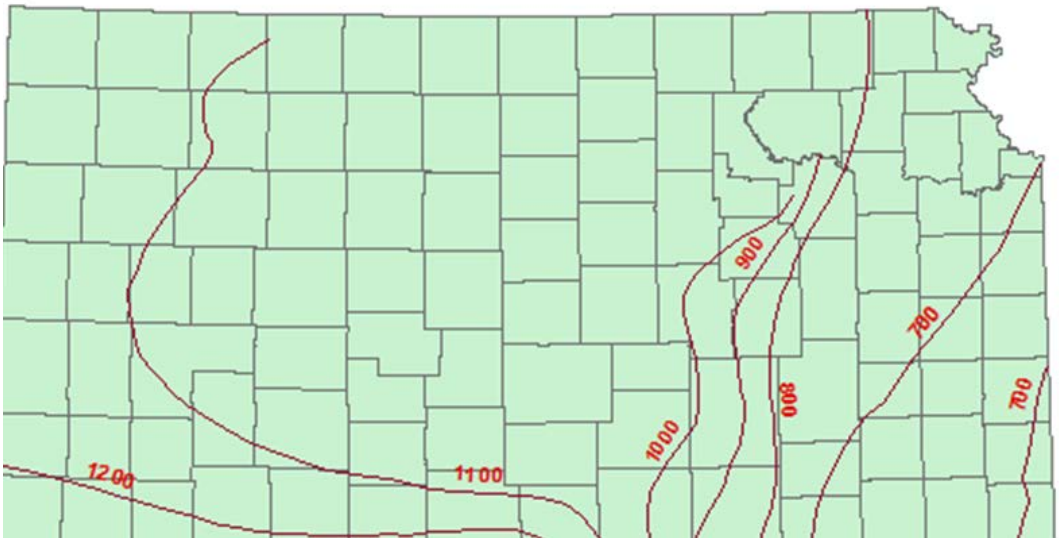

Figure 17. Potentiometric surface of Arbuckle. Merging of two regional flow fields (Rocky Mountains & Anadarko Basin). Groundwater flow across state takes approximately ¼ to ½ million years.

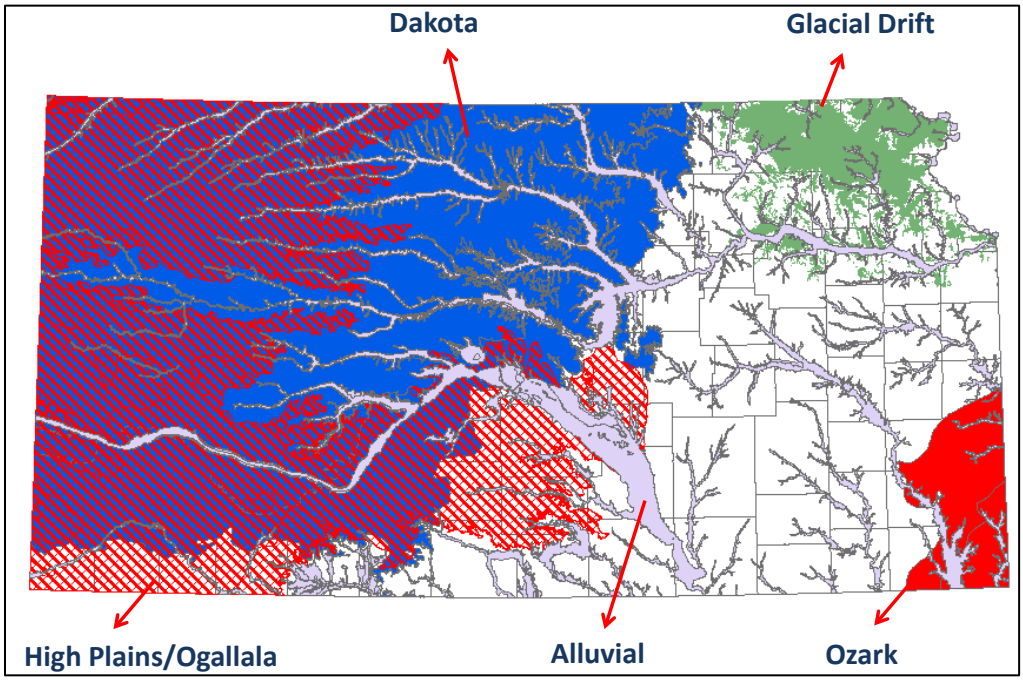

Figure 18. Spatial distribution of the shallow freshwater aquifers in Kansas.

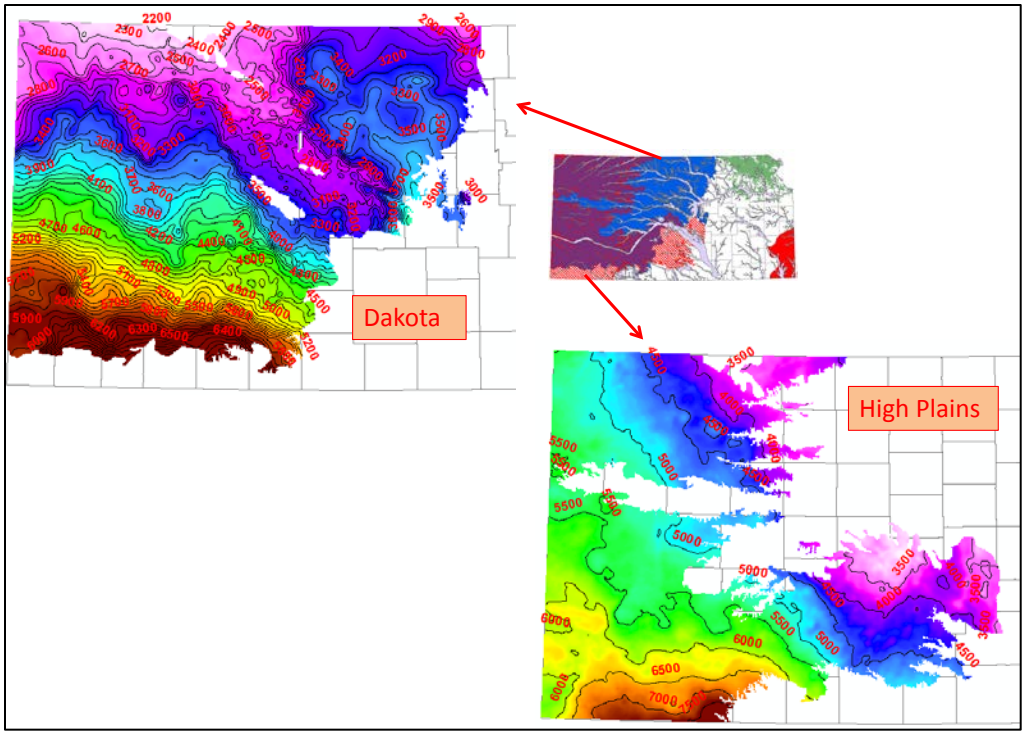

Figure 19. Vertical separation (ft) between Arbuckle and freshwater aquifers. Vertical distances of the top of Arbuckle to the Dakota and High Plains aquifers ranges from 2200 ft to over 6500 ft.

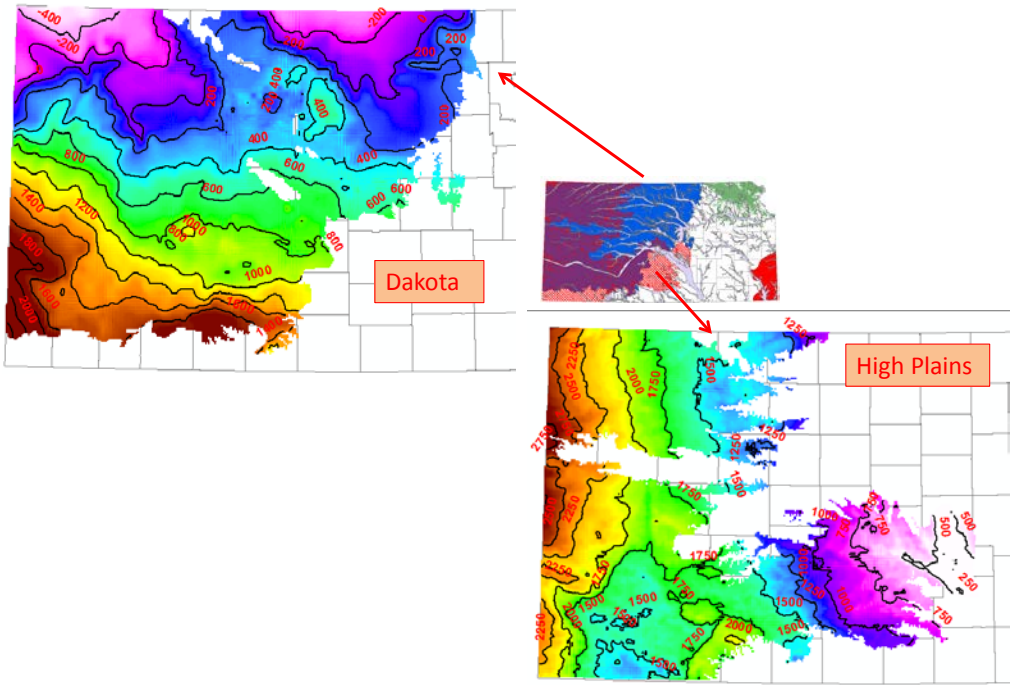

Figure 20. Head difference (in feet) between water levels in Arbuckle and base of freshwater aquifers range from a negative 400 ft (Arbuckle above the shallow zones) in northern Kansas to over 2000 ft in southwestern Kansas.

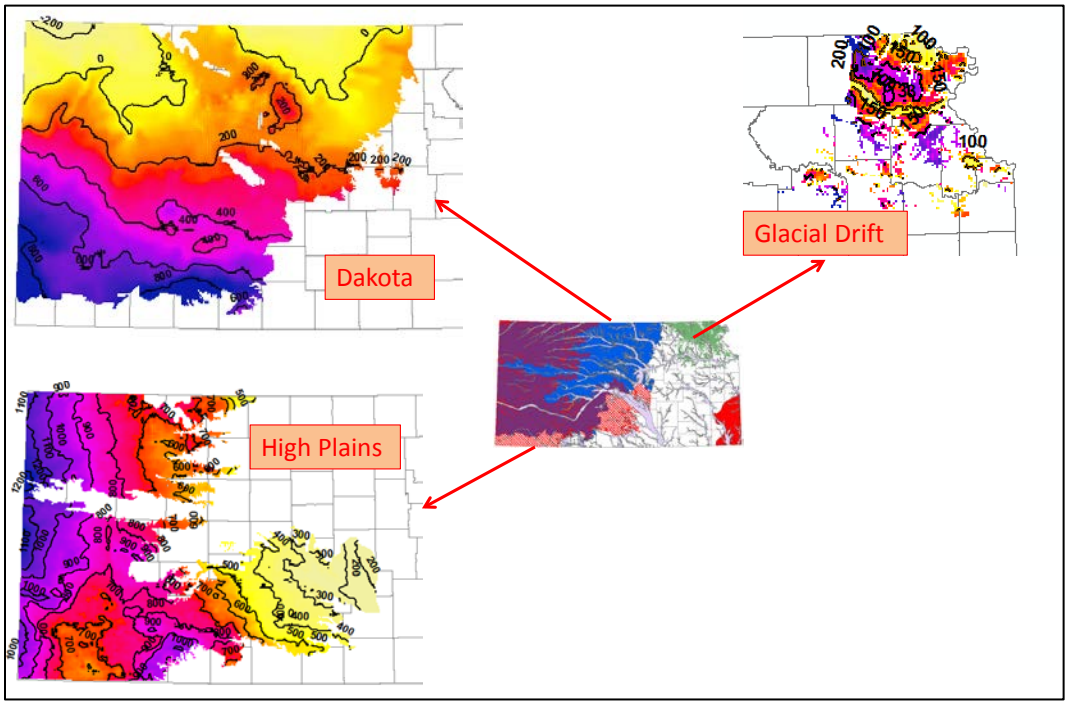

Figure 21. Required increase in pore pressure (psi) for migration of brines from Arbuckle into freshwater aquifers ranges from a negative 200 ft in northwest Kansas to over 700 ft in southwest Kansas.

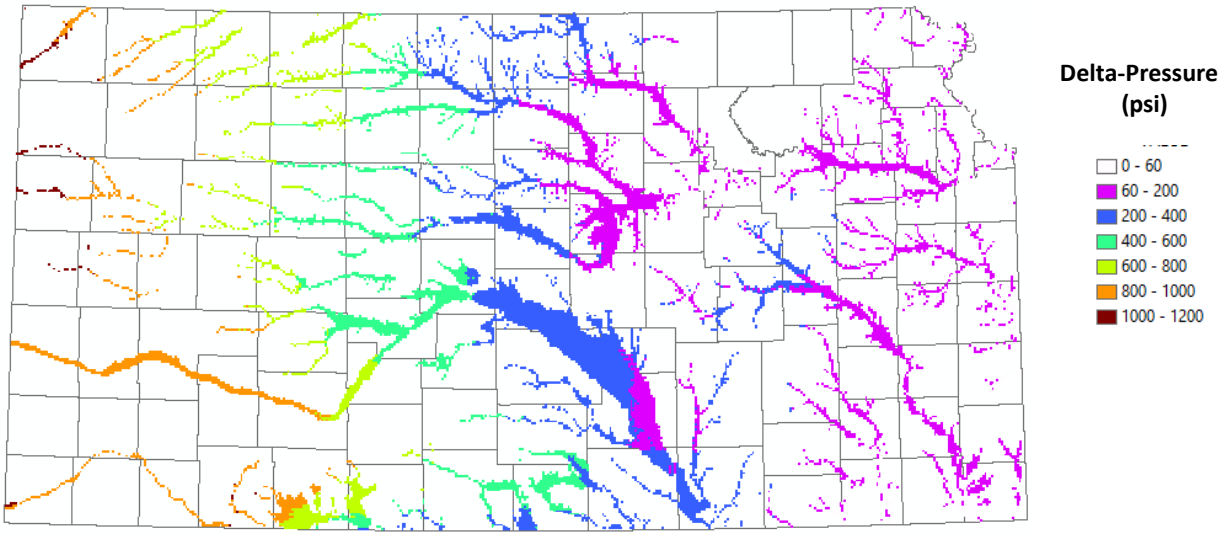

Figure 22. Required increase in pore pressure for migration of brines from Arbuckle into alluvial aquifers ranges from the 60 to 200 ft range in eastern Kansas, east of the Nemaha Uplift to over 1000 ft in far western Kansas.

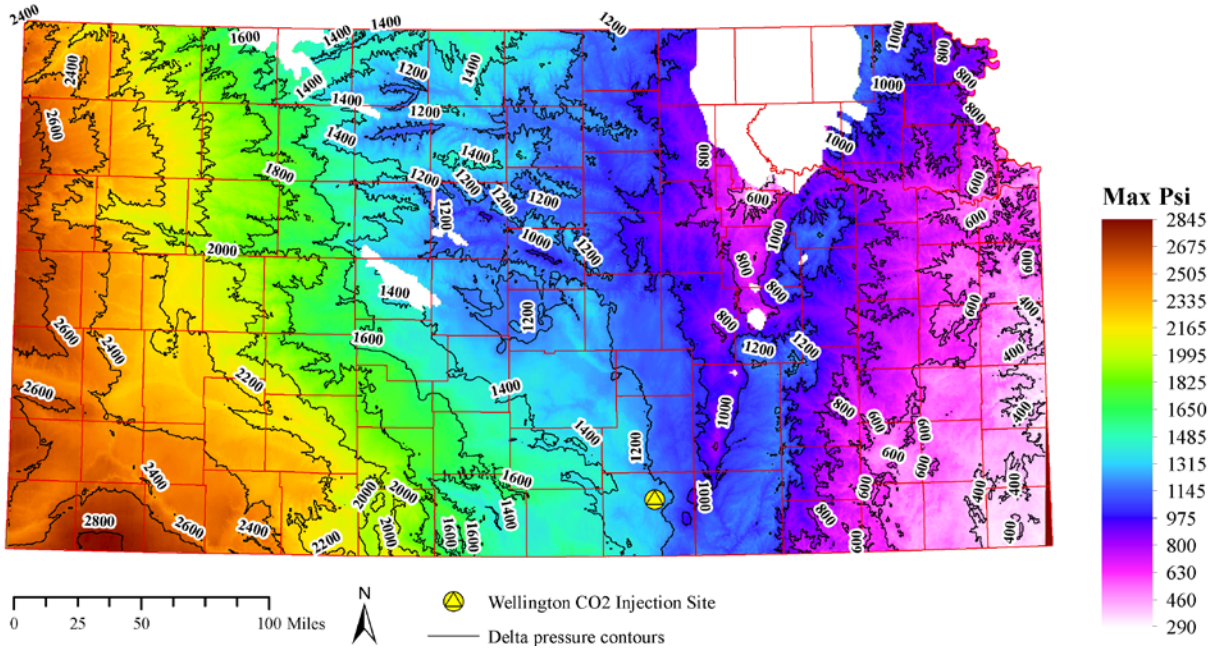

Figure 23. Maximum allowable increase in pore pressure (psi) to prevent fractures. fracture gradient in Kansas ~ 0.75 psi/ft. Values range from 400 ft in southeastern Kansas to over 2800 ft in southwestern Kansas.

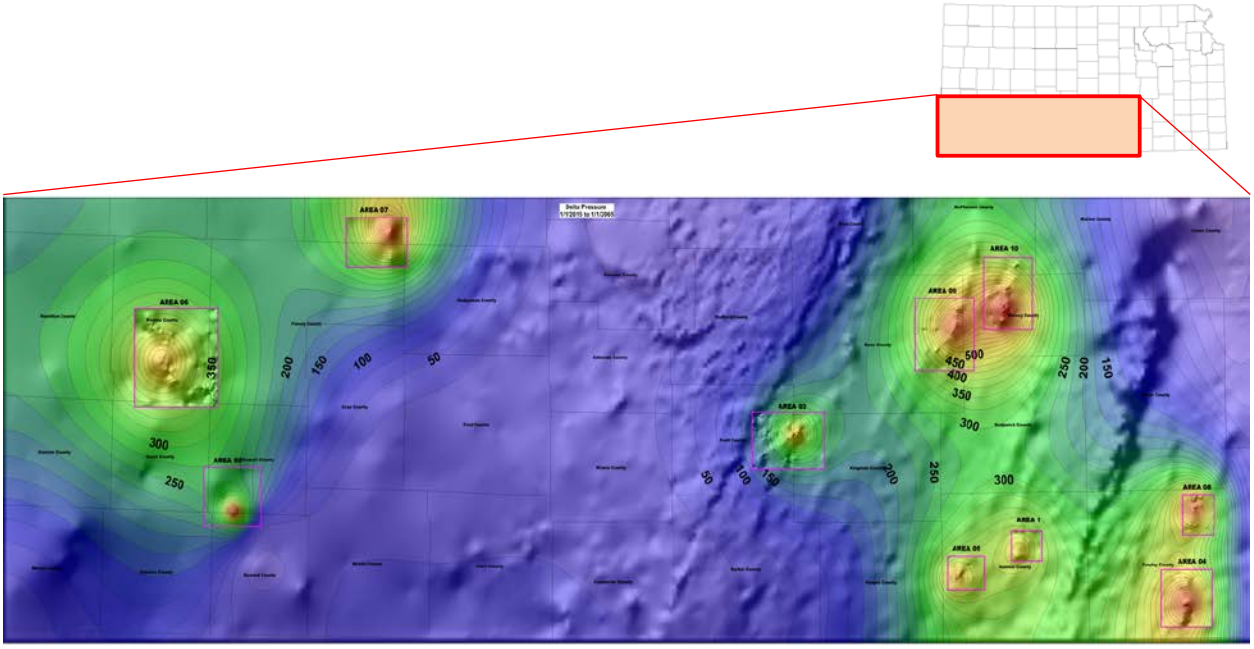

Figure 24. Simulated increase in pore pressures with commercial scale CO2 injection at 10 sites in southern Kansas over a 50 year period. Increase in pressure (psi) range from 400 psi to over nearly 600 psi. Pressures rapidly decrease after injection ceases.

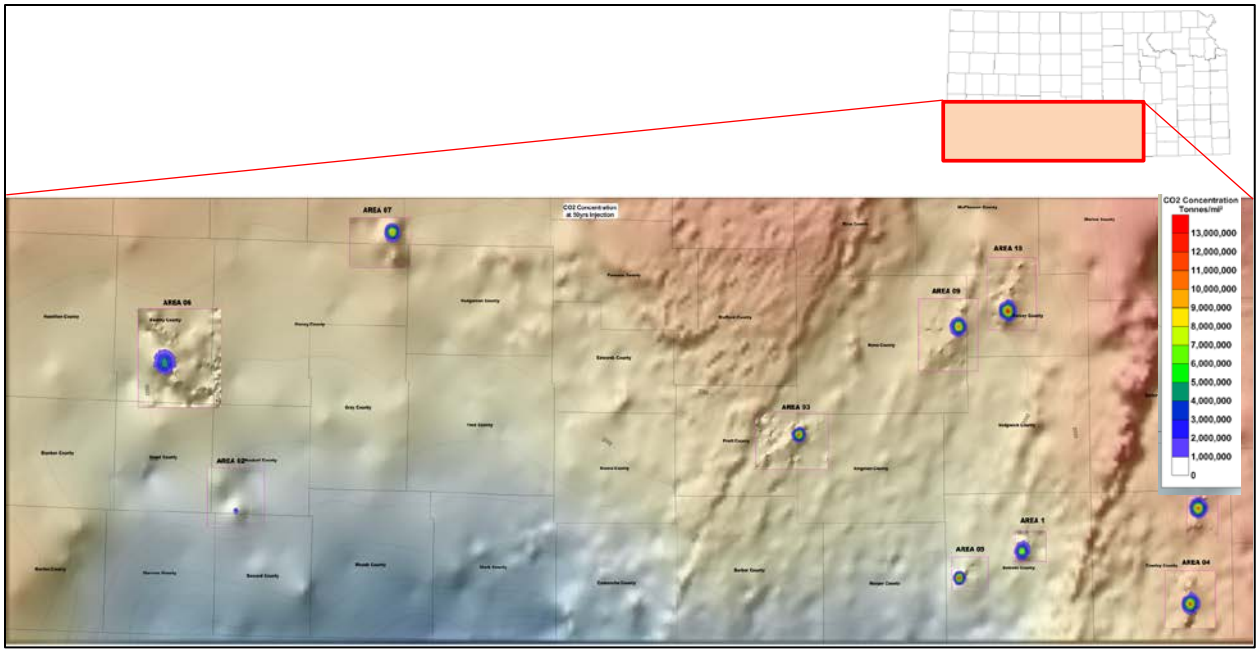

Figure 25. Simulated extent of the CO2 plume using CO2 concentration in tonnes/km2 at end of 50 years of commercial scale injection at the 10 modeling sites.

Conclusions

The saline Arbuckle aquifer has large capacity to store anthropogenic CO2 emission from Kansas and surrounding states for many decades.

CO2 injection however will cause elevated pore pressures.

Pressure constraint maps have been prepared to guide in developing an optimal state wide plan for commercial scale injection of CO2.

Task 11: Produced Water and Wellbore Management Plans

Subtask 11.1. Identify at-risk wells in Wellington Field

Subtask 11.2. Outline Best Practices and well recompletion plans for at-risk wells

Subtask 11.3. Outline Best practices and well completion plans for new CO_2 injector wells

Subtask 11.4. Summarize practices in place for disposal of produced water

Task 12. Regional CO2 Sequestration Potential in OPAS - 17 Counties

Subtask 12.1. Map reservoir compartments in Arbuckle aquifer in a regional context

Subtask 12.3. Generalized estimates of miscible CO_2-EOR in similar and larger oil fields in approximately 17 counties

The combined CO2 sequestration from the four fields studied in western Kansas is + million tonnes (**Table 1**).

Reservoir	Total PV RB	Total HCPV RB	Oil Res BBL RB	Water Res BBL RB	Gas Res BBL RB
Cutter Morrow (1/1/1961)	25,719,145	18,730,543	15,456,000	69,789,100	3,275,690
Pleasant Prairie (1/1/2012)	22,680,000	9,069,100	9,051,400	13,611,000	17,741
Eubank (6/1/2013)	62,751,000	22,662,000	22,131,000	40,089,000	530,650
Shuck (1/1/2013)	44,688,513	17,310,419	17,139,000	27,380,000	173,231
Total	155,838,658	67,772,062	63,777,400	150,869,100	3,997,312
CO2 FVF (RB/MCF)	0.45	0.45	0.45	0.45	0.45
CO2 MCF/Tonne	19.1895	19.1895	19.1895	19.1895	19.1895
PV in CO2 Tonne	18,046,751	7,848,281	7,385,683	17,471,256	462,905
Efficiency for Example	0.05	0.6	0.6	0.2	0.8
Potential Sequester Tonnes	902,338	4,708,968	4,431,410	3,494,251	370,324
			SUM = 8,295,985 tonnes		

Table 1. Total fluid recovery and efficiencies of the four fields studied in western Kansas.

Subtask 12.4. Estimate regional CO_2 sequestration potential of OPAS

(Milestone/Subtask 12.4)

(1) **Estimate of CO2 sequestration in the Arbuckle using total pore volume in the model and formation volume factor at 2000 psi--** We have completed our regional analysis of the Arbuckle Group saline aquifer in south-central Kansas to estimate its potential for CO_2 sequestration. This analysis was performed using data collected from wireline logs, core, seismic surveys, and gravity/magnetics data throughout the 25,000 mi^2 study area, in addition to two characterization wells that were drilled to basement and cored for testing. Information acquired from all core and fluid analyses, petrophysical data, and tests were used to establish a regional correlation framework to assess flow units and stratigraphic subdivisions across the study area. Key properties were used as input parameters to build refined geomodels that could simulate commercial scale injection in 10 sites in southern Kansas. Results from the fine-grid simulations were extrapolated to the entire study region to obtain a more accurate estimate of regional CO_2 sequestration potential. This "Mega Model" simulation contained more than 2 MM coarse and fine grid cells, and provided a realistic measure of capacity beyond a

volumetric-based storage assessment. Additional details will be provided in the final report. An overview of these findings is provided below:

The total pore volume of the MegaModel is 37.34 x 10^{12} ft^3 or 6.65 x 10^{12} RB

Assumptions:
1. CO_2 FVF at 2000+ psi is approximately 0.45 RB/mcf
2. CO_2 Density is 0.1167 lb/ft^3, or 19.19 mcf/tonne
3. P90 Efficiency is 0.4%, P10 Efficiency is 5.0%
   Assuming 100% efficiency (where 100% of the pore volume is saturated with CO_2), the CO_2 volume would be 155.9 billion tonnes.
   At 0.4% efficiency, the CO_2 volume would be **0.62 billion tonnes**.
   At 5% efficiency, the CO_2 volume would be **7.8 billion tonnes**.

Based on the properties of the Arbuckle reservoir, a 5% efficiency factor is appropriate for CO_2 storage. Thus, the final characterization results indicate that the regional storage capacity of the Arbuckle saline aquifer in south central Kansas is approximately **7.8 billion tonnes of CO_2**.

(2) CO2 sequestration in the Arbuckle estimated using effective (net porous and permeable) pore space and the methodology of DOE-NETL National Carbon Sequestration Atlas III.

A new and final P10 estimate of sequestration capacity of 5.3 billion tonnes using the DOE-NETL methodology is similar to that obtained in (1) described above. The DOE-NETL equation used, $G_{CO2} = A_t\ h_g\ \emptyset_{tot}\ \rho E_{saline}$, includes the Esaline factor that ranges between 0.40 and 5.5 percent over the 10th to 90th percent probability range. The P90 value using the DOE-NETL methodology is 60,619,189,540 metric tonnes.

(3) **Estimating CO2 sequestration the Arbuckle using MegaModel with megainjection wells.**

The MegaModel has been completed and a written report on the study and a transfer of the CMG model will be completed as the last step. Pressure at each well is set 40% higher than original pressure to stay within a conservative breakdown pressure of about 1.37 times initial pressure. Model results will be included in the final report.

The following figures summarize the MegaModel grid and provide examples of a two area CO2 plumes. (**Figures 26-29**).

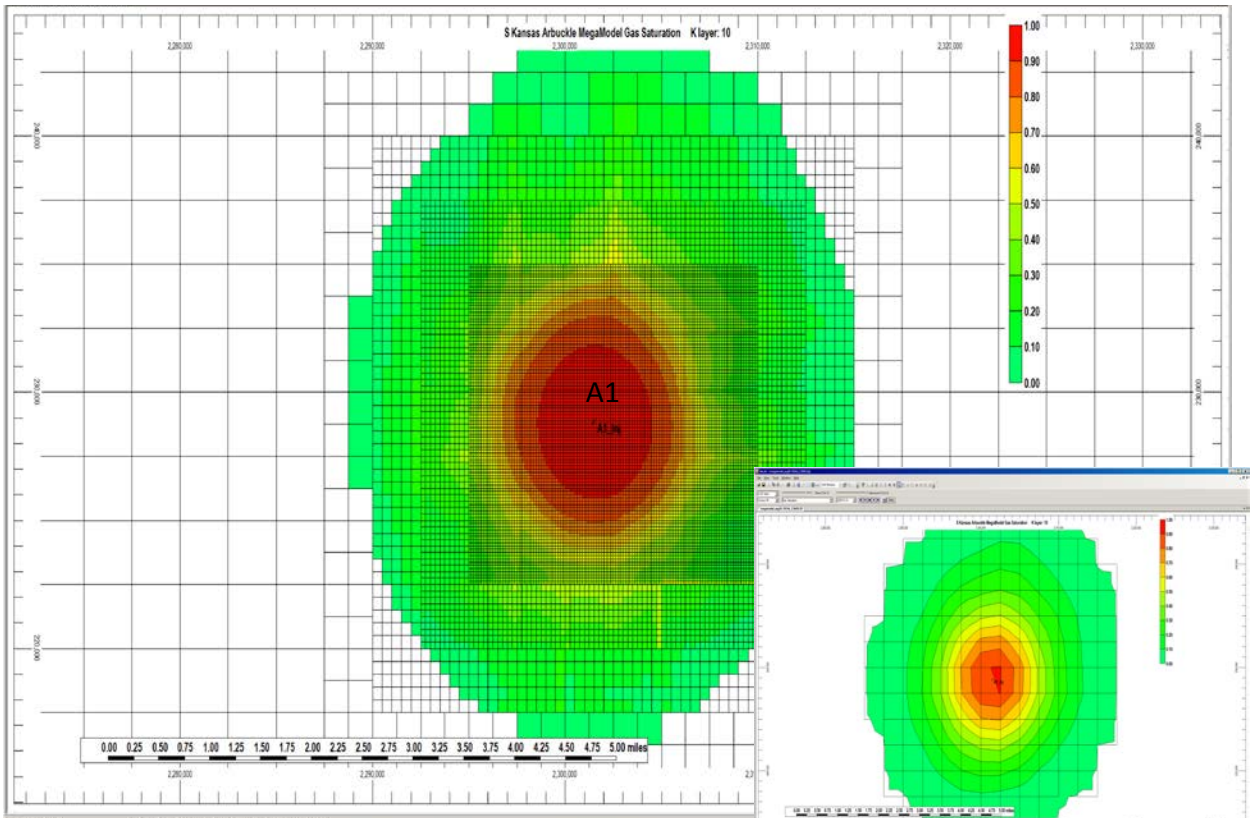

Figure 26. Area #1 Gas saturation.

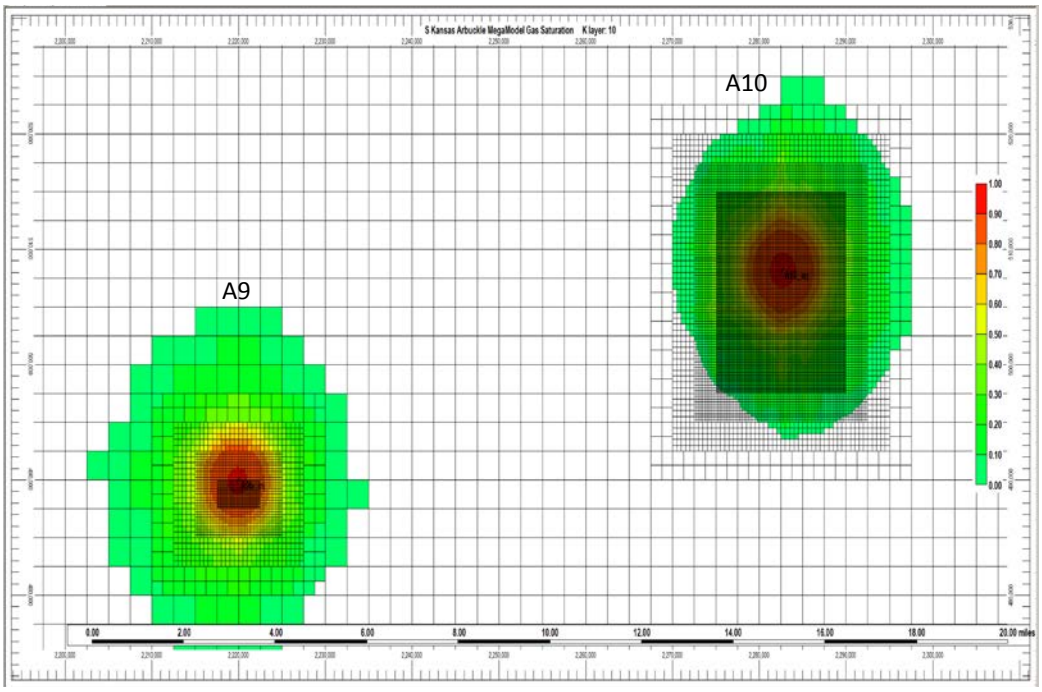

Figure 27. Size of CO2 plume conveyed by gas saturation for Areas 9 and 10.

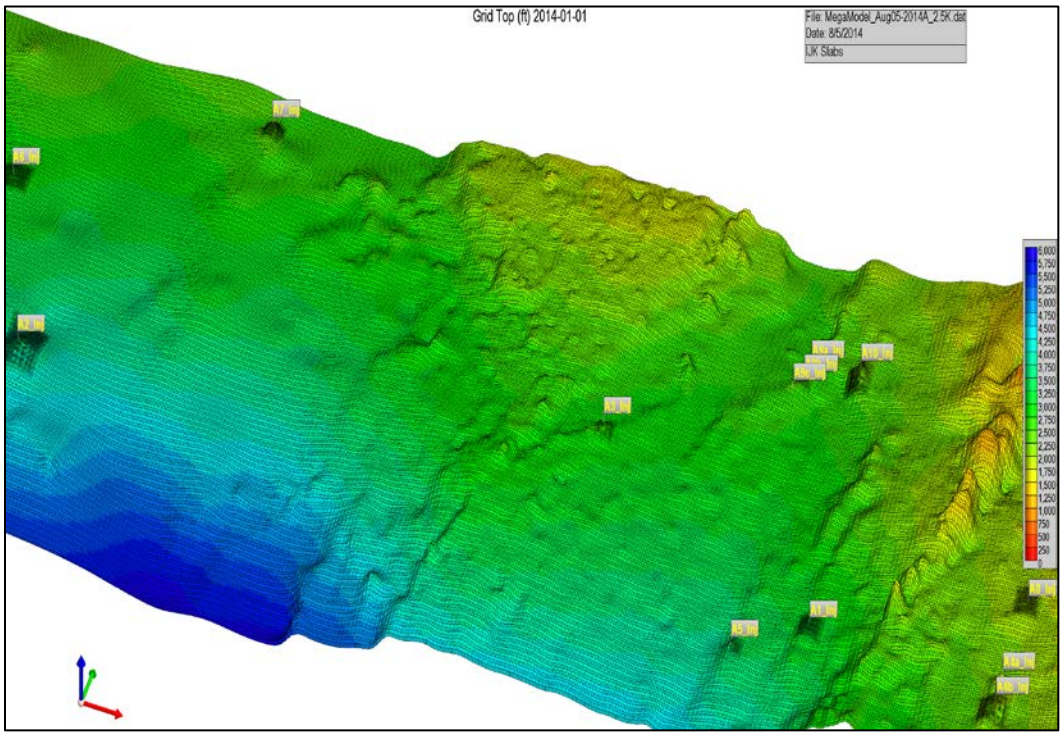

Figure 28. MegaModel showing local refinement with regional coarse grid of 2500 ft x 2500 ft used for the large simulation.

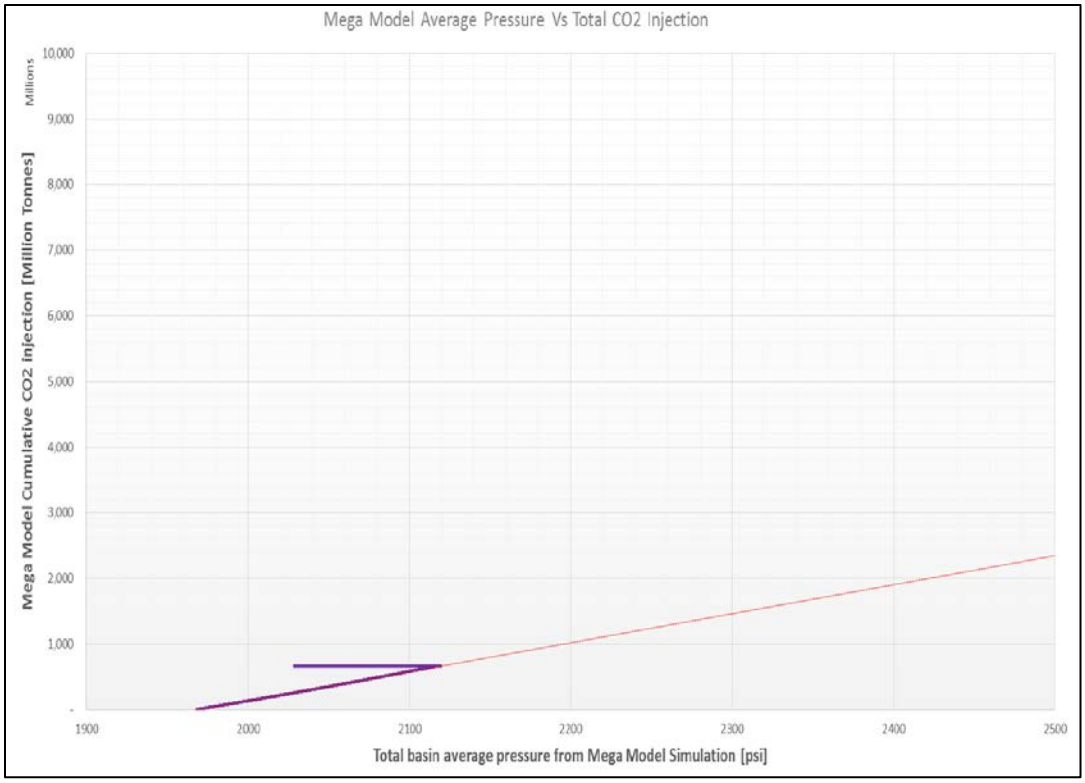

Figure 29. Simultaneous injection at wells per 200 mi2 and associated increase in total basin average pressure from MegaModel simulation (psi).

Task 13: Regional Source-Sink Relationships in approximately 17 Counties in South-Central Kansas

Subtask 13.1. Map major point CO_2 sources in Kansas
Subtask 13.2. Map major CO_2 sinks in Kansas

Task 14: Technology Transfer

Subtask 14.1. Build and maintain project website with interactive access to data and analyses via graphic display and analytical web tools
Subtask 14.2. Link project web-site to relevant DOE databases
Subtask 14.3 Submit project results to peer reviewed journals for publication

Task 15: Extend Regional Study of Ozark Plateau Aquifer System (OPAS) to the Western Border of Kansas – "Western Annex" and extend the type log database to include the whole state of Kansas to address fluid flow under commercial scale CO2 sequestration.

Subtask 15.1. Extend regional study by evaluating CO_2 sequestration potential in 5000 mi^2 area west of the existing 17+ county area and extend the type log database to the whole state of Kansas to address fluid flow under commercial scale CO_2 sequestration.

Subtask 15.2. Create consortium of companies

Subtask 15.3. Encourage development of business plan to sequester emitted CO_2

Task 16: Collect and Analyze Existing Data for Developing Regional Geomodel for Arbuckle Group Saline Aquifer in Western Annex

Subtask 16.1. Assemble, reprocess, and interpret existing 3D seismic and other data

Subtask 16.2. Analysis of KGS's gravity and magnetic data

Subtask 16.3. Remote sensing analysis

Task 17. Acquire (New) Data at a Select Chester/Morrow Field to Model CO2 sequestration Potential in the Western Annex

Subtask 17.1. Collect existing seismic, geologic, and engineering data – Chester/Morrow fields
Subtask 17.2. Select Chester/Morrow field to acquire new data

Subtask 17.3. Collect new multicomponent 3D seismic survey
Subtask 17.4. Process multi-component 3D seismic survey
Subtask 17.5. Develop initial geomodel for the selected Chester/Morrow field

Subtask 17.6. Select location for Test Borehole #3
Subtask 17.7. Complete permitting requirements for Test Borehole #3
Subtask 17.8. Drill, retrieve core, log, and run DST – Test Borehole #3
Subtask 17.9. Openhole Wireline Logging – Test Borehole #3
Subtask 17.10. Wellbore Completion – Test Borehole #3
Subtask 17.11. Analyze wireline log - Test Borehole #3
Subtask 17.12. Test and sample fluids (water) from select intervals – Test Borehole #3
Subtask 17.13. Analyze Arbuckle core from Test Borehole #3
Subtask 17.14. Analyze Chester/Morrow core from Test Borehole #3
Subtask 17.15. PVT analysis of oil and water from Chester/Morrow oil reservoir
Subtask 17.16. Analyze water samples from Test Borehole #3

Task 18: Update Geomodels and Conduct Simulation Studies - Evaluate CO_2 Sequestration Potential in Arbuckle Group Saline Aquifer and by CO_2-EOR in Select Chester/Morrow Field in the Western Annex

Subtask 18.1. Update geomodels of the Chester/Morrow sands and Arbuckle Group saline aquifer in selected field

Subtask 18.2. Optimize geomodel for simulation - Flow-unit identification, fracture characterization, and upscaling

Update on Cutter seismic interpretation (draft figures contributed by Clyde Redger)

Converted shear and P-wave in Upper Morrow oil reservoir were analyzed by Clyde Redger as part of this M.S. KU thesis. He also examined the converted wave 3D seismic at Cutter Field to examine the ability to map flow units in the Arbuckle and to examine the use of impedance to map porosity of the flow units. Finally, the fast and slow shear velocities were examined to determine if there is a directional anisotropy. A series of figures provide a perspective of this work that is currently bring incorporated in Mr. Redger's thesis. **Figures 30-47** are focused on the first part of the study dealing with Upper Morrow Sandstone oil reservoir characterization.

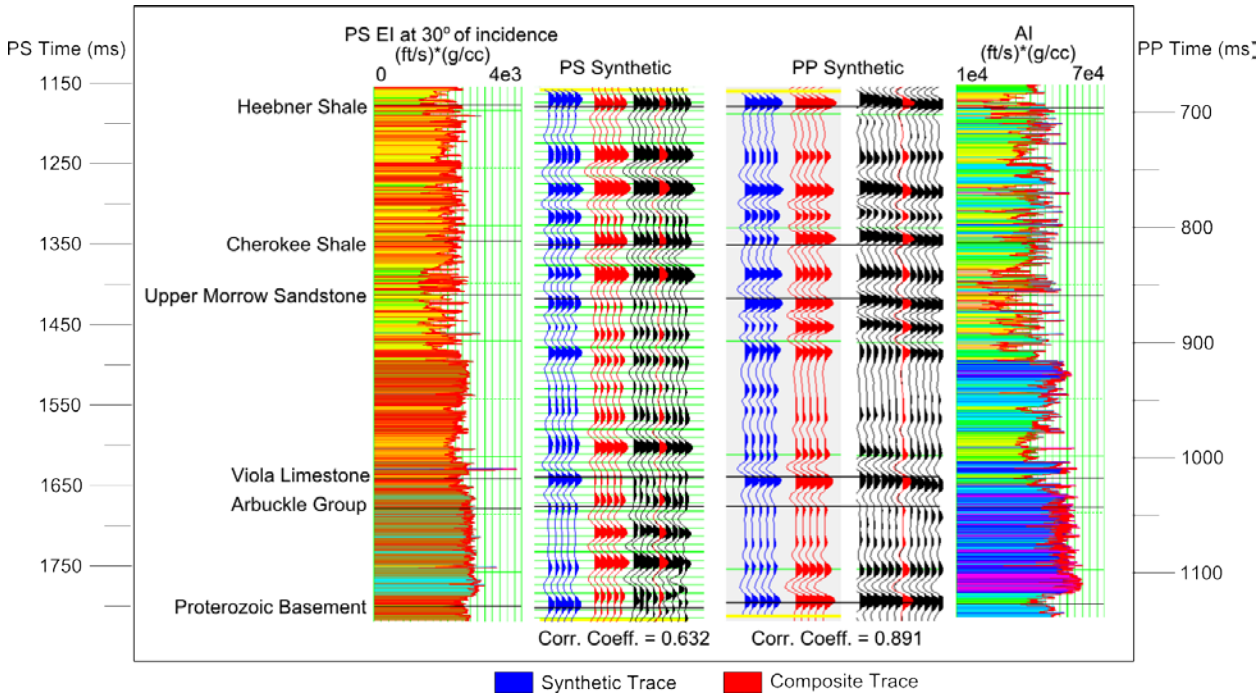

Figure 30. Synthetic seismogram for both converted shear and compression wave based on the Cutter KGS #1 spectral (Halliburton) sonic log compared to the composite trace extracted from the 3D seismic volume at the KGS #1 well location. There is a very good match for both the p- and s-wave data. Similarly, the acoustic impedance that are shown on opposite ends of the figure (left = log), (right – seismic volume) are very similar, again attesting to the quality of the correlations.

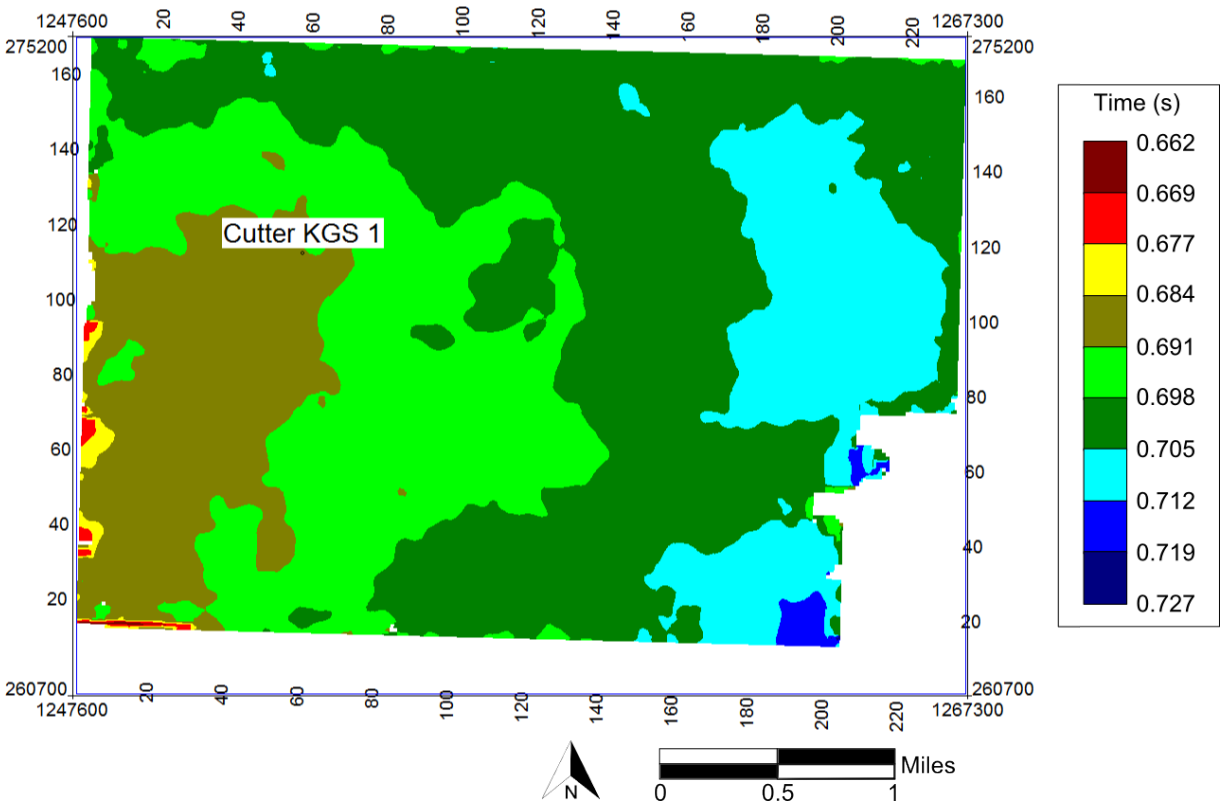

Figure 31. Time surface of the prominent marker, the Heebner Shale, well above the main reservoir, upper Morrow sandstone of Cutter Field suggesting that the location of the west side where the Cutter KGS #1 was drilled is higher.

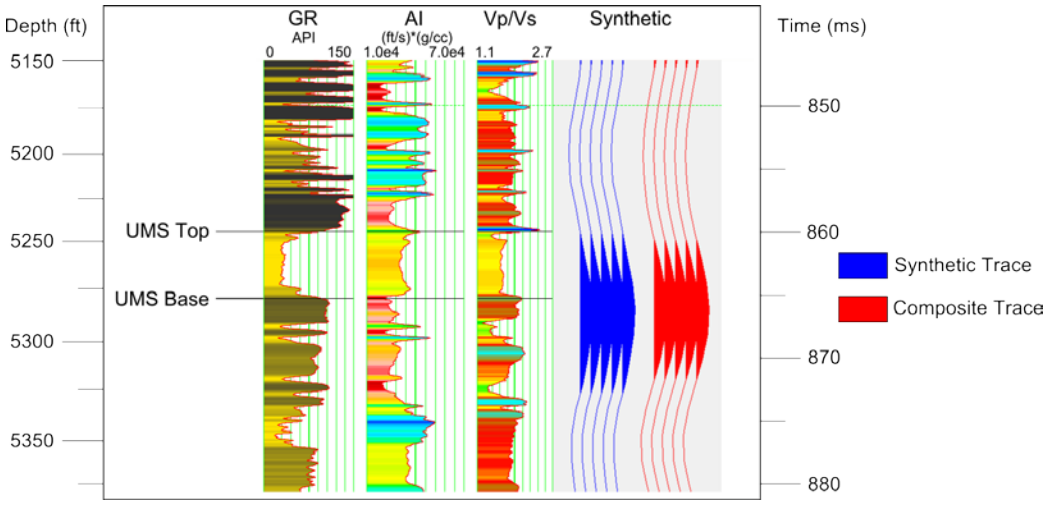

Figure 32. The closeup of the acoustic impedance Vp/Vs ratio and the synthetic waveform illustrate the resolution of the sandstone interval compared to the seismic data. Again, there is close correspondence of the log based and composite seismic trace attesting to the quality of the data.

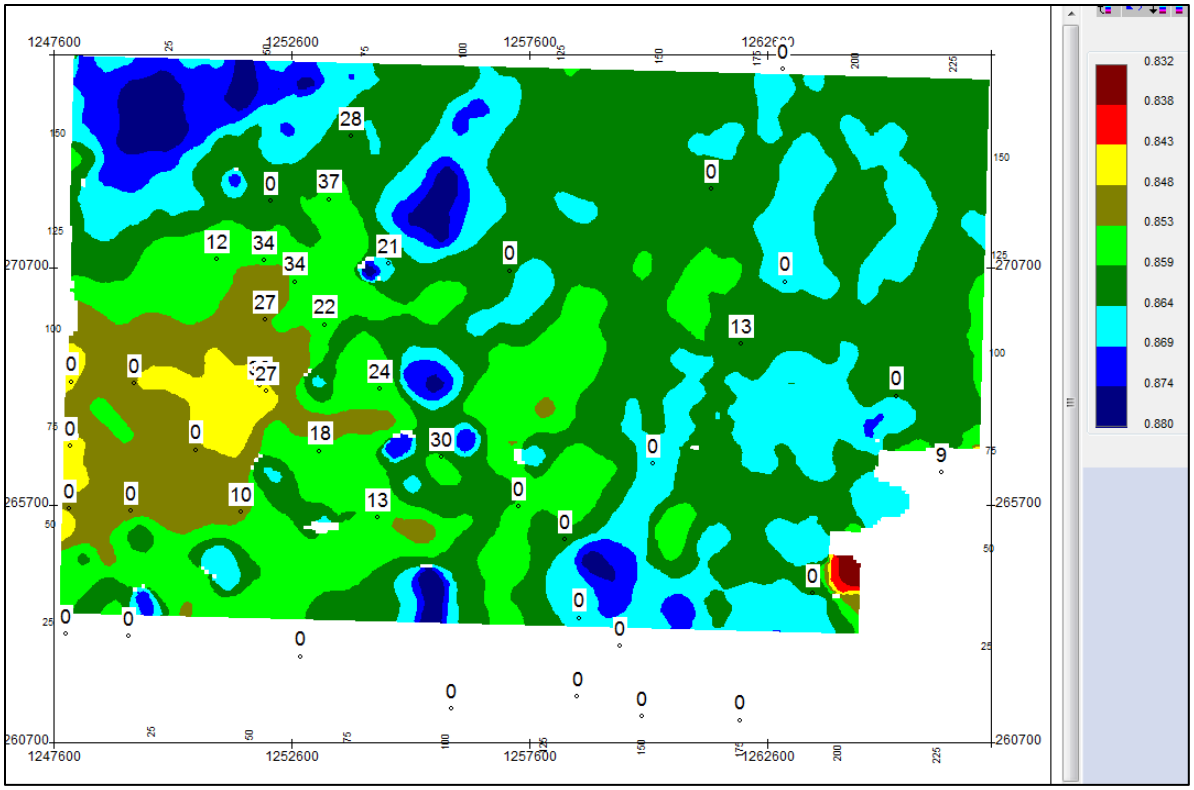

Figure 33. Upper Morrow sandstone (UMS) time structure with labels of the sand thickness from well log data.

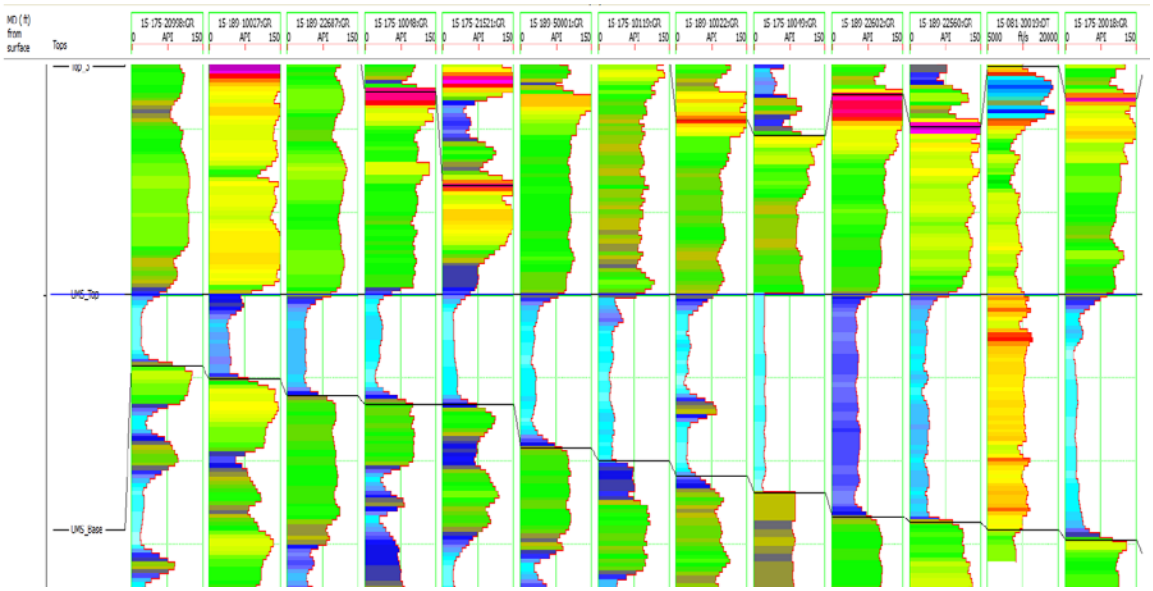

Figure 34. UMS Well Correlations using natural gamma ray from well logs, 17 wells.

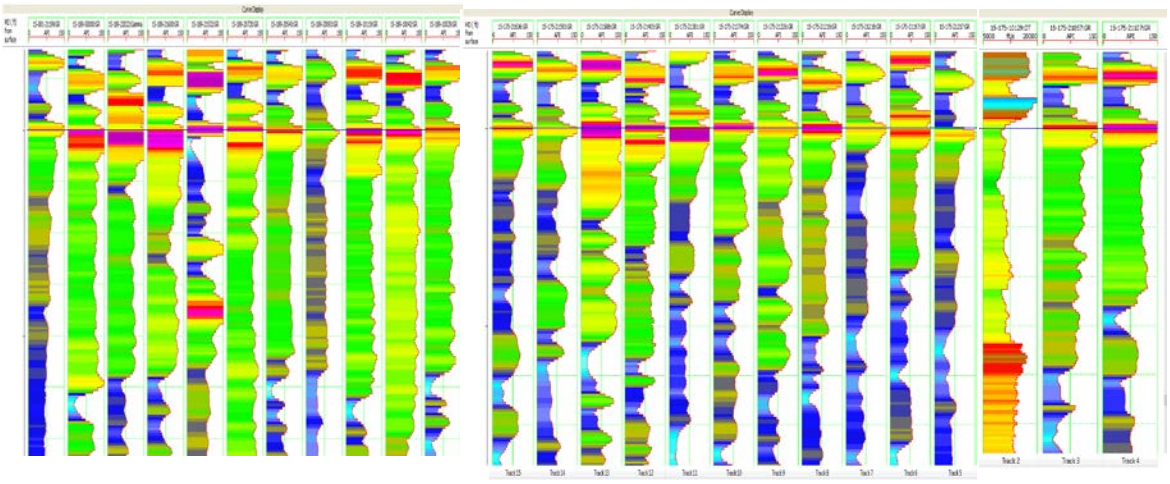

Figure 35. UMS Absent as indicated by gamma ray from well logs, 25 wells.

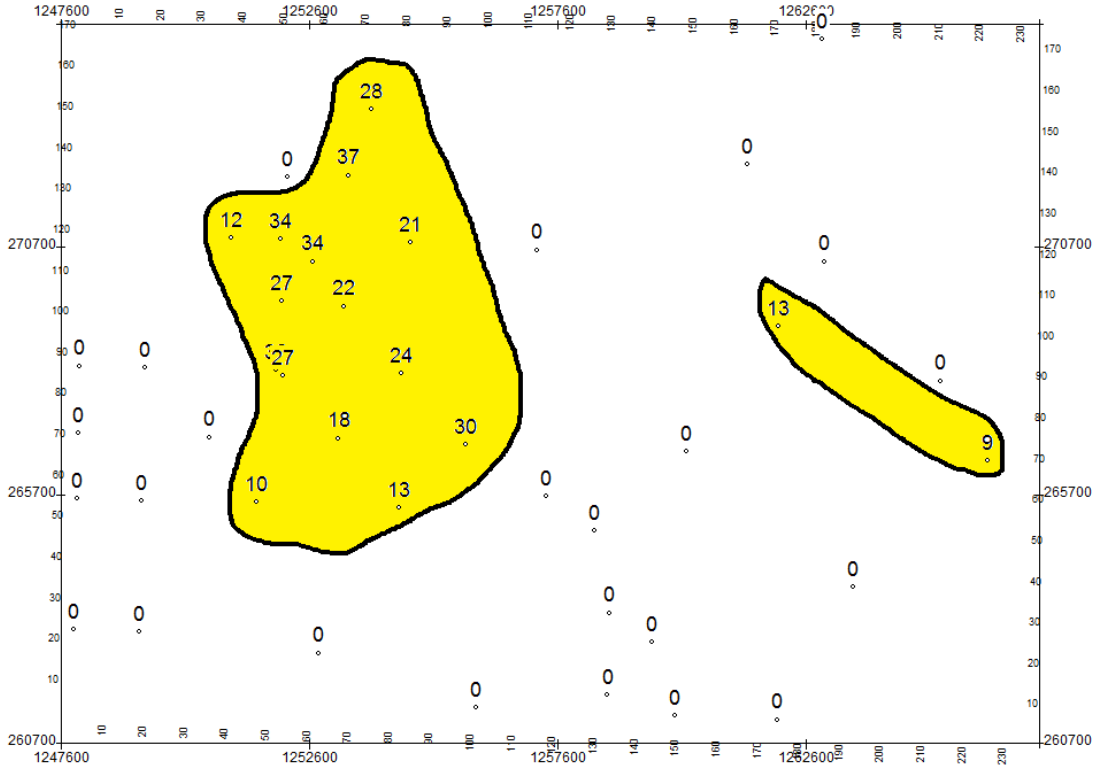

Figure 36. Thickness of UMS based on well logs.

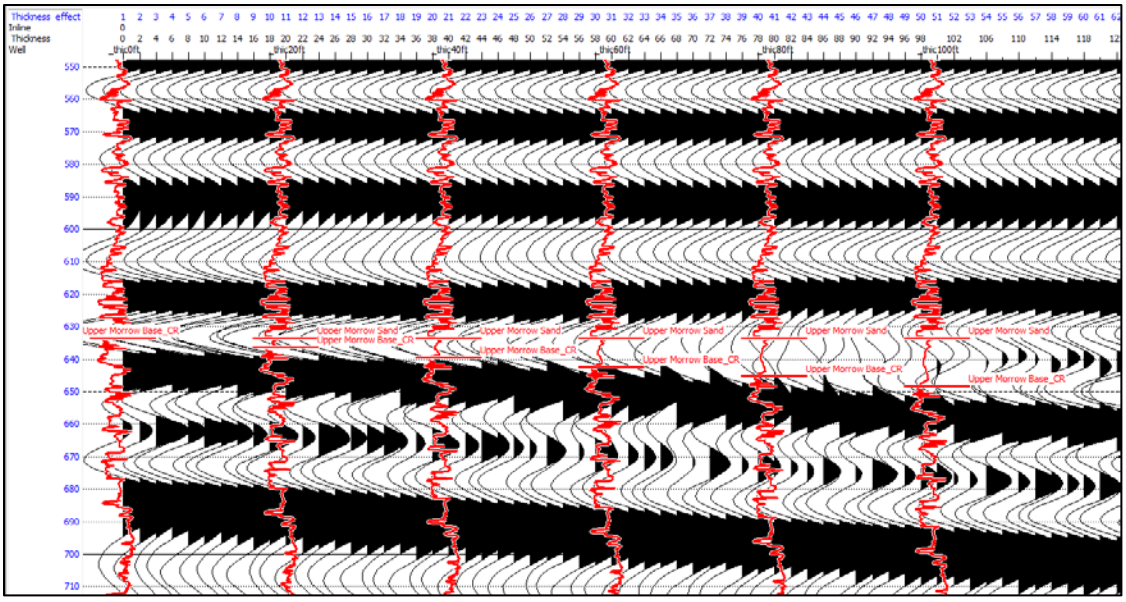

Figure 37. Hampson-Russell software solution of wedge model showing reflection response with increasing thickness of UMS.

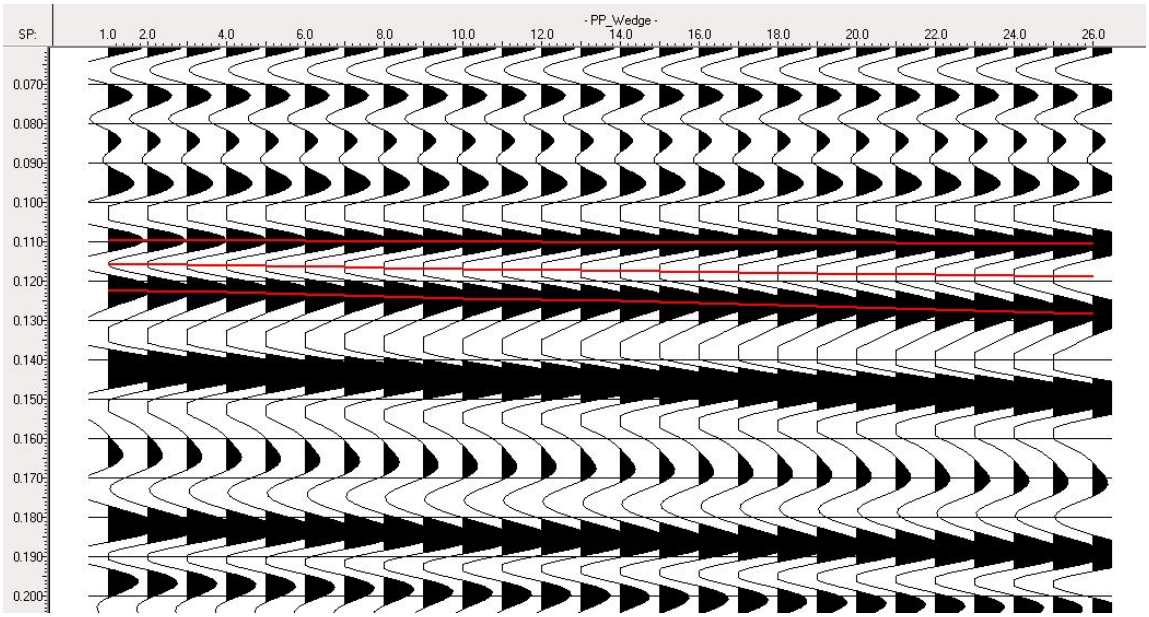

Figure 38. Observed wedge model with actual seismic traces. Changes in the amplitude are much more subdued compared to the model of Figure 37.

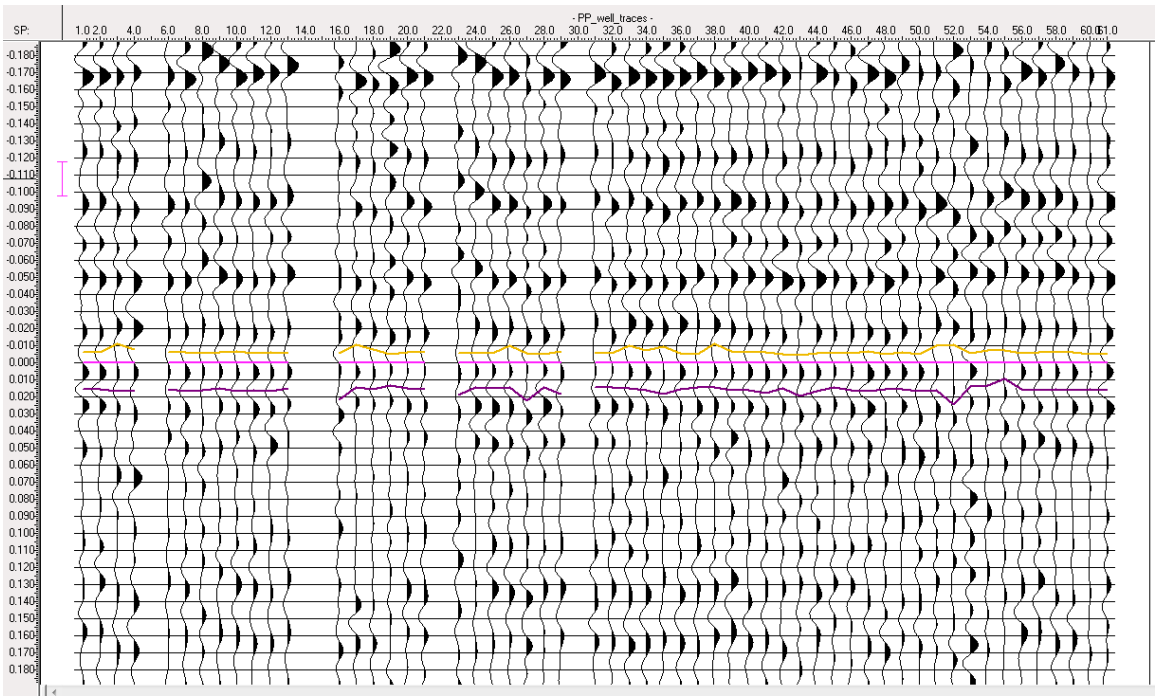

Figure 39. PP Traces extracted from well locations used for instantaneous frequency analysis.

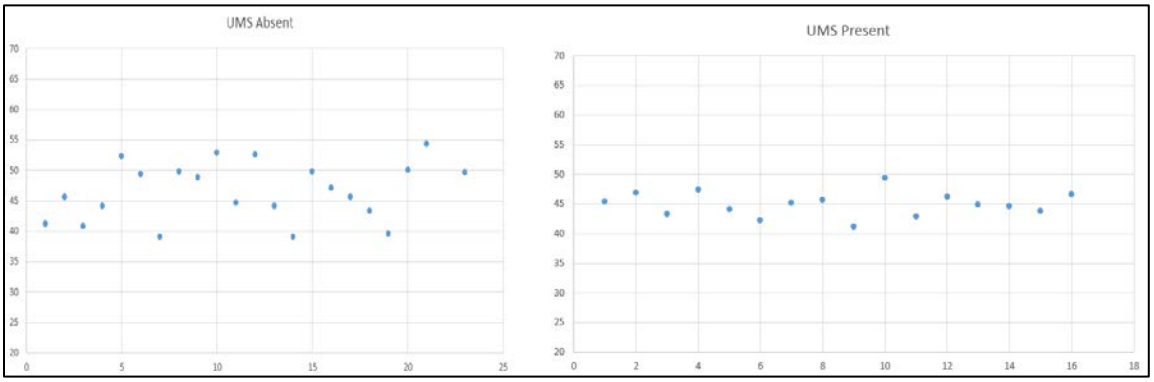

Figure 40. Instantaneous frequency values are more consistent in the presence of sand, but the mean value is essentially the same.

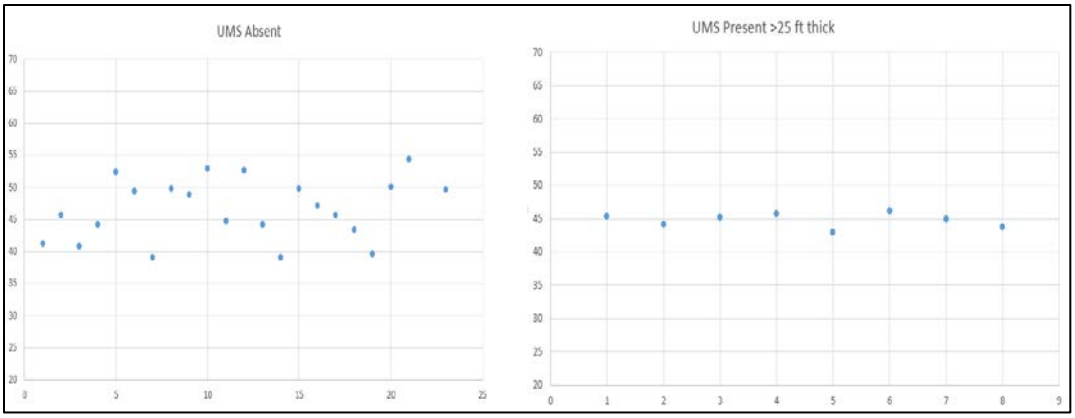

Figure 41. A comparison of instantaneous frequency at wells without sand are compared with wells that have more than 25 ft of sand. The latter has the least variability of all, which is expected.

	UMS Absent	UMS All Wells	UMS >25 ft
Average	46.5	45.0	44.8
Median	46.4	45.1	45.1
STDEV	4.8	2.1	1.1

Table 2. Instantaneous Frequency summary showing the statistics of wells with no sand, all wells with sand, and wells with sand thicker than 25 ft. Wells with the thickest sand have a lower average and median value and the standard deviation is lowest.

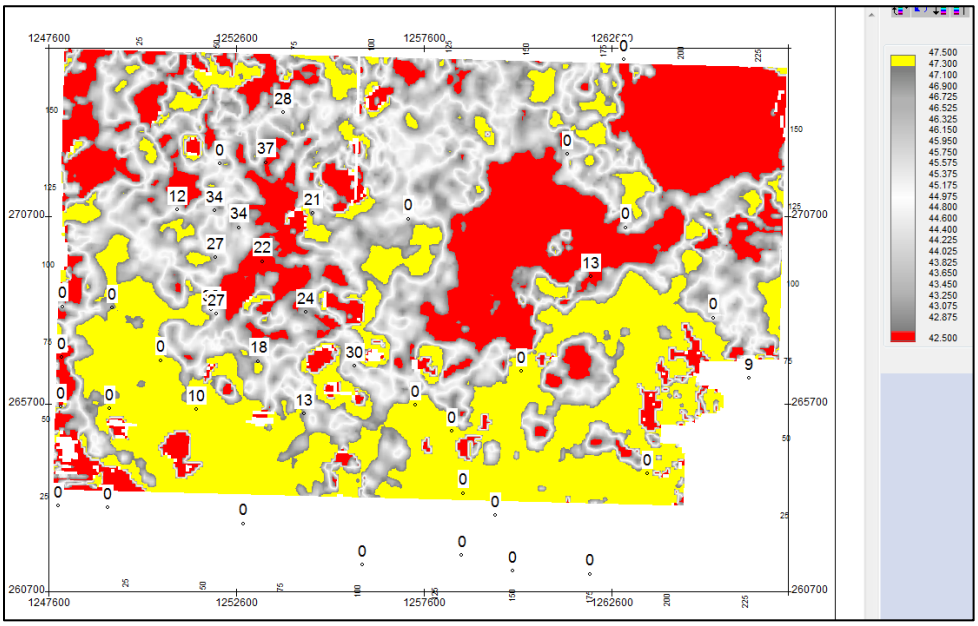

Figure 42. Map of instantaneous frequency indicating lower frequency in areas of thicker sand.

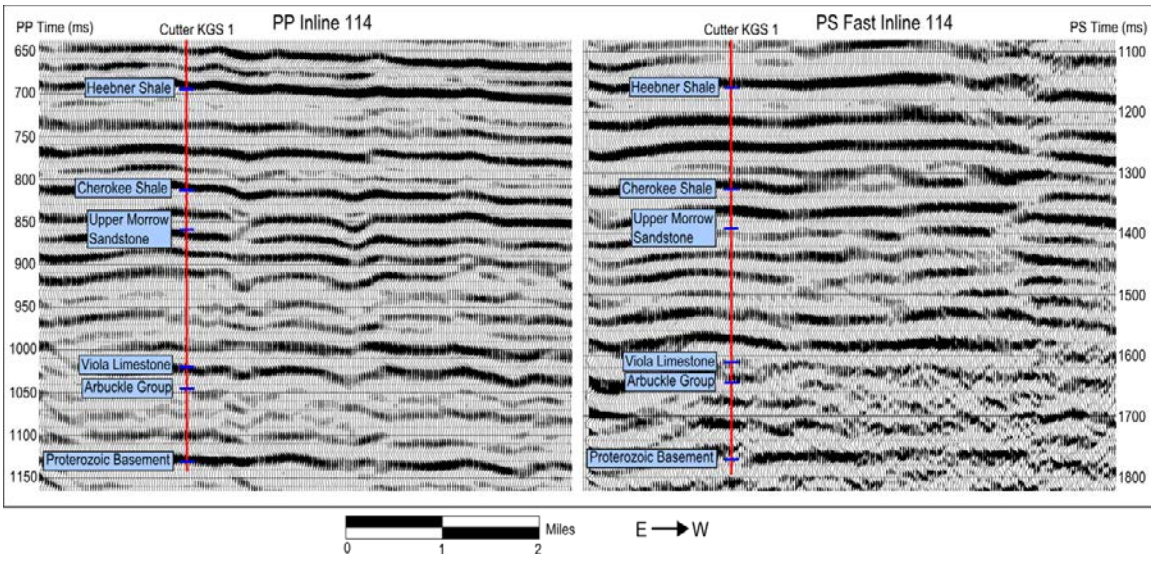

Figure 43. PP (left) and PSV (right) seismic correlation comparing data quality. Both have similar frequency content/resolution. The Viola section and below are noisier in the shear wave domain. Both PP and PSV show a good basement reflector.

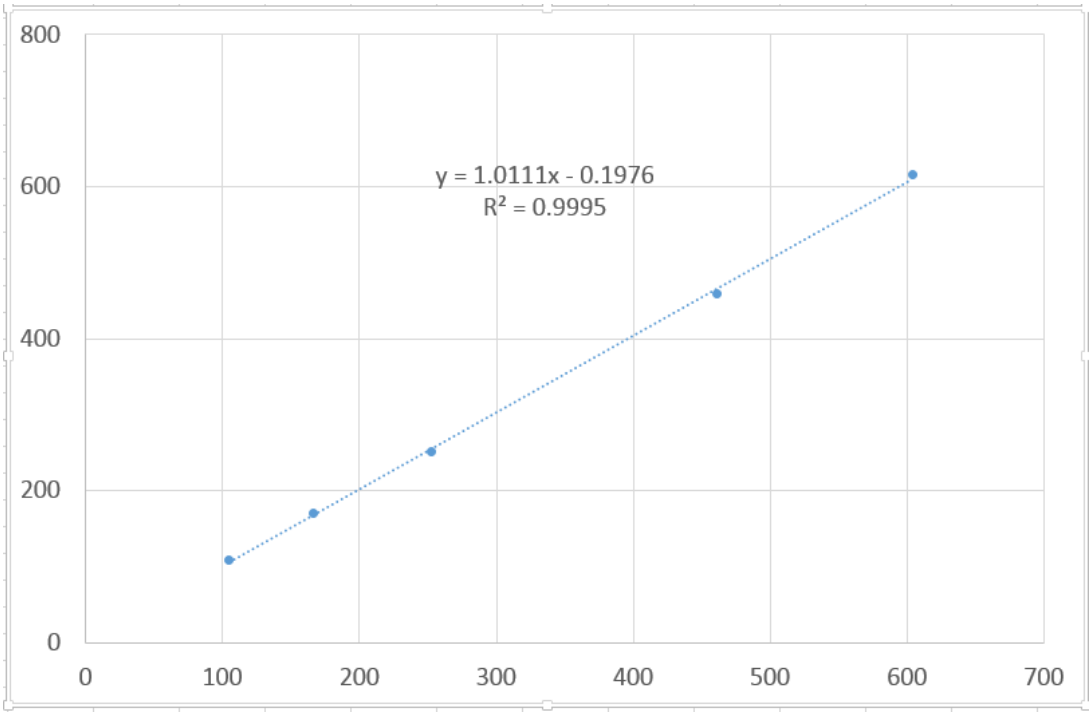

Figure 44. Observed vs estimated TWT P-SV travel times plotted against each other show and excellent correlation.

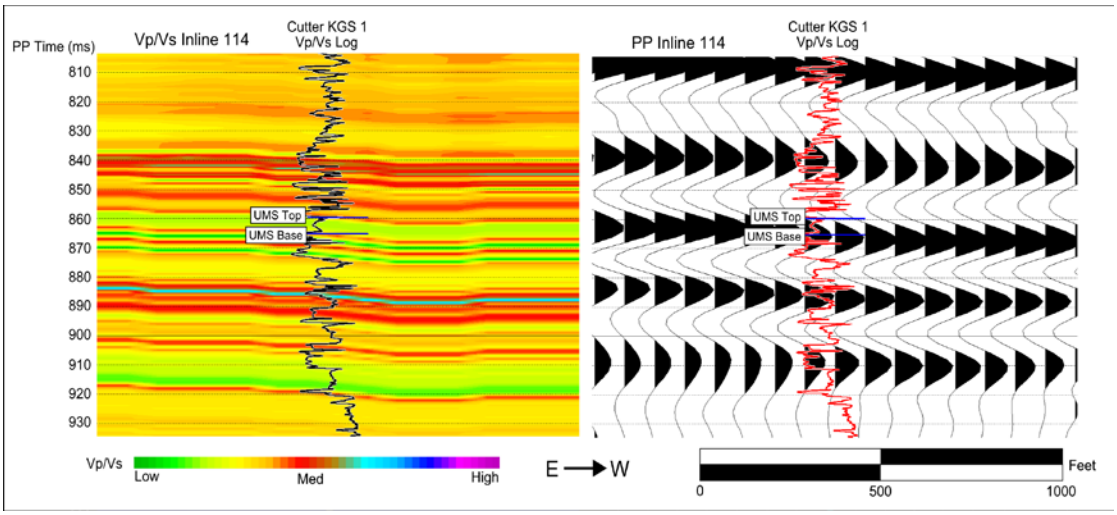

Figure 45. Vp/Vs along inline 114 profile closely compares with the Vp/Vs from the well log (left). The UMS has a low Vs/Vp ratio. On the right, the Vp/Vs log for the Cutter KGS #1 compared to the PP profile that passes through the well. The Vp/Vs profile is more highly resolved.

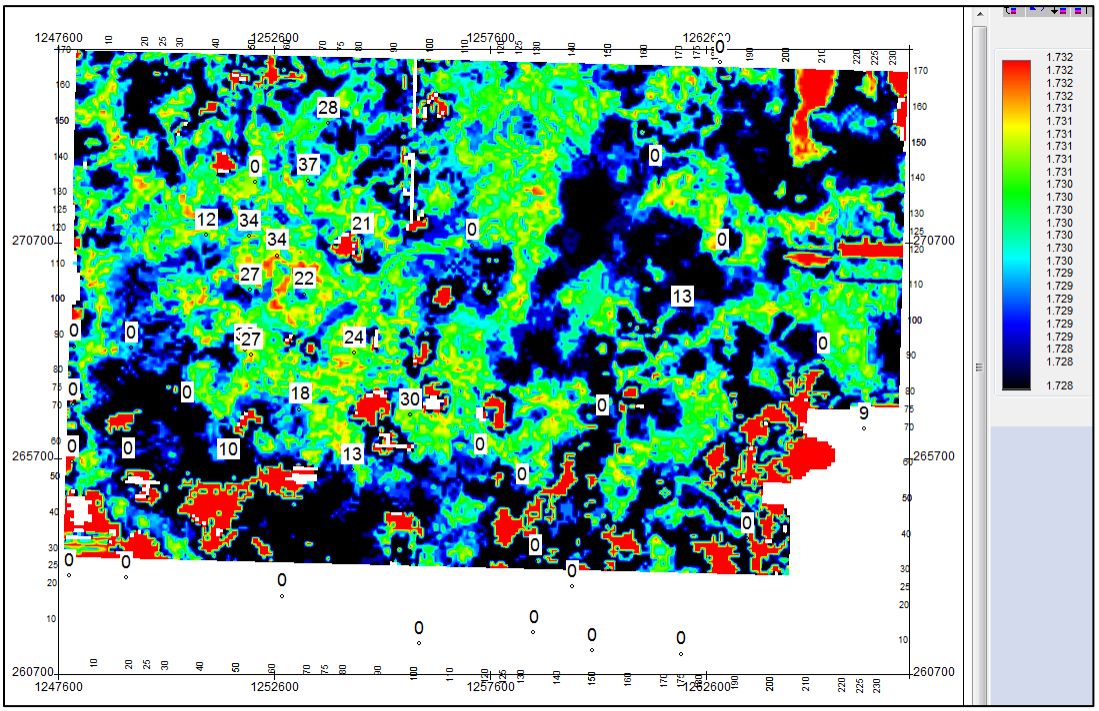

Figure 46. A map of the Vp/Vs Ratio has intermediate to higher values (greens & yellows) where the UMS is thicker. This appears to be counter to what is seen in the profiles.

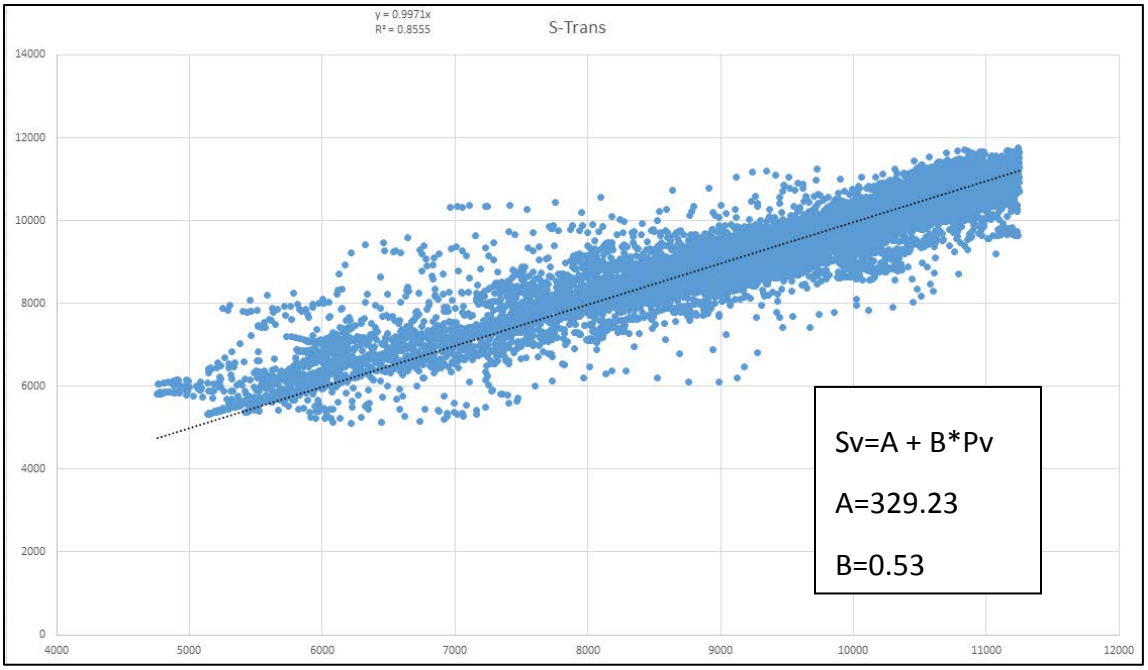

Figure 47. Castagna's Equation for Cutter Field plots the p-wave vs shear wave velocity. The fit of the curve is good and is indicative of a sandstone-shale siliciclastic system.

Remaining work with the Vs/Vp ratio includes:

- Calculate S-wave transforms
- Load additional wells into joint inversion workflow
- Recompute Vp/Vs volume and run joint inversion
- Acoustic Impedance
- Shear Impedance
- Density

The goal will be to improve the resolution of the sandstone that is not distinguished in a conventional p-wave seismic survey. The results to date are very encouraging.

Seismic Inversion, S- and P-Wave Characterization of the Viola-Arbuckle Deep Saline Aquifer beneath Cutter Field – Illustrations provided by Clyde Redger and commentary by L. Watney

The second part of the study conducted by Redger is to examine the Arbuckle saline aquifer to evaluate the structural features, whether flow units can be differentiated and characterized, and to evaluate general anomalies and heterogeneity in this interval. **Figures 48-67** are focused on the seismic inversion, and shear and p-wave velocity and amplitude variation as a means to characterize the heterogeneity of the deep saline aquifer interval.

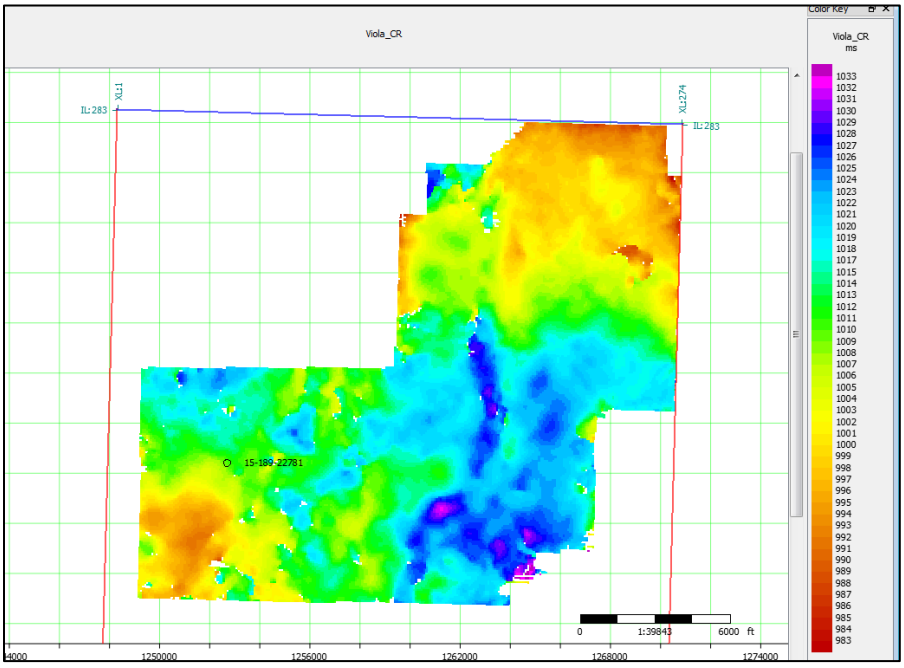

Figure 48. Viola Time Structure utilizes the best deep seismic reflector that is closest to the top of the Arbuckle. Rather than one high to the west as is the case with the shallower strata, the high has shifted to the southwest. This seismic volume shows a merged P-wave surveys that include the converted wave survey at Cutter. The location of the Cutter KGS #1 is shown to aid comparison.

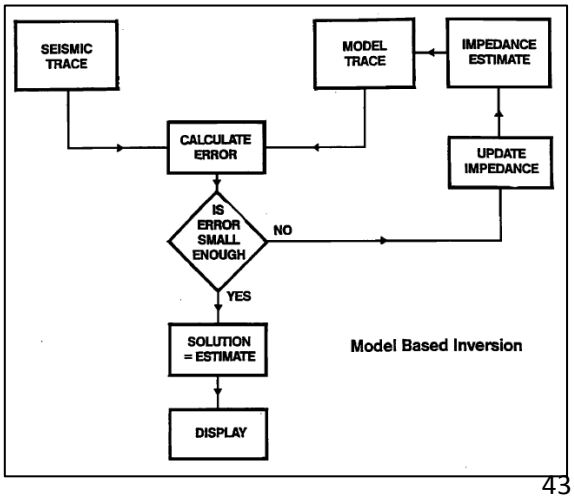

Figure 49. Seismic inversion is a means to convert the seismic reflection data to rock-property description and in this case follows a methodology outlines by Russell (1988).

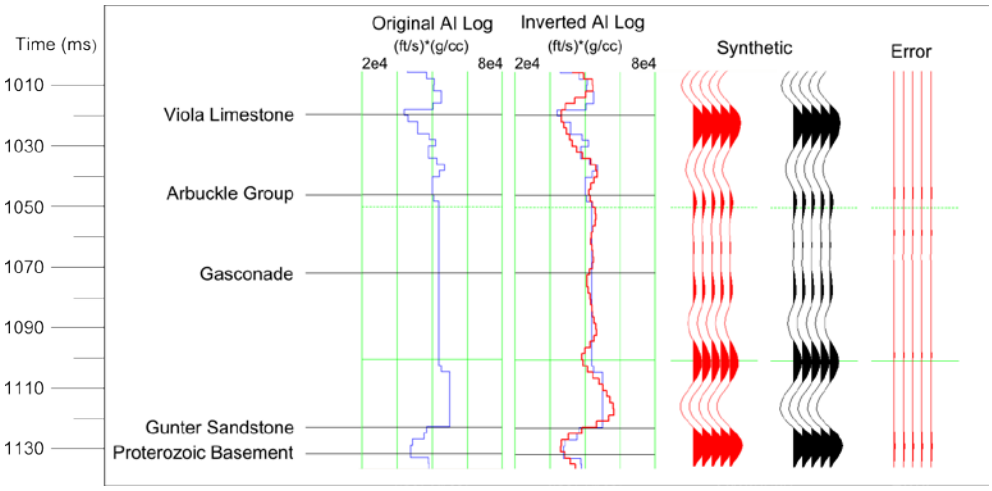

Figure 50. The seismic inversion is illustrated here with the original well log with computed acoustic impedance (left) alongside in inverted seismic trace (right in red). The fit is excellent suggestion the seismic is a good candidate for this inversion procedure.

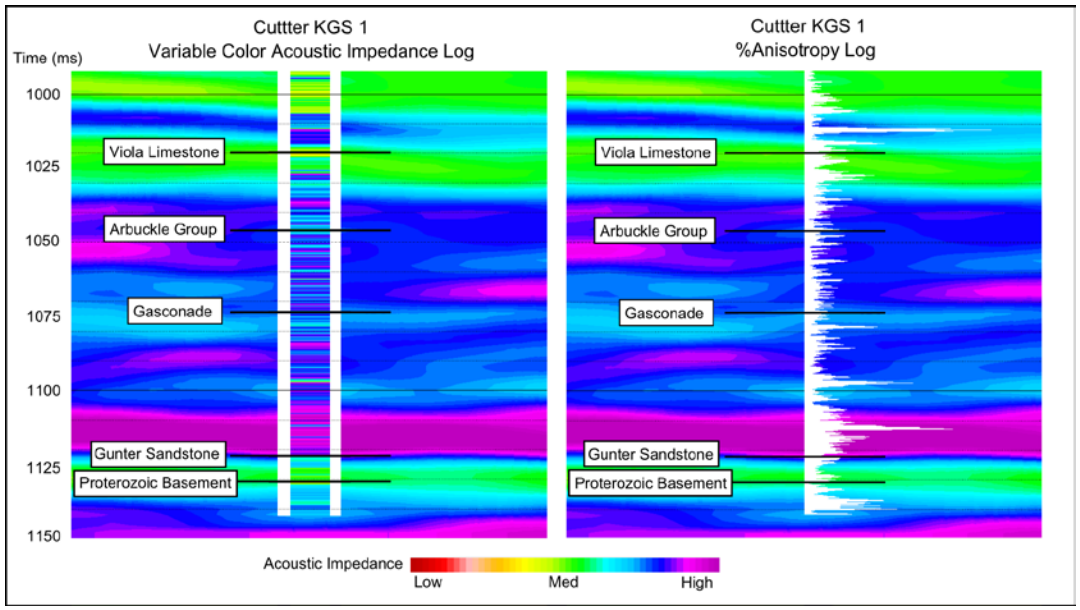

Figure 51. The preliminary inversion results are shown with acoustic impedance profile compared with the acoustic impedance log (left) and the percent anisotropy (right). Notice the close correlation of the log and seismic impedance and the lateral variability of the impedance. While the Viola Limestone that overlies the Arbuckle is uniformity medium impedance – a shaly wackestone, the interior of the Arbuckle suggests variable pods of high and low impedance. The top of the Gasconade Dolomite is regionally correlated and appears to represent a widespread subaerial unconformity overlain sharply by a shaly dolomite representing inundation of the carbonate platform on which the Arbuckle was deposited. The Cutter KGS #1 cut a core through the interval and found an interval of vuggy and brecciated dolomite. This appears to be matched by an interval of lower impedance (lighter blue).

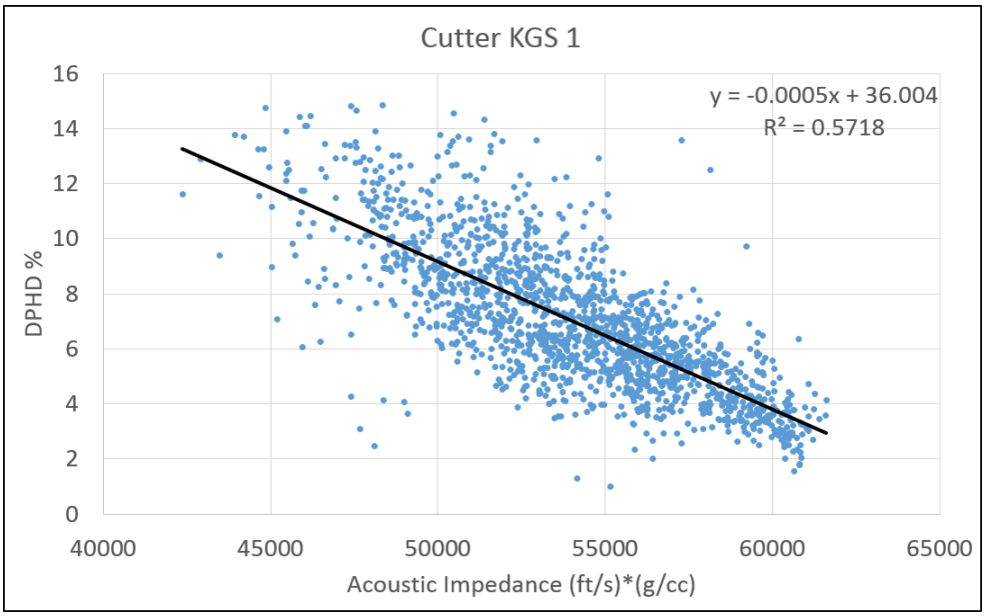

Figure 52. A crossplot of the acoustic impedance vs. density porosity of the Arbuckle interval shows a rather pore fit (R2 of 0.5718). This may reflect the range in the type of pore space in the dolomitic carbonate, from a grainstone with interparticle porosity, vuggy pores in part connected and others non-touching vugs, and also brecciated intervals. To make a better fit would require the distinction between these pore types.

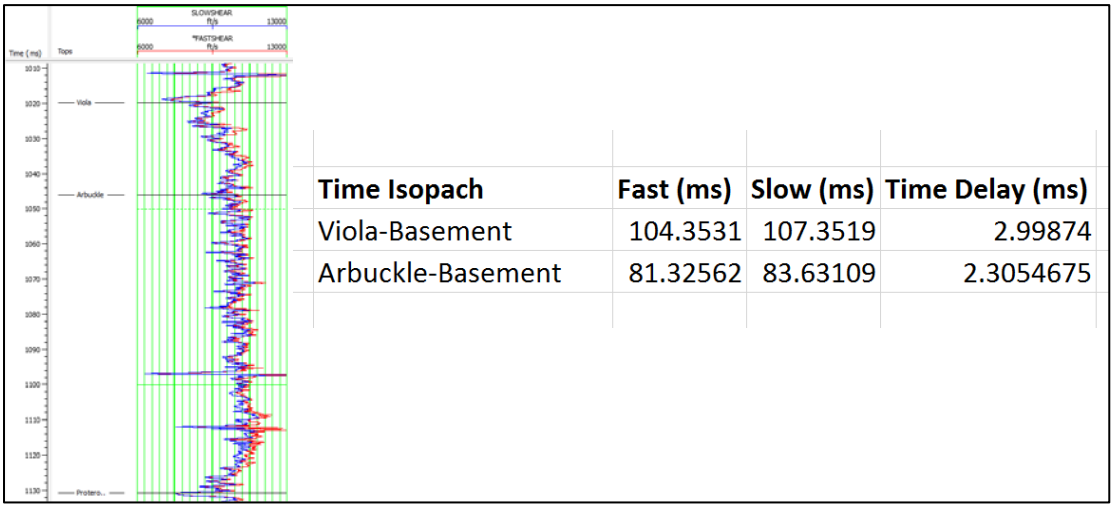

Time Isopach	Fast (ms)	Slow (ms)	Time Delay (ms)
Viola-Basement	104.3531	107.3519	2.99874
Arbuckle-Basement	81.32562	83.63109	2.3054675

Figure 53. Time isopachs between Viola and basement and Arbuckle and basement for fast and slow shear wave velocities are compared in this figure. The greater delay is includes the Viola suggesting greater anisotropy in the Viola than in the Arbuckle to basement interval. This is a rather counterintuitive compared to the impedance profiles, but it can be seen here that magnitude of shear wave variation in the Viola, albeit thinner interval, is considerably greater in the uppermost part of the Viola. The top of the Viola is another major unconformity and is associated with a thick chert breccia.

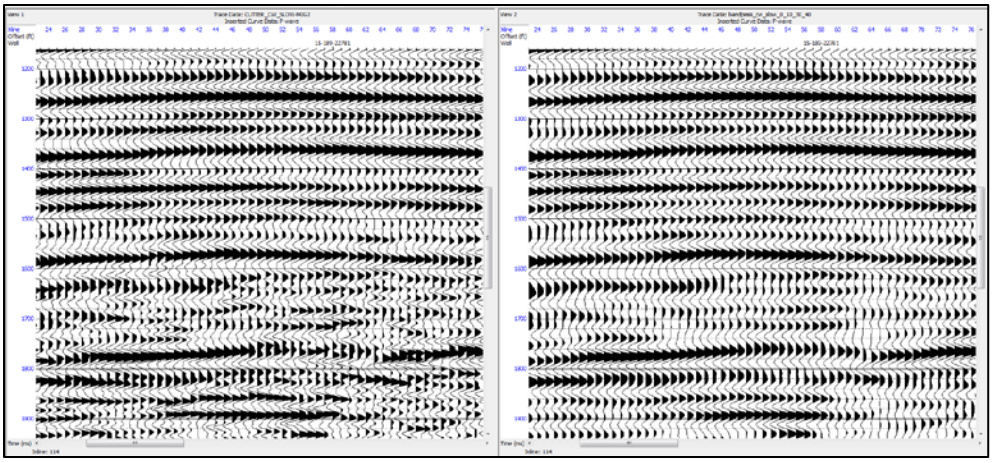

Figure 54. The slow shear amplitude profile (left) is compared with the P-wave amplitude and it is clear that the lower half in the shear wave domain is much more laterally discontinuous.

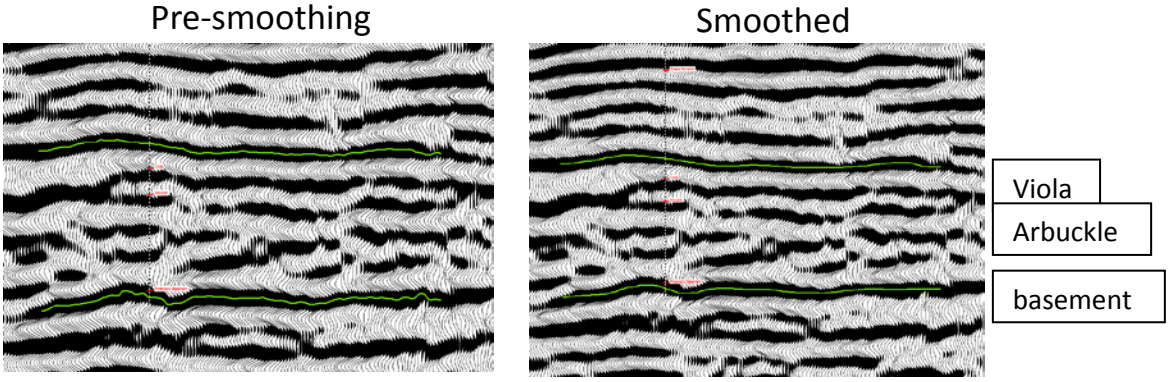

Figure 55. Seismic discontinuities are persistent even with smoothing including apparent dipping reflectors in the near the base of the Arbuckle. Also, the top of Arbuckle appears to be truncated along the base of the Viola Limestone/Simpson Sandstone with corresponding thickening of the Viola interval.

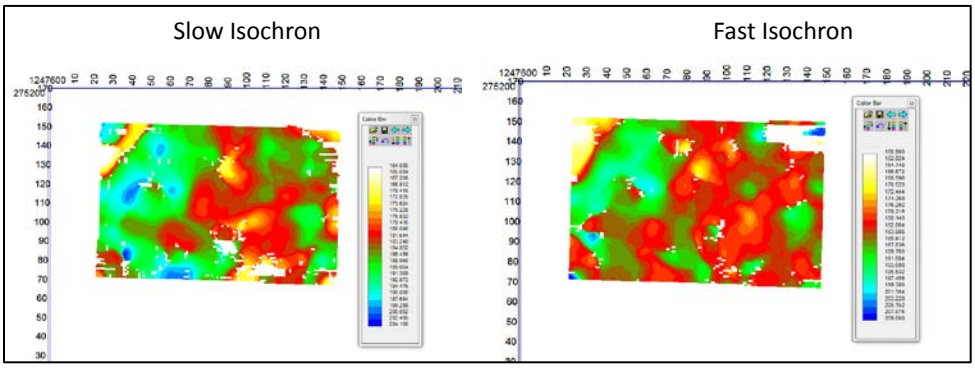

Figure 56. Both slow and fast isochrons along a surface in the Arbuckle show similar lateral variability.

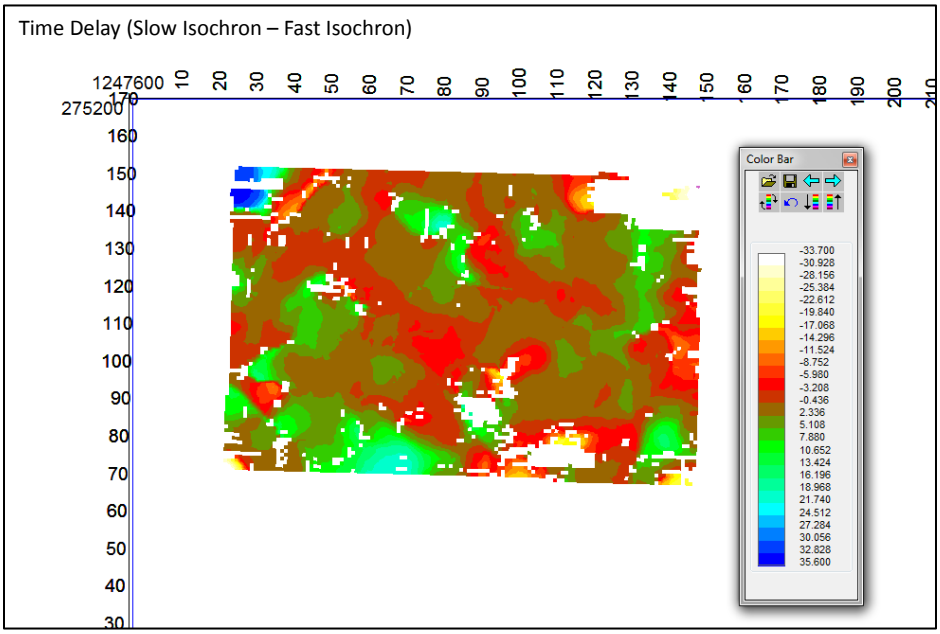

Figure 57. The difference between the slow and fast isochon is small and is questionable as to the significance of the pattern relative to the systematic noise of the interpretation. Yet, there appears to be NE- and NW-trends to the apparent anisotropy.

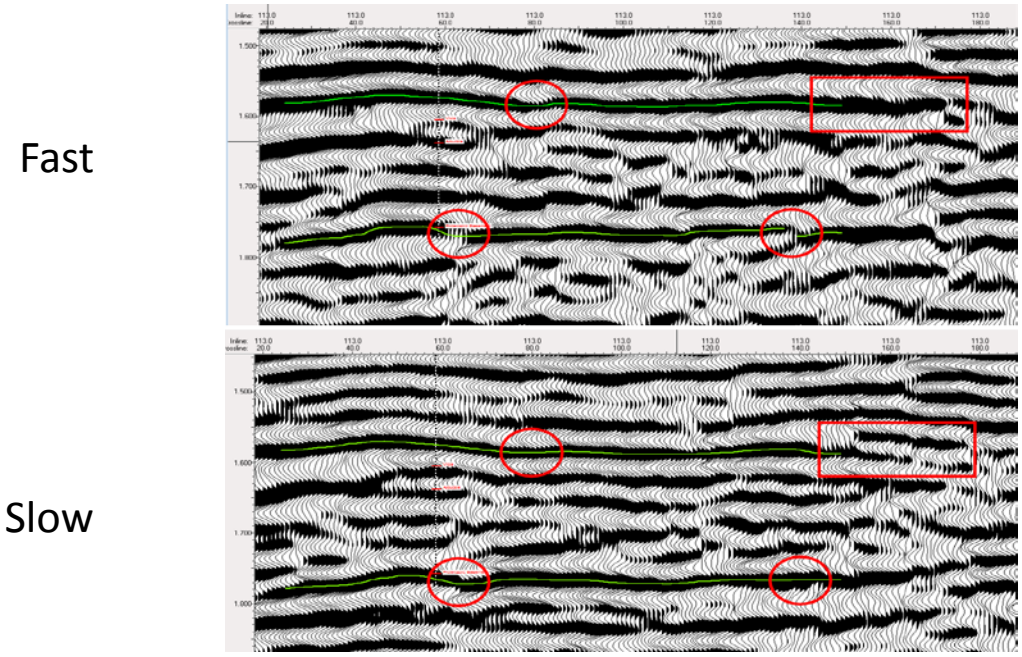

Figure 58. The differences between the fast (top) and slow (bottom) shear wave amplitude sections each show differences in the continuity of reflectors as highlighted in red. The east side of the profile has the most discontinuous reflectors, which is most marked in the slow shear wave domain.

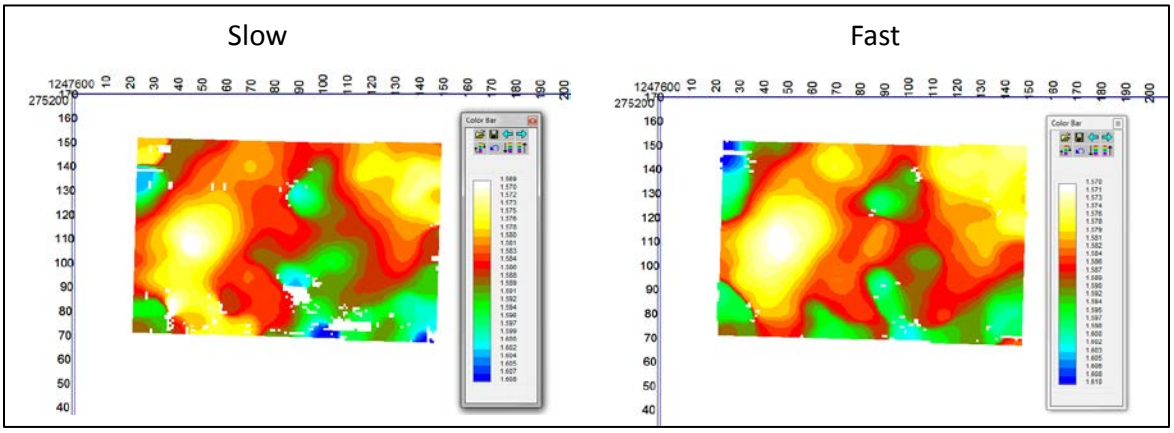

Figure 59. The slow (left) and fast (right) shear wave velocities along the top of the Viola, the prominent chert breccia below a major regional unconformity show similar low (warmer colors) and higher velocities. The pattern is roughly rectilinear with a NE- and NW-trend to the pattern. The lower velocities may reflect the thicker more porous chert at the unconformity.

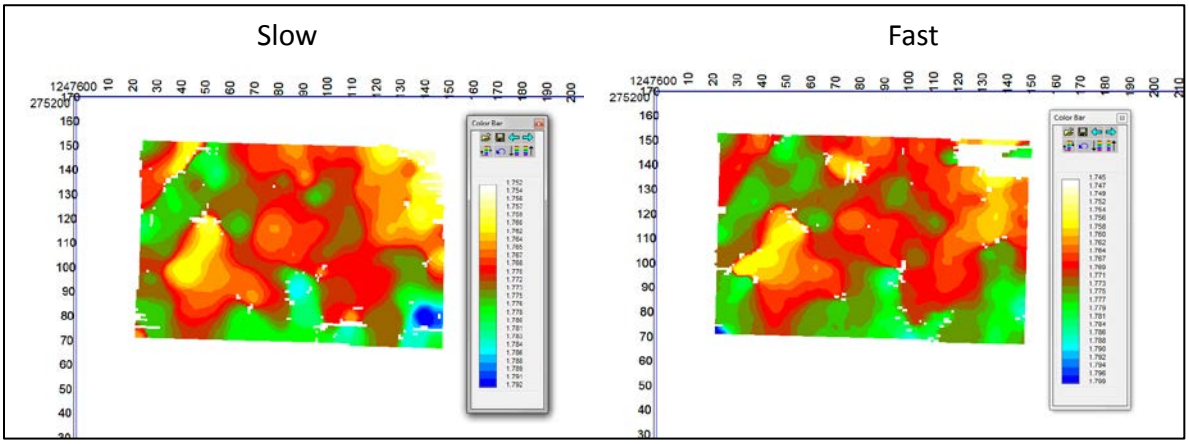

Figure 60. Maps are identical to Figure 59, but the interval is the top of the Proterozoic basement. The weathered surface on the granite may have variable residuum to account for the patterns. The grain again is NE- and NW-pattern.

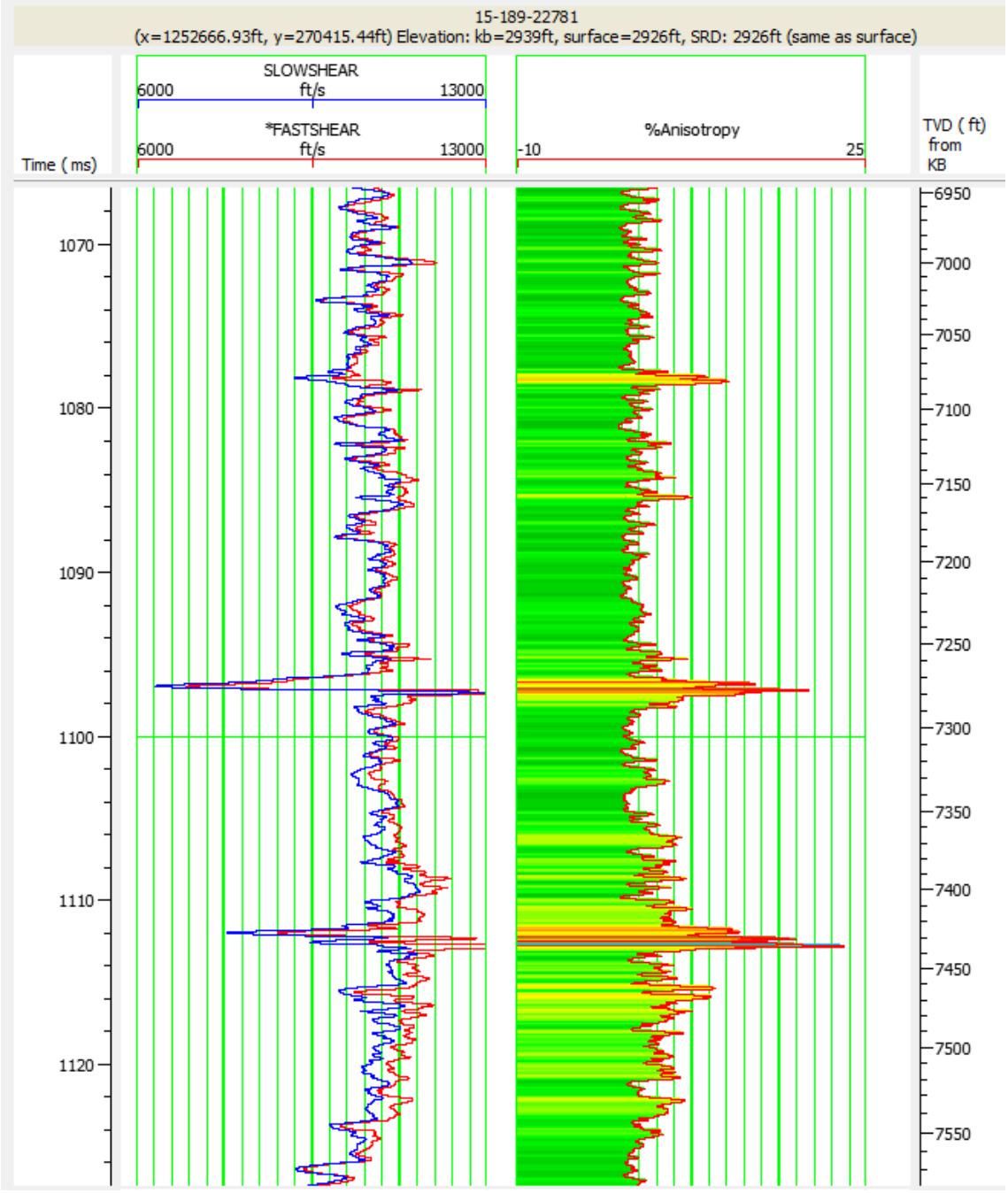

Figure 61. Distinct anomalous intervals are noted in the fast and slow shear wave velocities in the Arbuckle. The % anisotropy from the spectral sonic corresponds closely to lower shear wave velocities. The anomaly at 7425-35 ft is an interval with large vugs as noted in the microresistivity imaging log in Figure 62.

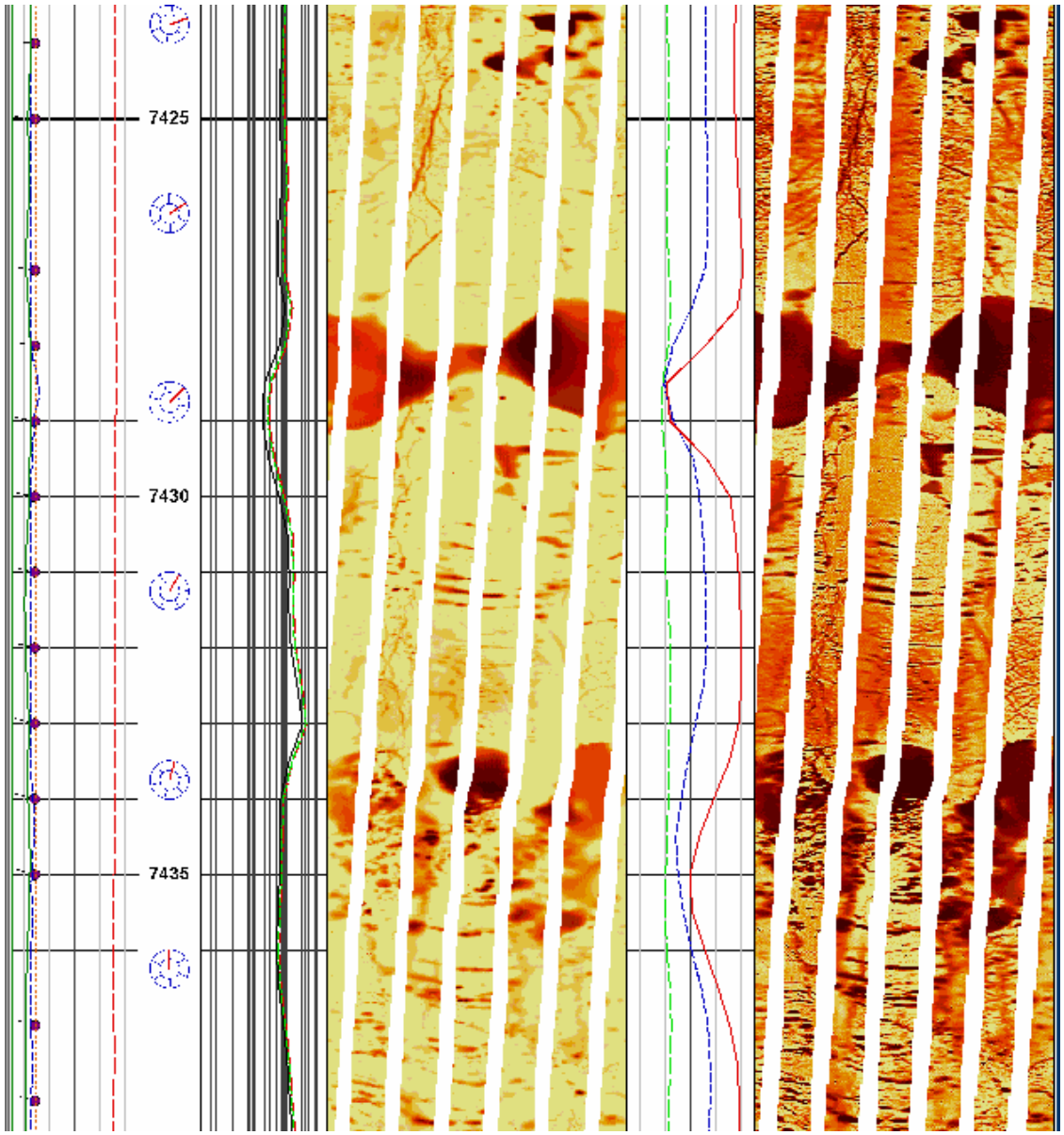

Figure 62. The microresistivity imaging log at 7425-35 ft displays an interval with large and small vugs and some small fractures.

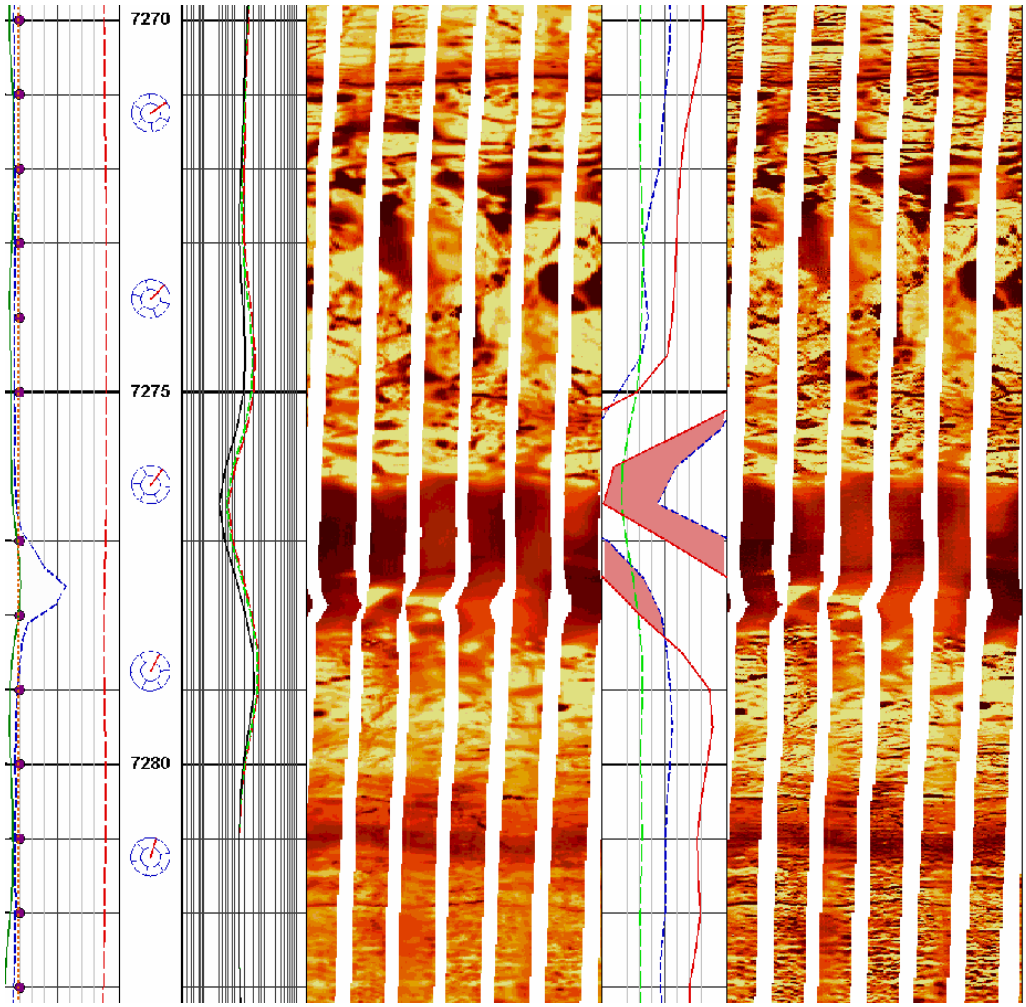

Figure 63. Image log 7270-80 ft corresponds to slow shear wave velocity and high anisotropy.

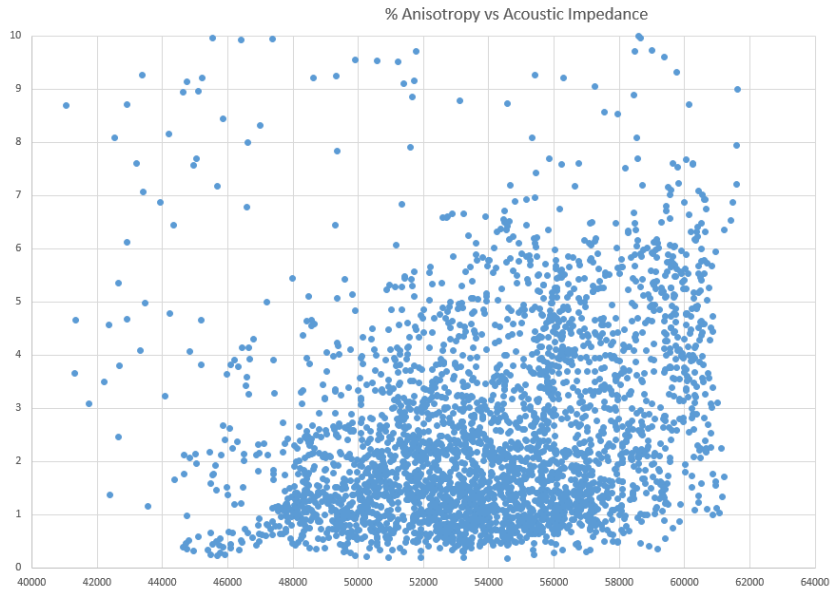

Figure 64.

Percent anisotropy vs. acoustic impedance shows no clear pattern. Again, the variation of impedance based on the pore type might be helpful in resolve some of this variability.

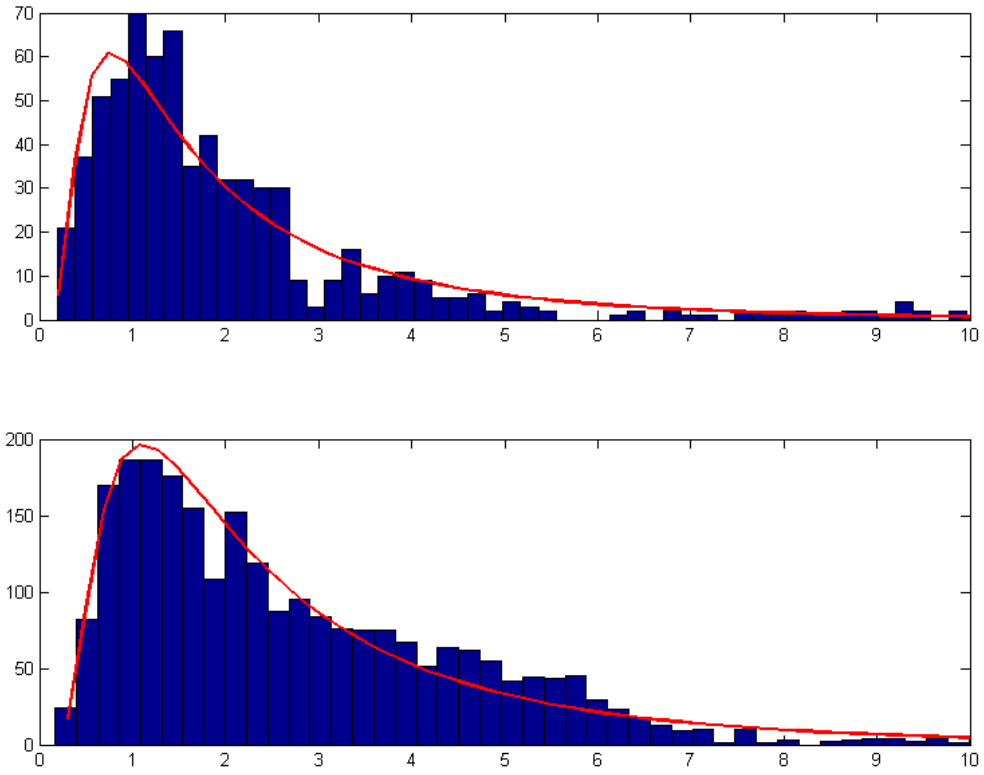

Figure 65. (Top) Low acoustic impedance (40000 – 51000) (ft/s)*(g/cc). (Bottom) High acoustic impedance (51000 – 62000 (ft/s)*(g/cc). Differences are small.

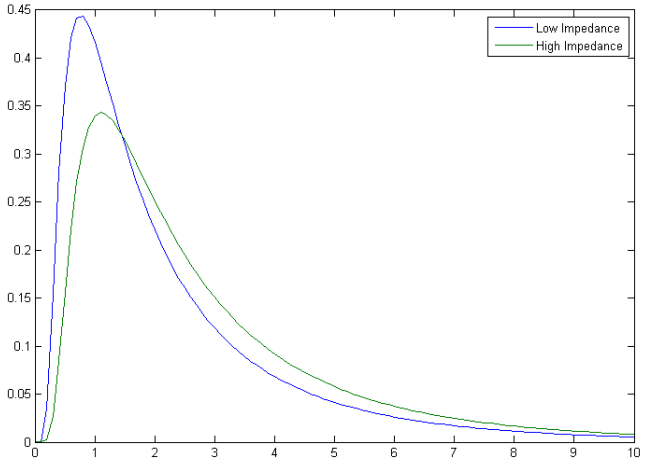

	A	B	C
1	%Anisotropy	Low AI	High AI
2	>1	72.1	84.3
3	>2	40.8	53.5
4	>3	24.4	33.7
5	>4	15.4	21.9
6	>5	10.0	14.6
7	>6	6.7	9.9
8	>7	4.5	6.8
9	>8	3.1	4.8
10	>9	2.2	3.8
11	>10	1.6	2.4

Figure 66. (left) Acoustic impedance vs. percent anisotropy showing low impedance has lower anisotropy. (right) The table to the right indicates that higher anisotropy is correlated with lower acoustic impedance.

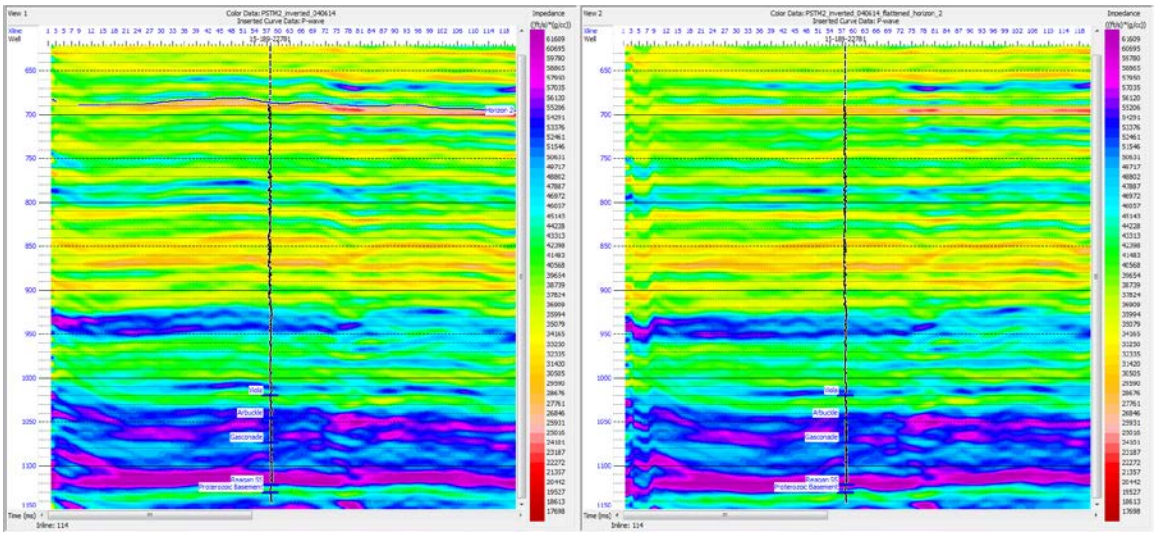

Figure 67. Inversion interpretation of seismic profile through Cutter KGS #1 illustrating 1) highly variable and complex impedance patterns in the Arbuckle (purple/blue high AI), 2) compared to the lower, laterally continuous impedance of the Viola (green AI).

Figures 68-71 illustrate the preliminary steps taken to analyze the inversion information in the Arbuckle so as to compare with Arbuckle flow units that have been correlated across the study area in southern Kansas using core and well log data. The flow units, while related to a succession of petrophysically distinct strata relating to vertical and horizontal permeability and porosity, they are also constrained by the regional stratigraphic divisions that were established earlier based on lithofacies and log character.

As described above the results from seismic inversion can be used to relate to the flow units by resolving porous strata, albeit a complex suite of pore types comprising the Arbuckle. This preliminary analysis sets the stage for additional work that is being conducted as the thesis is completed. The approach should help guide future work analysis of this publically-accessible seismic volume.

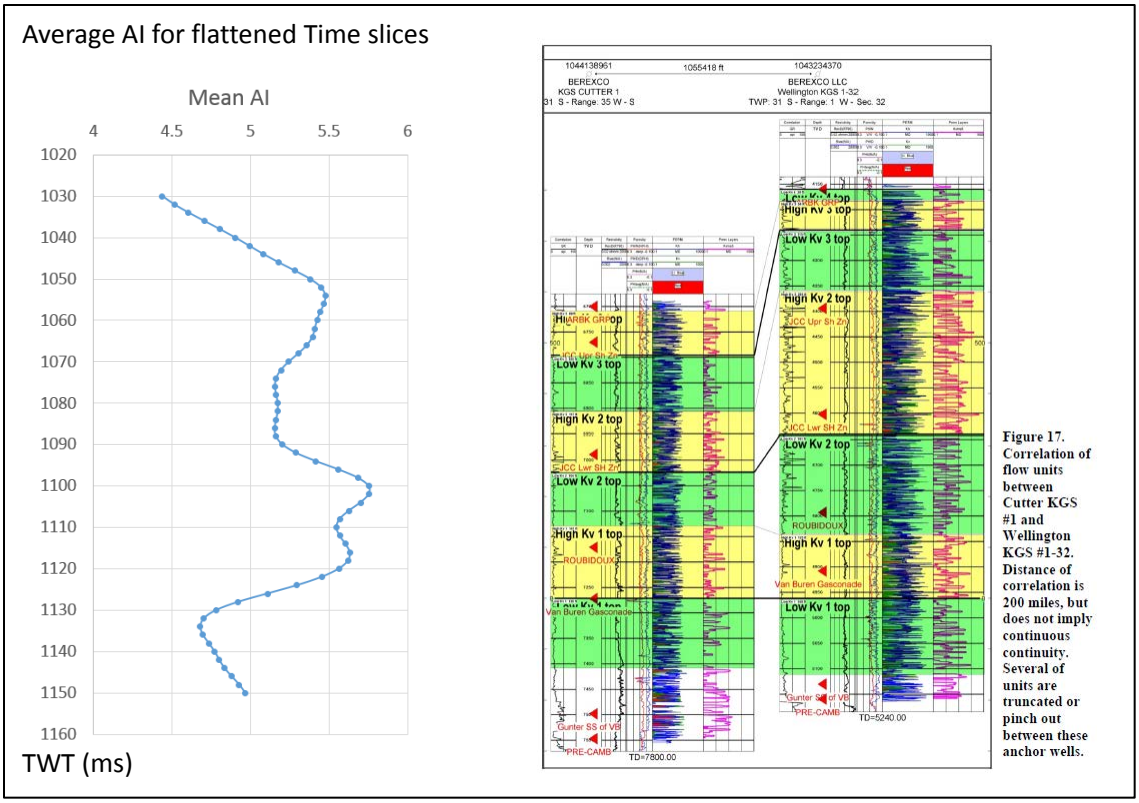

Figure 68. A first step taken to compare the flow units with the acoustic impedance (AI) was to obtain the mean AI for flatten time slides with the assumption that the flow units are conformable parallel units, not varying in thickness and not undergoing internal tilting, pinchout, or truncation. As noted previously the amplitude sections suggest that the internal layers in the Arbuckle at not uniform. This is also the case regionally where flow units thin, thicken, and locally pinchout due to changes in sediment accommodation due to varying topography or even episodic structural deformation.

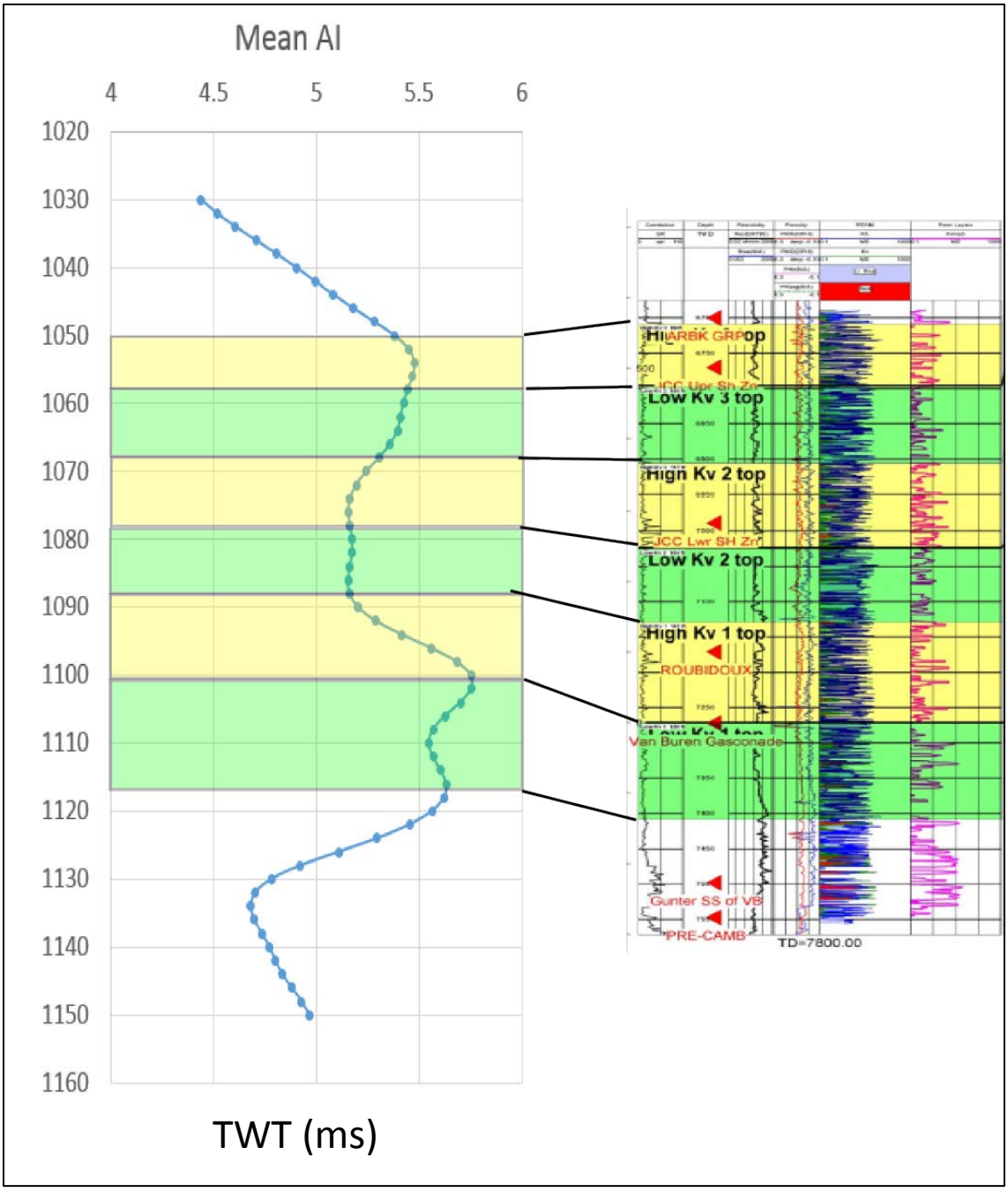

Figure 69. Flow unit correlation using a mean AI profile compared to the petrophysical classification of the Cutter KGS #1. The low quality flow units (green) and high (yellow) vaguely correspond with lower AI, particularly in the internal from the top of the High Kv flow unit to the base of High Kv 1 flow unit. This is also the interval with the better quality reservoir interval, centered around the Roubidoux Formation of the Arbuckle as labeled in the well log profile above.

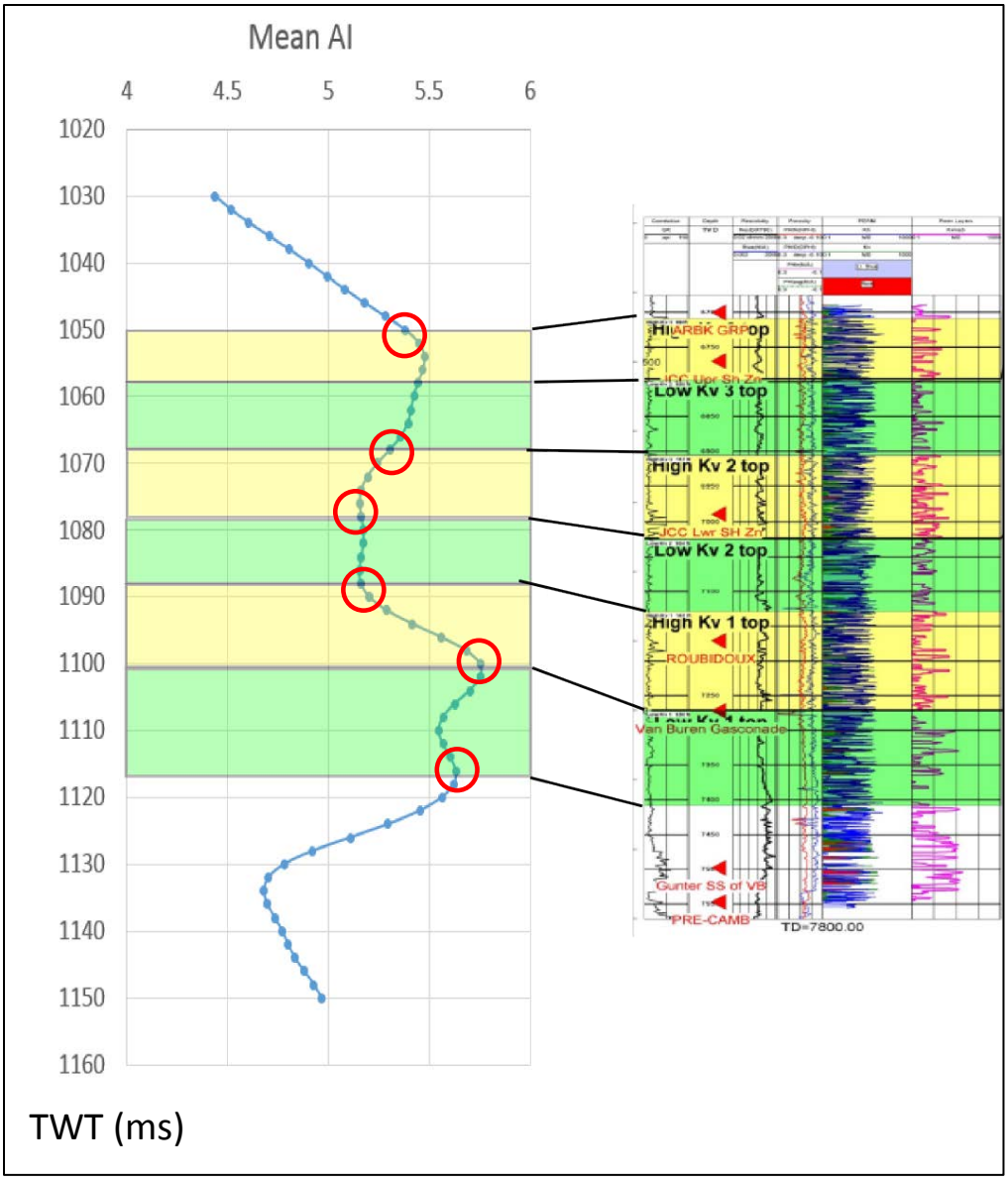

Figure 70. The AI profile highlighted with the inflections of this curve help to illustrate correlations.

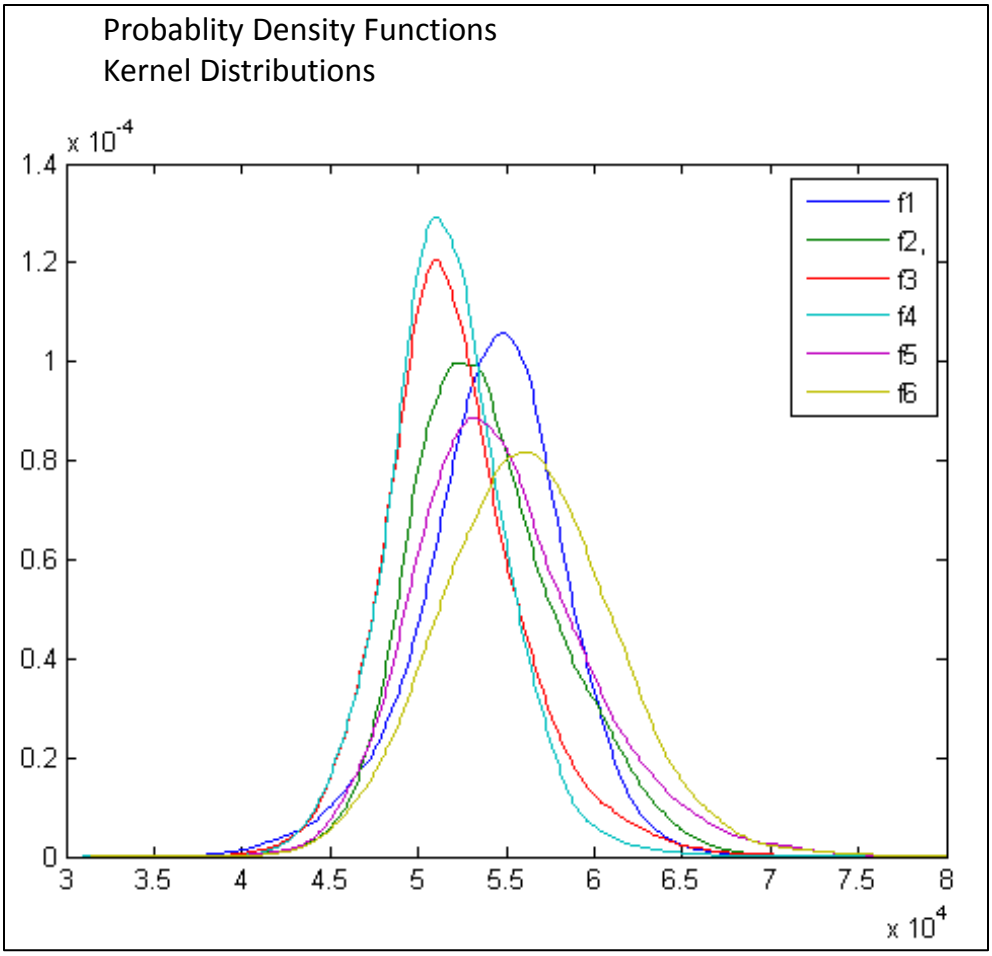

$$\hat{f}_h(x) = \frac{1}{nh}\sum_{i=1}^{n} K\left(\frac{x - x_i}{h}\right) \quad ; \quad -\infty < x < \infty ,$$

where n is the sample size, $K(\bullet)$ is the kernel smoothing function, h is the bandwidth.

	A	B	C	D	E
1	**Flow Units**	**Depth (ft)**	**Mean AI (ft/s)*(g/cc)**	**Kernel Function**	**Kernel Distribtion Bandwidth**
2	High KV 3 top	6709	54167	Normal	326.274
3	Low Kv 3 top	6796	53893	Normal	350.787
4	High kv 2 top	6905	52038	Normal	297.019
5	Low kv 2 top	7027	51646	Normal	268.222
6	High kv1 top	7130	54771	Normal	374.207
7	Low kv 1 top	7272	56251	Normal	396.754

Figure 71. The AI distributions (upper figure) for each flow unit show no variation (f4 [High Kv 2], and f5 [Low Kv2]) while other flow units do show slight to moderate variation. The lowest mean AI (more porous?) corresponds to a Low Kv 2, while the highest AI (less porous?) corresponds to a low Kv, in Low Kv 1. As previously mentioned it is likely the heterogeneity expressed by the AI profile in Figure 67 may not be captured in the times slice approach to comparing AI and log based flow units.

Update On Analysis of the Regional 3D Seismic (Dennis E. Hedke with contributions by Lynn Watney)

From the powerpoint based report -- Seismic Evidence Related to Significant Regional Structural Domain and the Question of CO2 Leakage Potential, Dennis Hedke, Hedke-Saenger Geoscience, Ltd., October 18, 2014

The volumetric curvature attribute and the amplitude 3D volumes in the seismic volumes that have been donated to this project often show signal disruption below the incised valley systems. This are interpreted to be steeply dipping and/ or chaotic beds. The velocity in the IVF is different than either side, but it does appear to be the cause of the long and vertical disruptions.

The focus of this discussion is the Shuck Field seismic volume and the topic of the signal disruption. This basis of the information conveyed here is also included in the final report on Shuck Field.

Overview

The large 3D seismic volume in the Shuck area provides significant detail to examine a typical Incised Valley Fill system (IVF) that contains important oil and gas reservoirs in the study area as well as assessing the geologic context. This legacy data obtained from earlier 3D seismic efforts, as acquired and delivered by Anadarko Petroleum, provide excellent imaging context for the IVF systems.

General Description

Approximately 79 square miles of surface template 3-dimensional (3D) seismic data, which was designed to yield 82.5' x 110' bins, was analyzed using conventional time and amplitude mapping, as well as post-stack seismic inversion, and volumetric curvature datasets.

Production in the area occurs in multiple zones, but this study will focus primarily on Pennsylvanian Morrow-aged and Mississippian Chester-aged targets that occupy the IVF systems. The northern portion of this study area is approximately 12 miles south of the Cutter field area.

Definition of major geologic controls on reservoir (IVF) via seismic data

The quality of the processed seismic dataset is such that well defined incised valley fill is quite evident in the combined Meramec Time Structure image below (**Figure 72**). The image contains data that covers all or parts of many significant fields including Hitch, Shuck, Archer and Wide Awake, among others.

While geologic structure has some bearing with respect to some production in the area, the more significant control is related to stratigraphic context, and the stratigraphic complexity is notable.

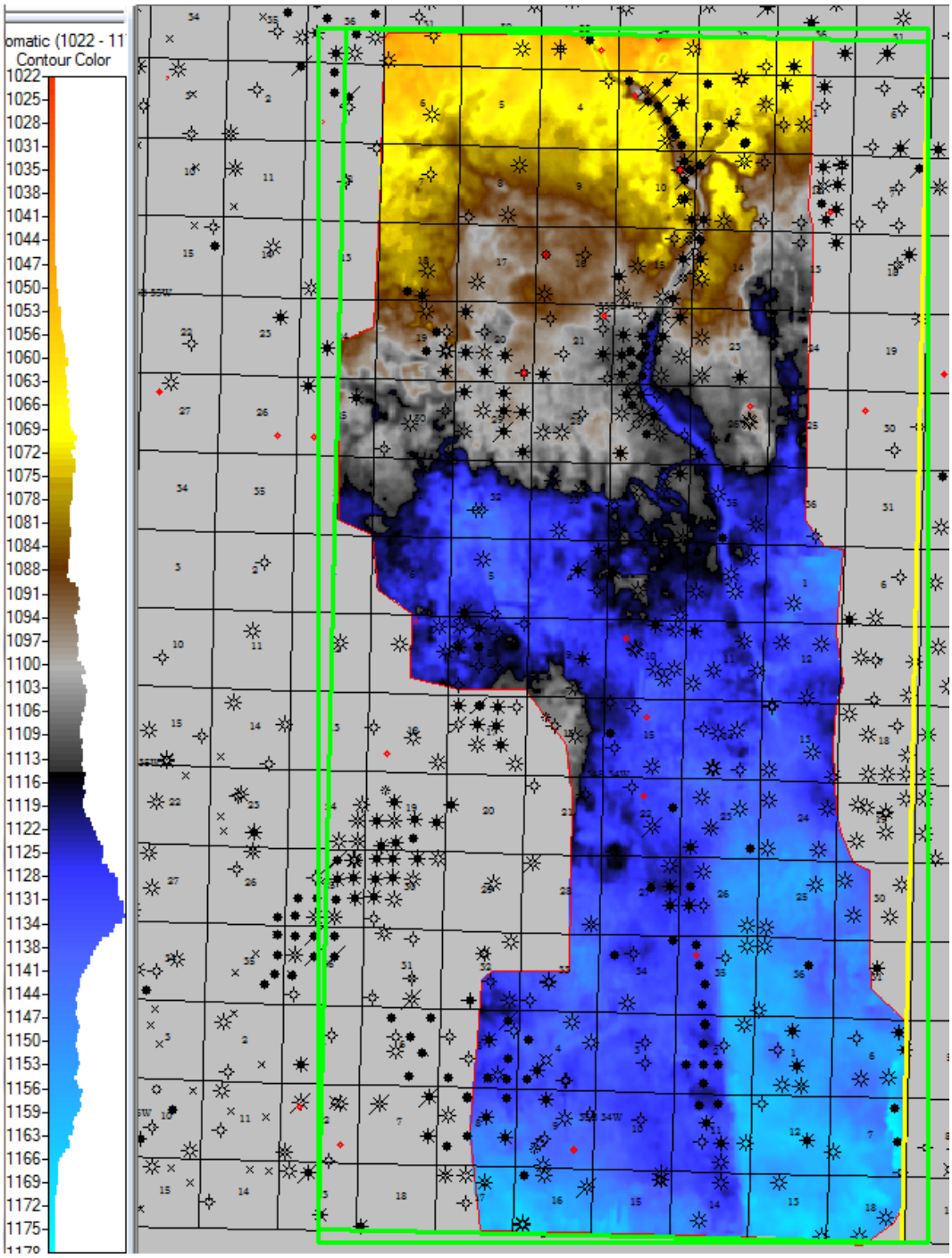

Figure 72: Meramec Time Structure image covering Shuck field, which occupies much of the IVF in the northern reaches, as well as areas outside the IVF, south to Wide Awake field. Boxes are 1 mi2.

The meandering, and in some cases very linear nature of the IVF is clearly visible. With abundant well control, we can construct a fairly reliable Depth Converted Meramec Structure map, as illustrated below in **Figure 73**.

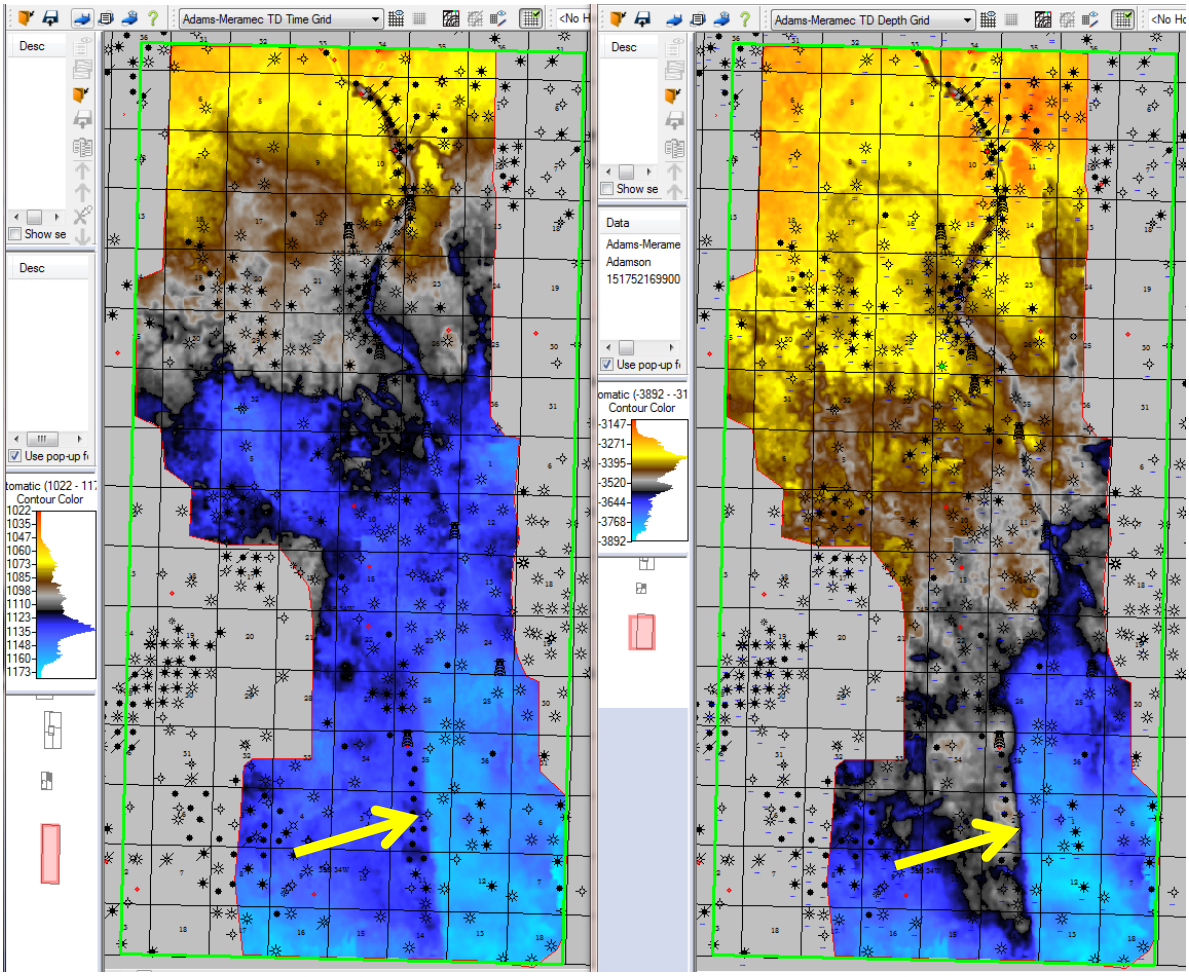

Figure 73: Meramec Time (left) vs Depth (right). Structural relief at Meramec is in excess of 750 feet. Relief from upthrown to downthrown block in lower right is ~240 ft, with producing wells identified to yellow arrow on upthrown side of the southern N-S trending fault.

Meramec Time Structure has been 'corrected' to yield the more accurate geometry and landform definition at Meramec time via Depth Conversion utilizing all available well control at Meramec. For example, the upthrown block in the lower middle part of the time map yielded very little, if any indication of the true structure that supports the production in that upthrown block.

The time relief from north to south is approximately 150 ms, while the depth relief is approximately 750 feet, yielding a rough estimate of 5 ft of structure per millisecond of time. Notice that there are numerous productive wells on the downthrown block in the southeast corner of the map.

The isochron from Morrow to Meramec illustrates similarity with the Meramec Depth map, and is illustrated below in **Figure 74**.

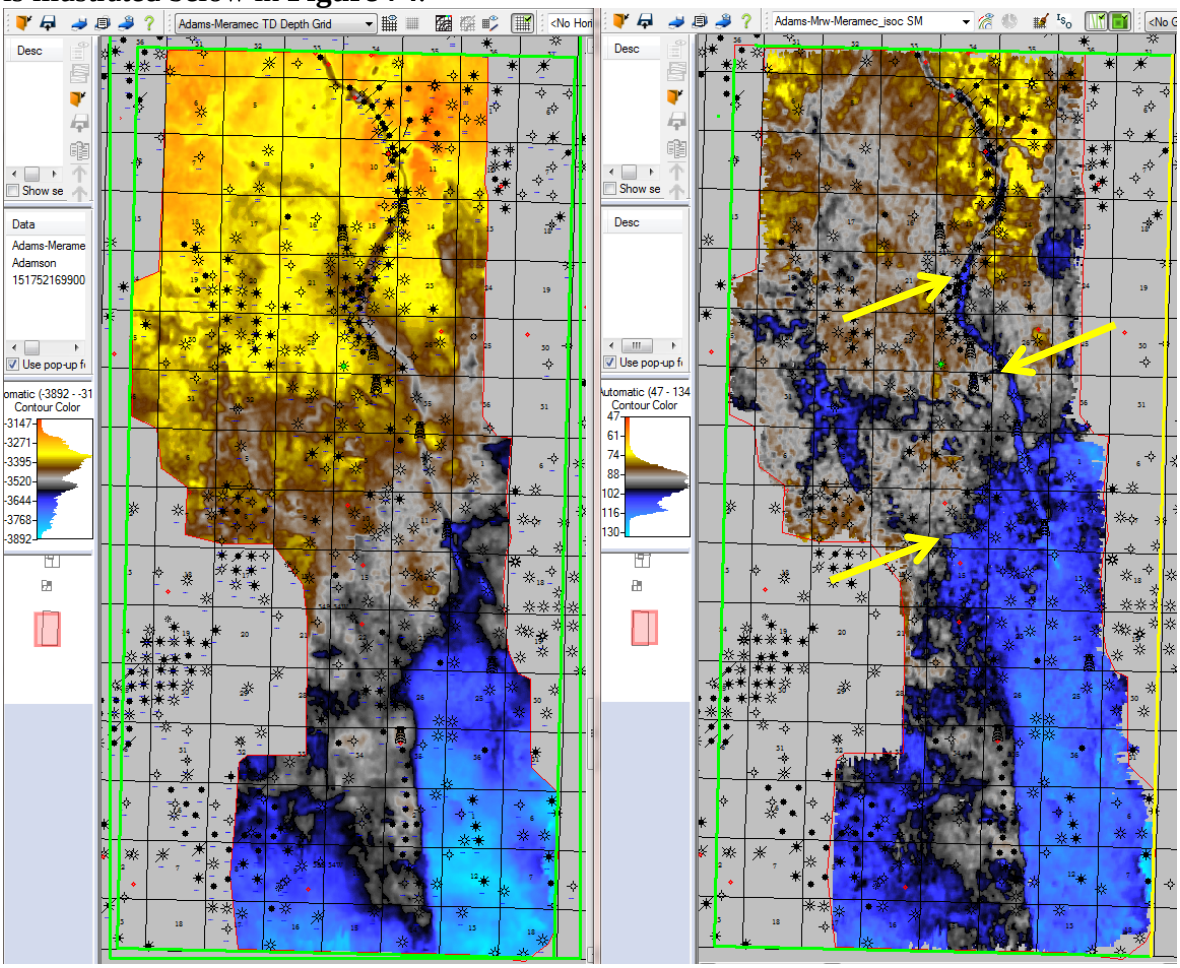

Figure 74: Meramec Depth (left) vs Morrow - Meramec Isochron (right). Mouths of the three tributaries that enter the west side of the main IVF trunk valley are highlighted with yellow arrows on the isochron map. Top and bottom tributaries trend NW as does the upper (northern) reaches of the main IVF.

While there are multiple linkages that can be observed between these two key maps, it is worth noting that the significant tributary feeding in from the west just above center of the isochron map does not traverse the minor 'bridge' that is barely noticeable in the depth context.

It is also the case that the trending of the leftmost meandering system that ultimately reaches up to the northwest corner of the mapped area has a strong parallel relationship to the main IVF system. That relationship is difficult to discern in the Depth map. One can also get a weak sense of where the southern part of the IVF heads after leaving the quasi platform just above the blue region, which is at about 100 ms isochron thickness. We will show evidence later where the system goes once it passes into a thicker stratigraphic package to the south, crossing apparent fall line dividing incised bedrock with different resistance to being incised.

While the IVF is striking enough in its detail, it is worth taking a closer look at the geometry of the meandering system that makes up the main tributary (**Figure 75**).

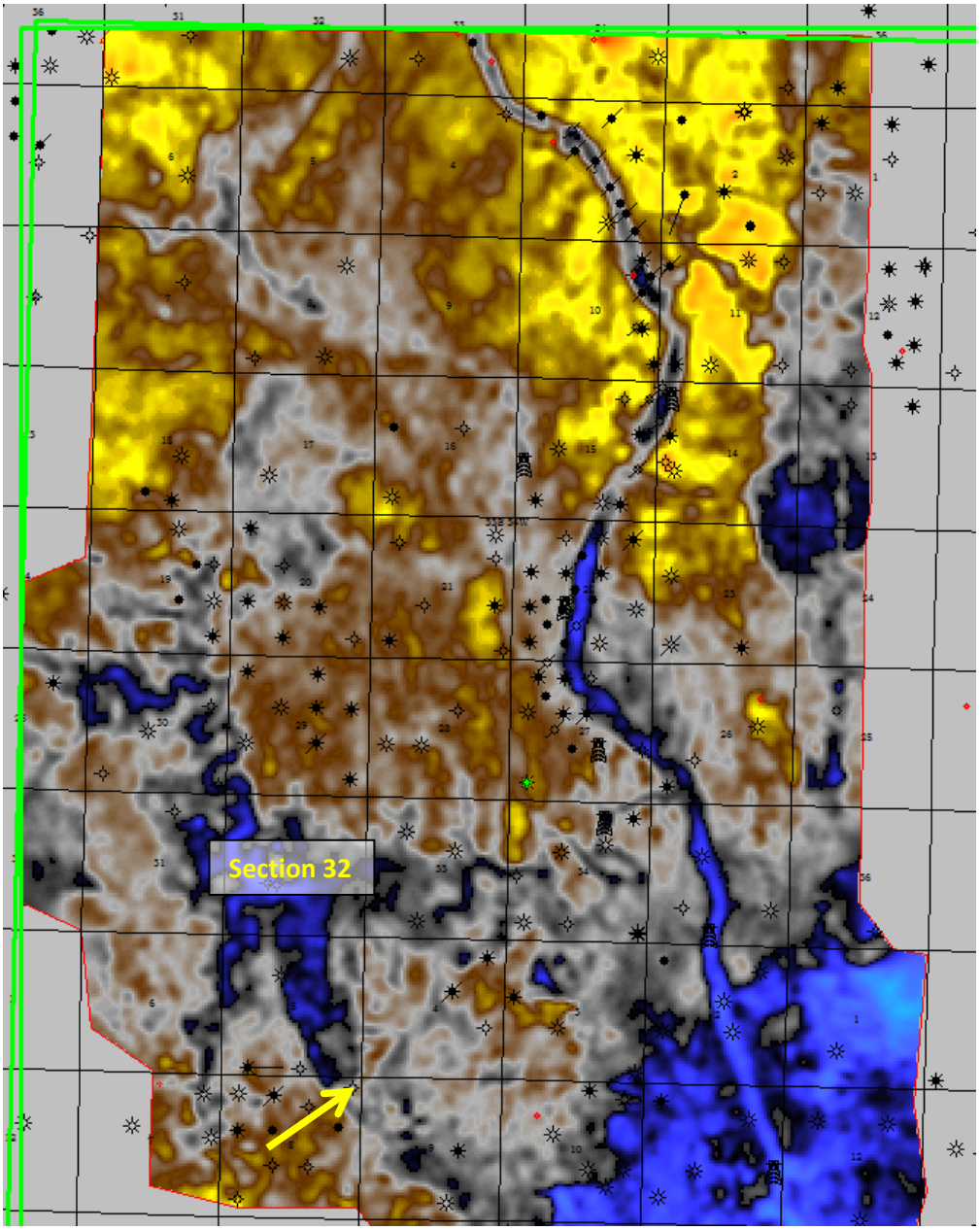

Figure 75. Morrow-Meramec Isochron detail to highlight meander belt. Minimum resolved meander system width is approximately 275 feet in section 34, equivalent to about 3 trace widths in the crossline direction. Derrick symbols are at locations where sonic log control was utilized.

The maximum isopach thickness of the meander system (section 32, **Figure 75**) is approximately 650 feet, while the minimum thickness is approximately 450 feet in the northwest corner of section 34. Please note the 'bridge' mentioned earlier in the northwest corner of section 8 (yellow arrow).

Both the depth map and the isochron map show the existence of another tributary that makes its way through sections 5, 8 & 9, T 33S R34W. Production occurs in this system in section 15 - T33S R34W (Anadarko-Koch 6A). The Morrow - Meramec thickness at that location is 629 feet. Production occurs in Chester, from an overall interval of 5927-6270.

For comparison to a well in the IVF proper, the Anadarko Etzold Unit North 2-5, located approximately E2 E2 NW section 22-T33S R 34W, has a Morrow - Meramec thickness of 709 feet, produces from Chester sands from a single net interval of 6230-6274.

The well with the derrick symbol in the tight meander loop in section 34 contains a Morrow-Meramec interval of 678 ft, and produces from a Morrow sand in an interval from 5962- 5966. Cumulative production from 1997 to present has been about 0.3 BCF gas.

There are dry holes in the IVF in between producing wells, and updip, so the system is more complex than meets the eye.

Acoustic Impedance Inversion Results

Data availability for this area was limited to stacked, off the shelf p-wave 3D. Sonic logs were utilized at the derrick-indexed symbols, totaling 8 discrete locations both within and outside the IVF, and one case within the meander belt. Four of the eight wells had availability of bulk density logs. After extracting a statistically significant wavelet from the actual seismic data (**Figure 76**) the logs were correlated to seismic via creation of a synthetic seismogram, and a model was built to integrate with the 3D volume.

Figure 76. Wavelet extraction.

In general, the quality of model building was high and an example of the inversion analysis, prior to making an inversion run is shown in **Figure 77**.

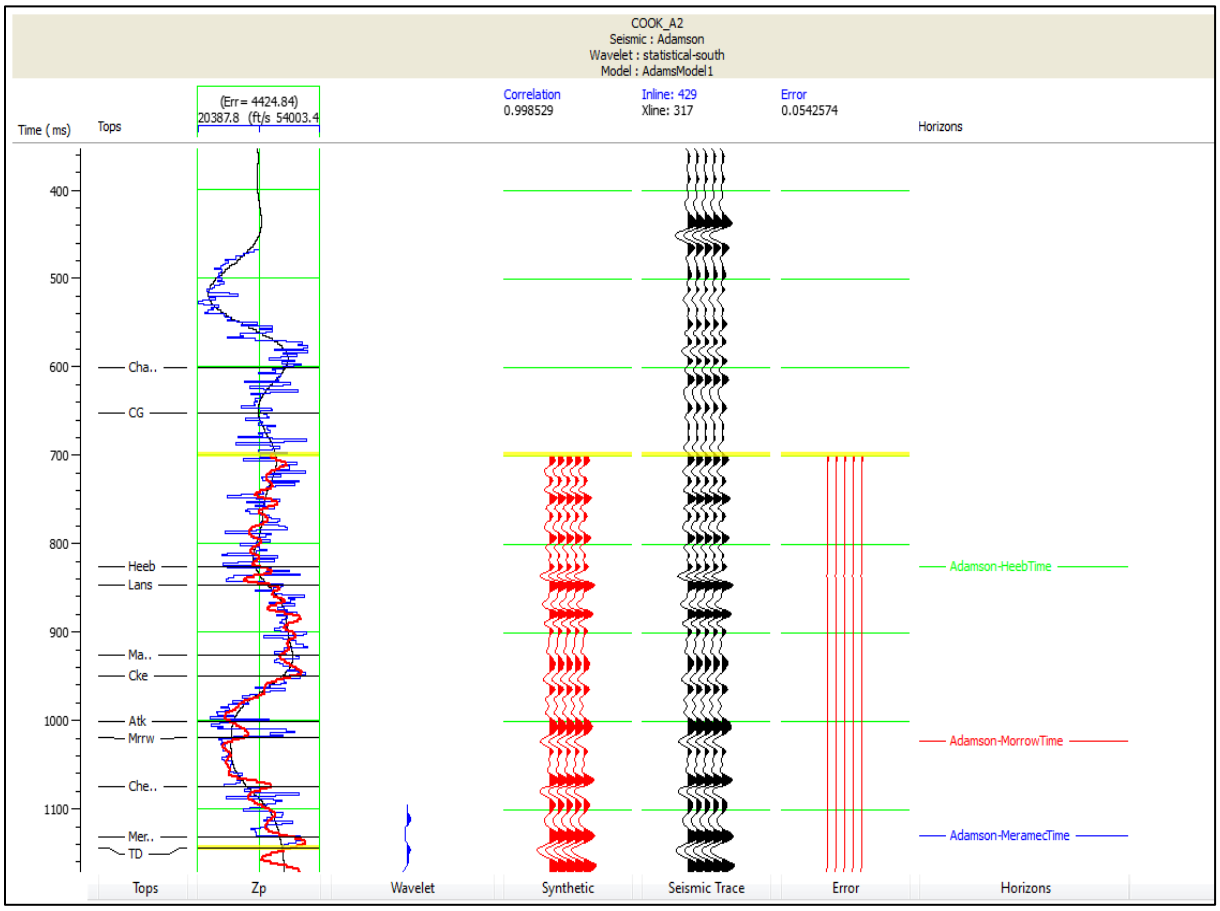

Figure 77: Inversion analysis; blue curve = input log, black = initial model; red = inverted log.

Virtually all wells used in the model building process exhibited quality similar to the well above, which is located in the heart of the IVF system, section 35, T34S R34W. The impedance log in this case (blue curve) is based on both actual sonic and bulk density curves. If a bulk density log is not available, an estimate of density character can be obtained via a Gardner's equation transform[1]. Gardner's relation is generally a good estimate for most lithologies, including clastics and carbonates. It is generally not reliable in evaporites.

[1] $p_b = aV^b$, where p_b=calculated bulk density, a=empirical constant, generally accepted to be 0.23, V= p-wave velocity, b = empirical constant, generally accepted to be 0.25.

Multiple models were built and tested for quality control. One such model is presented below and includes the sonic log control that related to that immediate area (**Figure 78**).

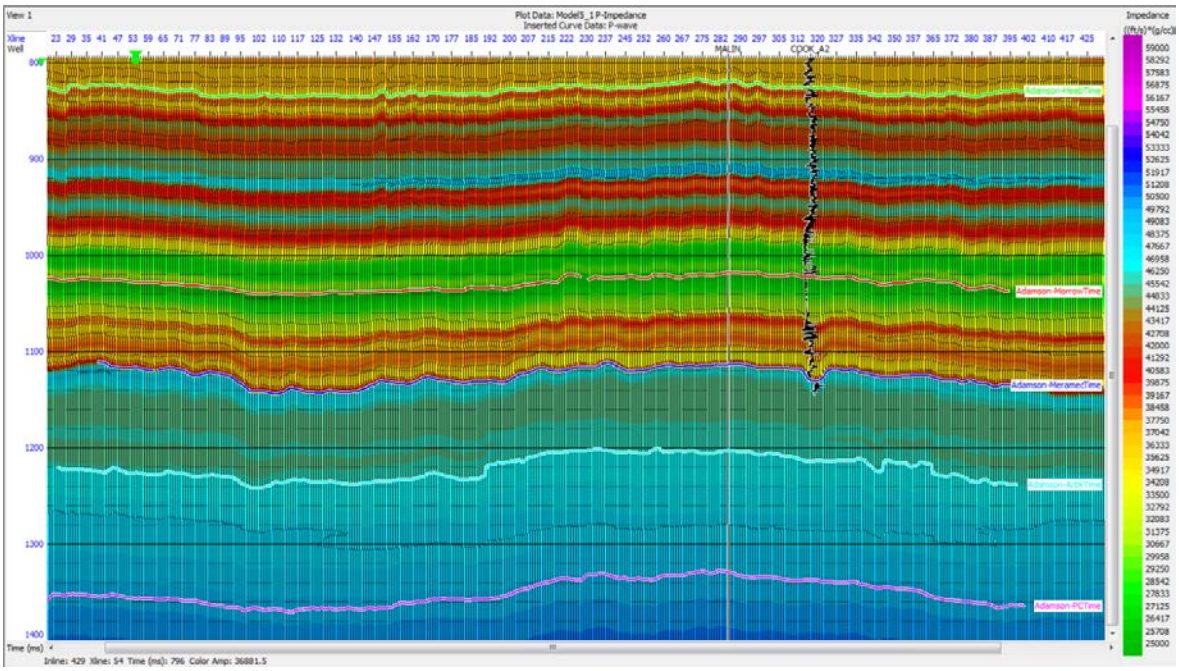

Figure 78: West-East profile illustrating model, including inserted sonic log from Anadarko Cook A2, SE SE SW, Sec 35 - T33S R34W. Topmost horizon =Heebner; Red horizon = Morrow; Horizon near base of inserted log = Meramec; Light blue horizon = Ordovician; Red horizon at base = Pre-Cambrian.

This IVF well also had actual density, so the impedance at this location is of highest quality possible. The sag on the west half of the diagram is in the thickest portion of the meander loop discussed earlier.

The higher impedance zone (red color) approximately midway between Morrow and Meramec is the top Chester. In the model this zone appears to be relatively uniform. Once the model and real data come together it will be seen that sorting out real geology is challenging.

The model is built by incorporating horizon control from prior picking into extrapolated sonic log locations, which are widely spaced. That being said, it is interesting that the model did pick up some contrast in the stratigraphic section between Meramec and Ordovician sediments. Certainly, there is considerable variation in that part of the geological section, which is evident in the inverted outcome.

The horizon characterization is based on correlation of events in the conventional amplitude domain. In that context and event such as Meramec time usually fits in the center of a peak amplitude event. Once an inversion is run, that event is translated to a high impedance correlation, with a generally sharp boundary with the lower impedance sediments above. Conventional amplitude events on inline 429, with emphasis on the stratigraphic section from Morrow to Basement are shown in **Figure 79**.

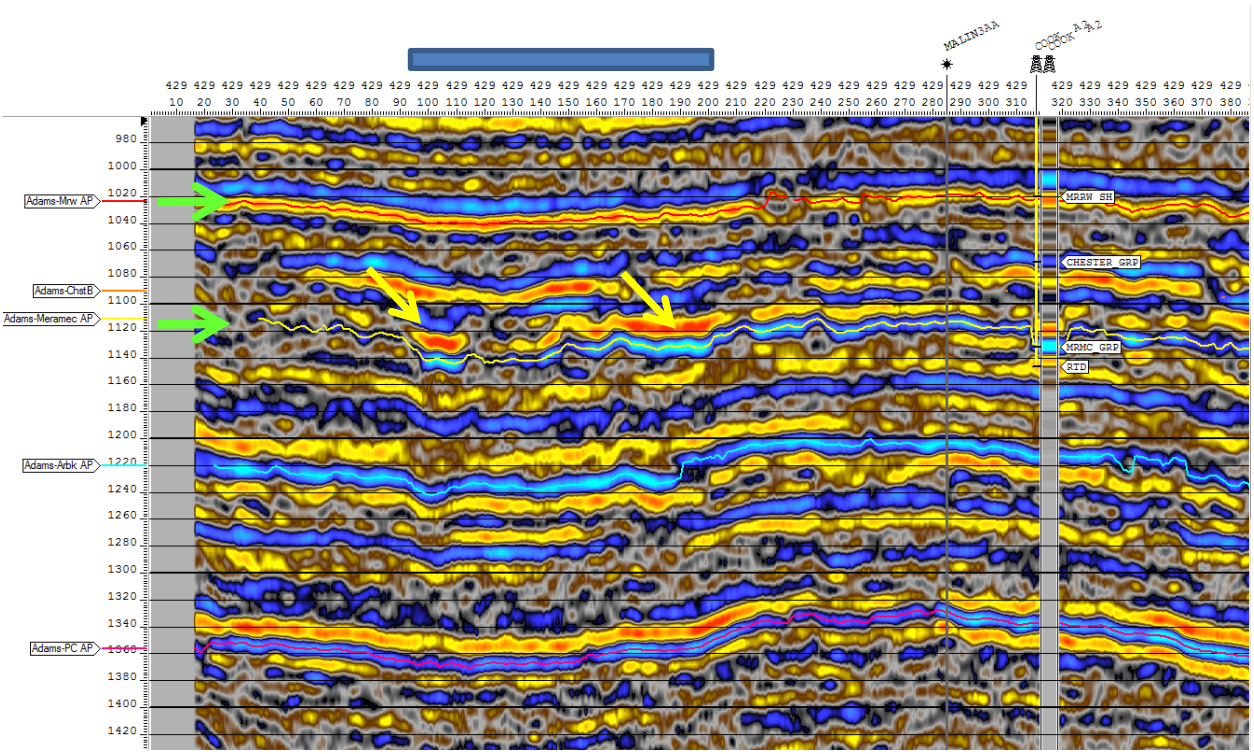

Figure 79. Conventional amplitude (variable density) profile (traces omitted to emphasize details), illustrating complexity between Morrow and Meramec (green arrows), as well as relative complexity throughout the remainder of the stratigraphic section. Blue colors relate to positive amplitude, bright colors to negative amplitude. Alluvial deposits in a meander belt are highlighted with yellow arrows. Blue bar at top delimits possible faulted graben that appears to be Chester in age.

The stratigraphic complexity observable in the conventional amplitude data between the Top Morrow and Top Meramec is obvious. The synthetic seismogram from the Cook A2 is inserted in the variable density display, and the overall quality of the correlation from synthetic to real data is good. The hotter amplitudes on the left part of the profile just above Meramec (yellow arrows) are related to alluvial sediments within the meander belt.

The case can be made for a nearly vertical fault at or near crossline 200, with offset commencing at approximately Chester time, continuing through the Ordovician and likely continuing into Pre-Cambrian, although offset at the unconformity is softened. A similar condition exists on the west edge of the system at around crossline 95 (See blue bar in **Figure 79**).

On the right side of the image (east), the Morrow - Meramec isochron is generally around 95 ms, with the exception of the IVF, where the isochron time thickness is >105 ms. In the meander belt on the middle left (west) portion of the image, the maximum isochron is ~103 ms.

The companion impedance profile is shown below, again without trace overlay to expose as much detail as possible (**Figure 80**).

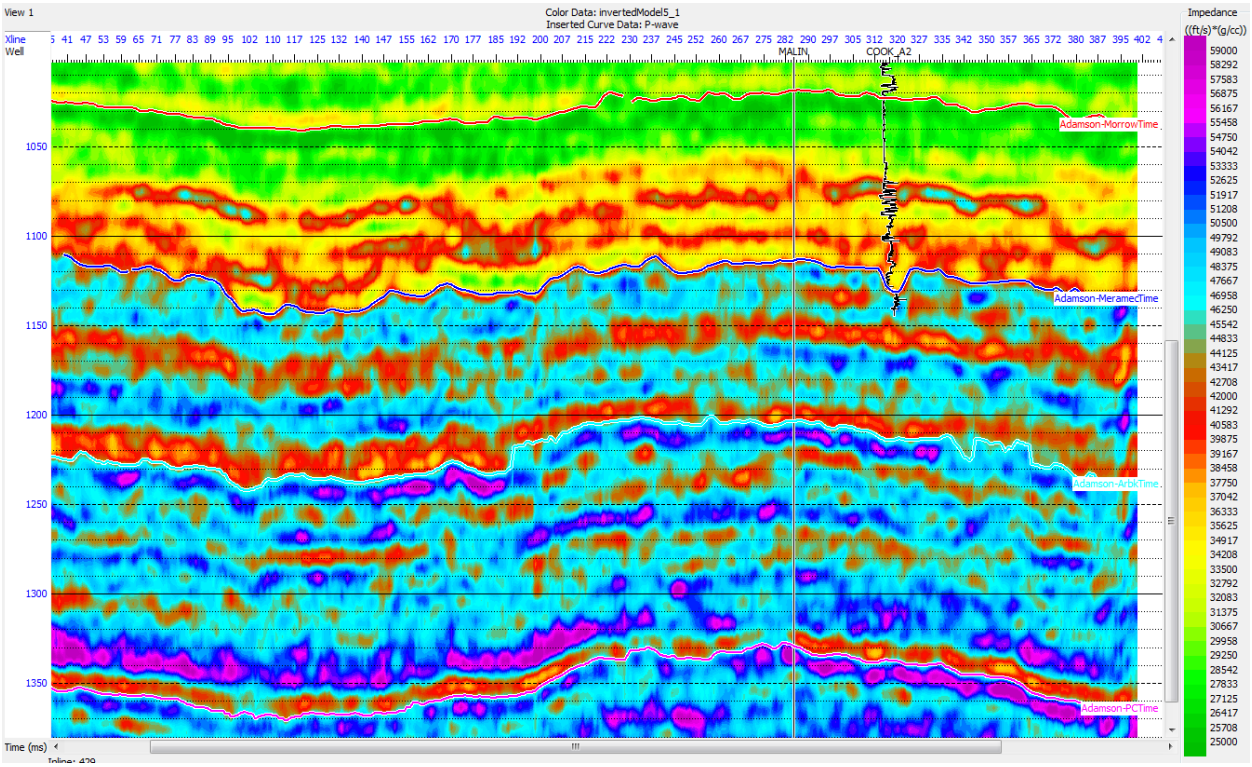

Figure 80: Acoustic impedance on inline profile 429. Cook A2 P-wave log trace overlies profile.

This profile is coincident with the preceding amplitude profile (**Figure 79**). Notice the sharp boundary at the interface with Meramec sediments, at a time of around 1110 ms on the left edge of the profile. Sediments above register in the range of 25,000 - 30,000 impedance units; sediments immediately below are in the 45,000 - 50,000 unit range.

Lighter blue shading in the Chester sequence most likely relates to carbonate rocks, with green shading leaning toward shales. Magenta colors will be tighter, denser carbonates. Generally speaking, the most optimum range for sandstone is from about 30,000 - 35,000 impedance units. In the Cook A2 well, the Lower Chester sands have an impedance range of 33,000 - 34,000 impedance units.

A bounded time horizon slice has been extracted from the 3D volume that covers the lowest 15 milliseconds of the Chester sequence, which will relate to approximately the lowest 90 feet of sediments in the IVF (**Figure 81**). Many of the commercially productive wells in the IVF have come from this part of the system, although some wells will produce from shallower sands in the Chester, and some wells will produce from Morrow sands above Chester.

In map view we can then associate and compare impedance with amplitude (**Figure 81**).

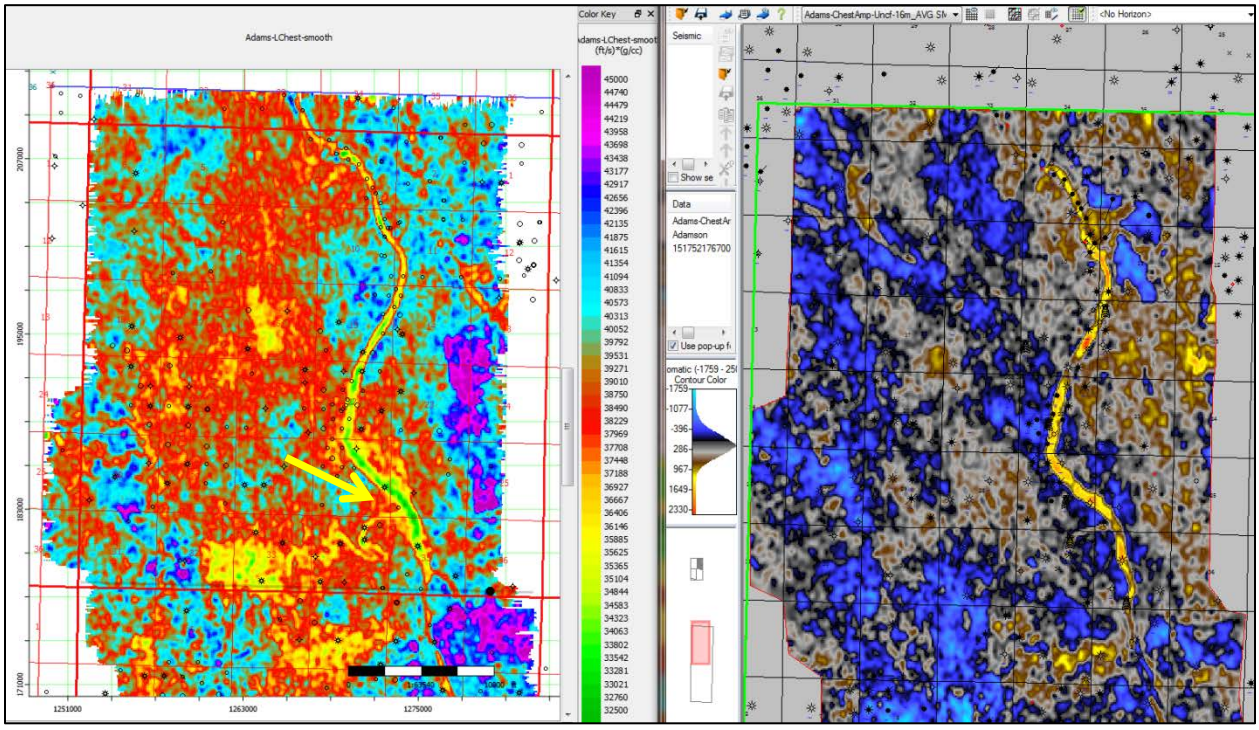

Figure 81: Lower Chester extracted impedance time window (left) vs extracted amplitude window (right). North half of study area. Color scheme for impedance changes with more limited geographic extent. Now, greens are more likely to be sands. Yellow arrow is mouth of a tributary as it enters the main IVF.

The color scale in the impedance map view has been adjusted slightly from the scale that pertained to the impedance profile, such that the lowest impedance on the color scale is now set at 32,500 and the highest at 45,000. This allows for better discrimination of the sand system.

Note that the impedance mapping clearly tracks the tributary feeding the main IVF (yellow arrow **Figure 81**), while the amplitude mapping tends to lose track of this anomalous character. It is also the case that the impedance mapping has a much greater ability to discriminate lithologies overall.

In the case of the southern portion of the 3D volume (**Figure 82**), a significant faulted structure exists with the downthrown block located east of the fault. However, it is worth noting that the lithological character for the most part continues relatively unabated across the fault, certainly implying that the fault post-dated the stratigraphic distribution that existed pre-fault.

On the other hand, it is apparent that a significant stratigraphic discontinuity also occurs, outside and independently of the IVF, in the vicinity of the Archer field, sections 15, 22, 23, 26, 27 T34S R 34W. The NNW -SSE edge defining that system is not at all apparent in the amplitude mapping of the Lower Chester.

It is also important to note that the southward continuation of the IVF is easier to discern again in the impedance domain. It is also apparent that an additional arcuate feature (red arrow) can be identified in sections 23, 24 and 25, T34S R34W, which does not seem to have expression in the amplitude extraction. The Oxy-Gleeson C3 well is located in this feature, and it appears it was completed as a gas well in Chester sediments.

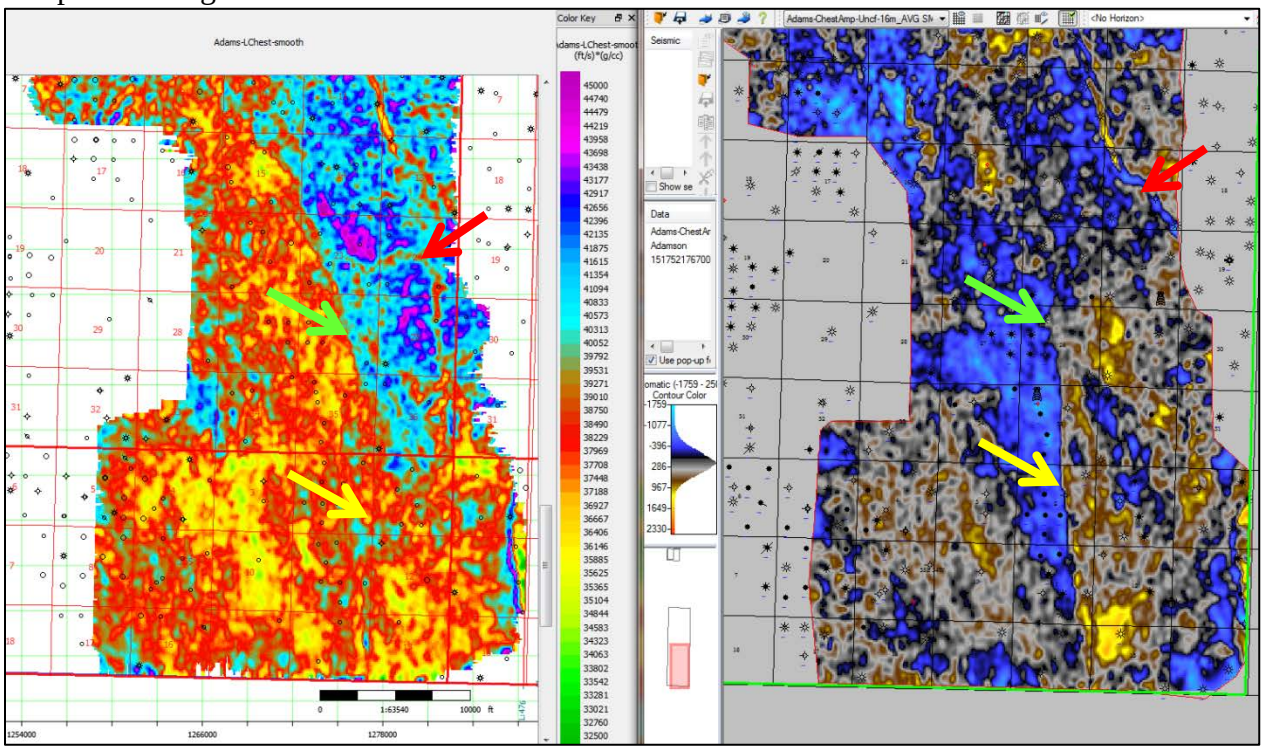

Figure 82: Lower Chester extracted impedance vs amplitude, south half of study area. Color scheme consistent with Figure 81. Green arrow = lithologic discontinuity; yellow arrow fault with no apparent lithologic change across it in this time slice; red arrow = arcuate feature.

Volumetric Curvature Characterization

The 3D volume was also processed to enable volumetric curvature, specifically Most Negative Curvature, in order to evaluate possible preferred orientations related to fracture systems and /or discontinuities (**Figure 83**).

The approach taken was one of maximum resolution, with a 3 trace average in an x-y sense, and a 2 sample smoothing in a vertical sense.

The results have provided an opportunity to view both structural and stratigraphic context simultaneously in some cases, again with focus on the IVF system / Lower Chester sediments. However, the evidence of preferred orientation across a broad vertical range is fairly consistent, and we see the azimuthal expression very well defined in a time slice at 1072 ms. The dominant azimuthal trends seem to be very close to N 45W/S 45E, with the conjugate set generally settling

around N 35-40E/ S35-40W. Locally, these ranges vary, but they do seem to be fairly persistent even into the Basement. Deeper into the volume we see the clear expression of the IVF anomaly, and simultaneously we can note the persistence of the linear anomaly in the south central extremity of the survey.

The big picture grain and the combined structural/stratigraphic look are shown in **Figure 83**.

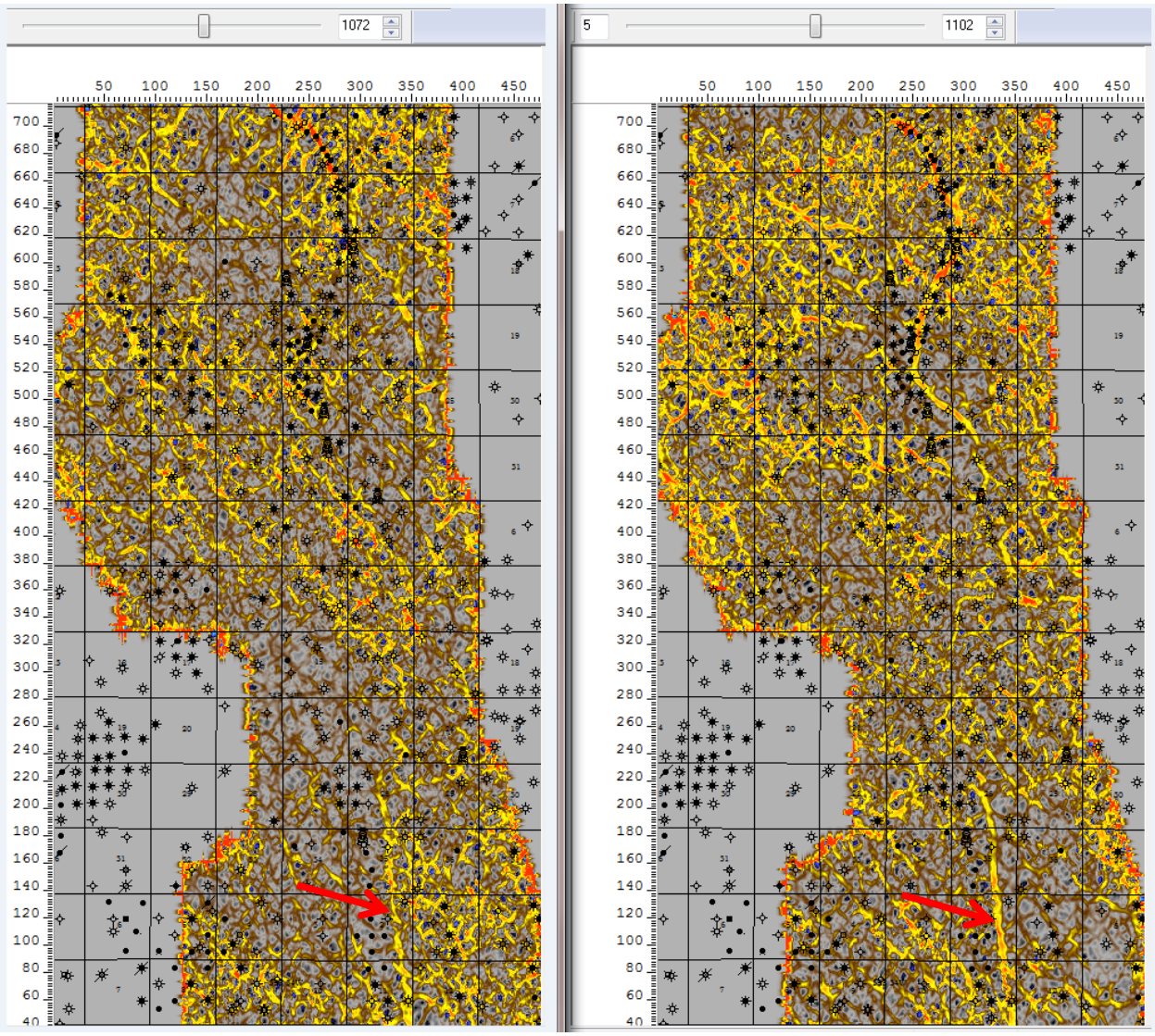

Figure 83: Most negative curvature. Left plate from 1072ms, illustrating the appearance of the dominant NW-SE grain in the middle of the frame, and in the right plate, the combined structural element in the bottom center, and the stratigraphic component related to the IVF in upper right. Red arrow at location of a fault verified with offset.

While these are smaller in scale, we can certainly note that the fault bounding discontinuity in the bottom center is expressed in both plates. This structural element is first seen somewhat defocused at about 1020 ms, which places it at approximately Morrow time. It is virtually continuous through approximately 1140 ms.

The wedge shaped character outlined west of the linear anomaly appears likely to be related to the upthrown block that is expressed on the depth converted Meramec structure map shown earlier.

The IVF anomaly at 1102 ms in **Figure 84** is very clearly expressed and, as in other study areas in the region, the vertical extents of the IVF curvature anomalies can be seen to be well connected over many hundreds of feet. The image below is an extracted north-south profile that transects multiple IVF related features.

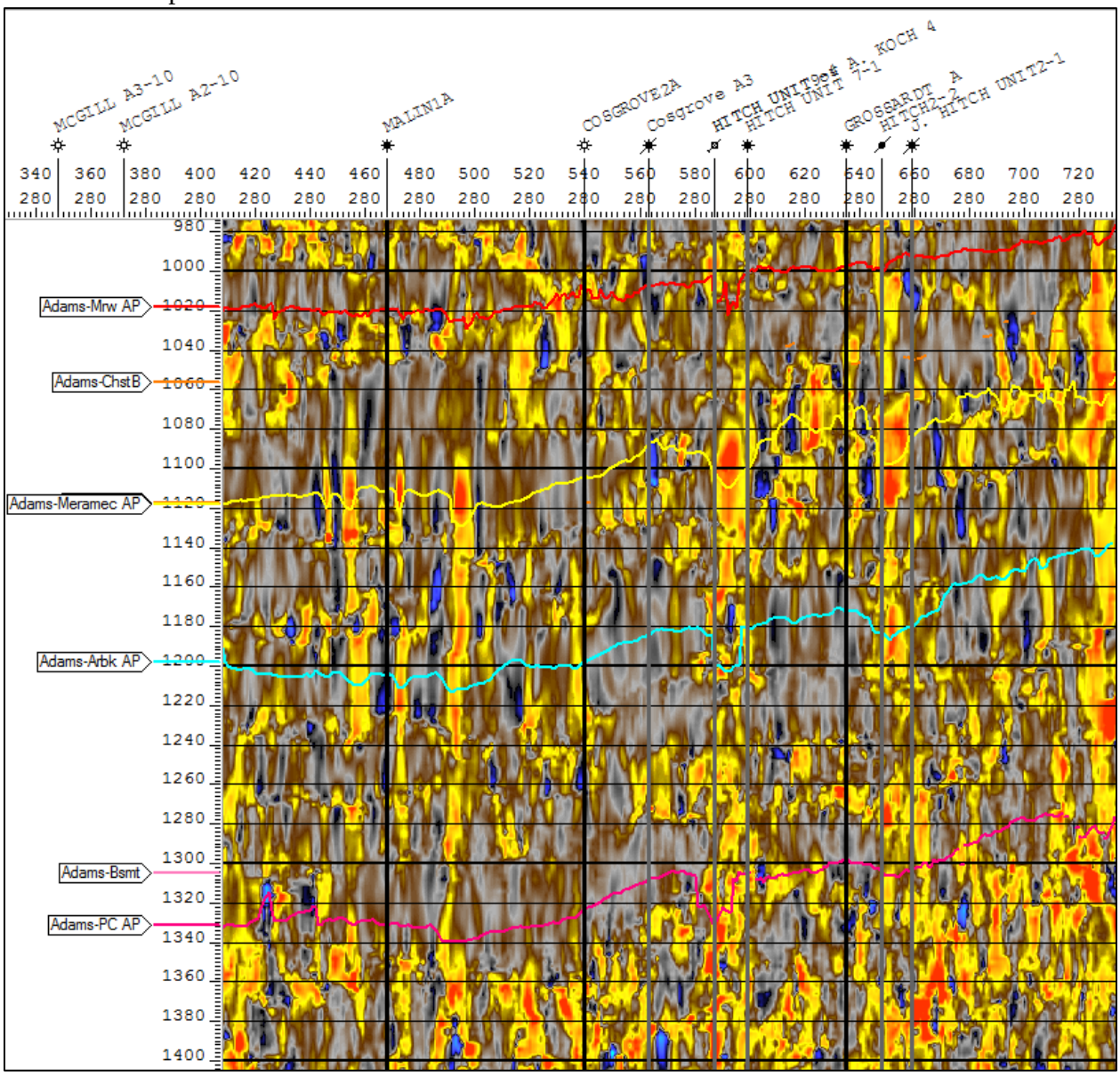

Figure 84: Most negative curvature, vertical profile, crossline 280, south (left) to north (right). Vertical anomalies from Chester to Basement.

The larger vertical anomalies at stations 280/655, 595 and 495 are related to the primary IVF system. The virtually continuous 'pipe' extends in an accentuated sense from just above 1100 ms

well into Basement at 1400 ms, and beyond. At that location, the Meramec occurs at a depth of about 6300 ft, while Basement would likely be penetrated at about 8500 feet below surface. Therefore, the vertical extent of the anomaly appears to exceed 2000 ft.

The smaller anomalies in the vicinity of the Malin-1A well are related to the tight meander belt discussed earlier in section 34, T33S R34W.

Conclusions on the Shuck Field Seismic Discussion

This dataset provides an opportunity to see with high spatial resolution multiple elements that relate to the IVF system, both structurally and stratigraphically. Significant well control afforded the opportunity to truly tune the structural details that related to the IVF and tributaries, as well as the fault block in the southern study area.

Acoustic impedance inversion provides an ability to realistically discern between various lithologies, including sand, shale, and carbonates. While pre-stack data was not available, and therefore presented some limitations in terms of further quantification of for example VpVs ratio, the available post-stack volume did provide some qualitative differentiation of lithologies.

Volumetric curvature, applied at the highest resolution, yielded insight related to likely fracture system background that has likely driven at least in part the genesis of the IVF system. Zones of weakness were in certain time intervals quite obvious. The vertical connectedness of certain anomalous features would seem to suggest that the IVF may very well be sourced from underlying Basement structure.

Shuck / Adamson Seismic Characterization --Documentation that a Prominent N-S Fault in the Southern Portion of the Seismic Survey has a Prominent Strike-Slip Component

The regional seismic volumes were examined together to evaluate fault type, timing, and effect on sedimentation, i.e., evidence for episodic structural activity. A portion of this review is presented here and will be expanded on in the final report. The conclusions are

1) high angle reverse and strike-slip faulting is more common than believed;
2) faulting is clearly linked to the tectonism of the Ouachita-Amarillo-Wichita-Arbuckle system in both timing and apparent stress regime that was imposed on the southern Kansas shelf;
3) peak movement of the faults consistently occurs in late Morrow-Atokan that led to the reorganization of the shelf, uplifts, and the depositional system;
4) evidence for the contribution of tectonics to deposition is complicated by concurrent changes in sea level;
5) faulting greatly diminishes above the Upper Pennsylvanian, but examples have been identified where faults change their sense of movement during the early Tertiary Laramide tectonism associated with the Rocky Mountains and even younger, late Tertiary affecting deposition and deformation of the High Plains Aquifer; and
6) many structure characterized by the 3D seismic show multiple episodes of structural deformation expressed by growth/differential sedimentation across the structure including

lower Paleozoic, e.g., notable thickening of the Arbuckle and Mississippian strata across major faults.

Evidence for a major strike-slip fault in the Shuck Field area is presented in **Figures 85-91.**

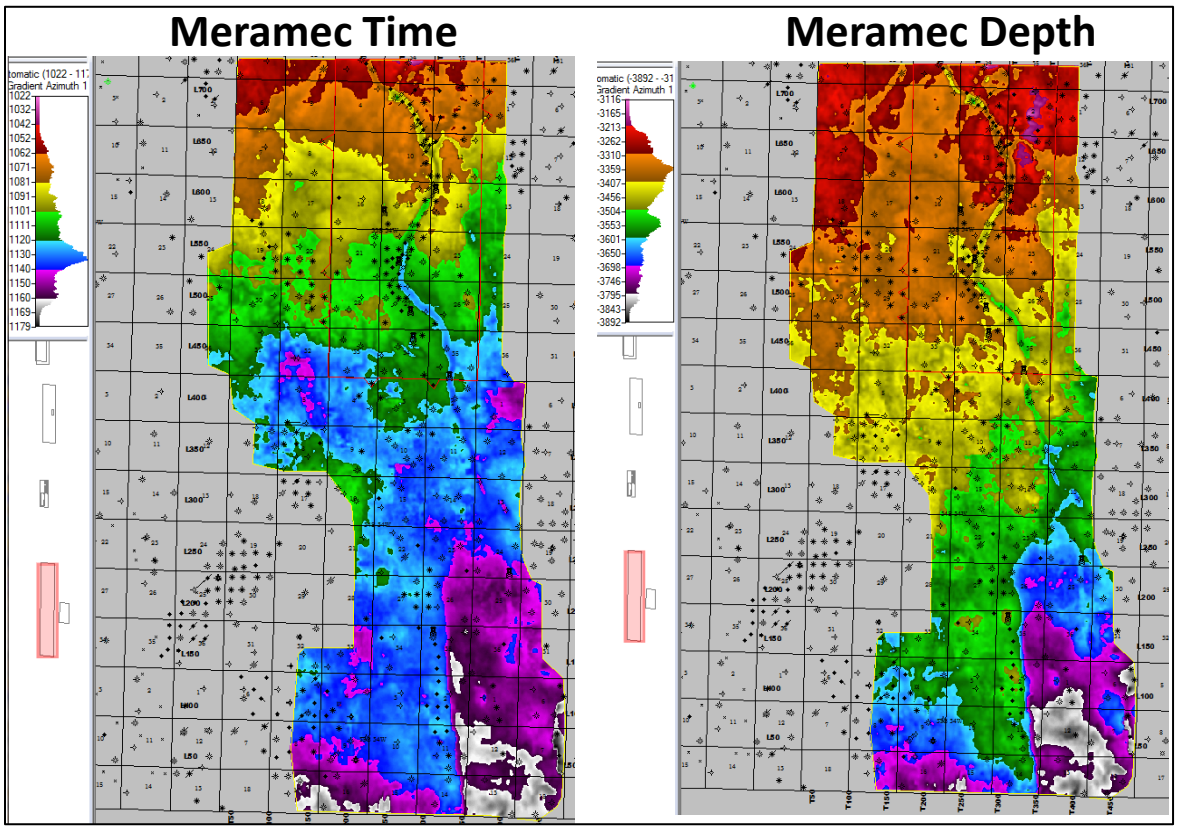

Figure 85. Near surface velocities coupled with real stratigraphic complexity render the overall time structure indications to be of somewhat limited use. However, Depth Converted Structure is reasonably well adjusted due to significant well control availability. The structural nose in the south central portion of the Meramec Depth contains a reverse fault on the east flank.

Depth 1 – Slightly reduced detail **Depth 2 – Slightly increased detail**

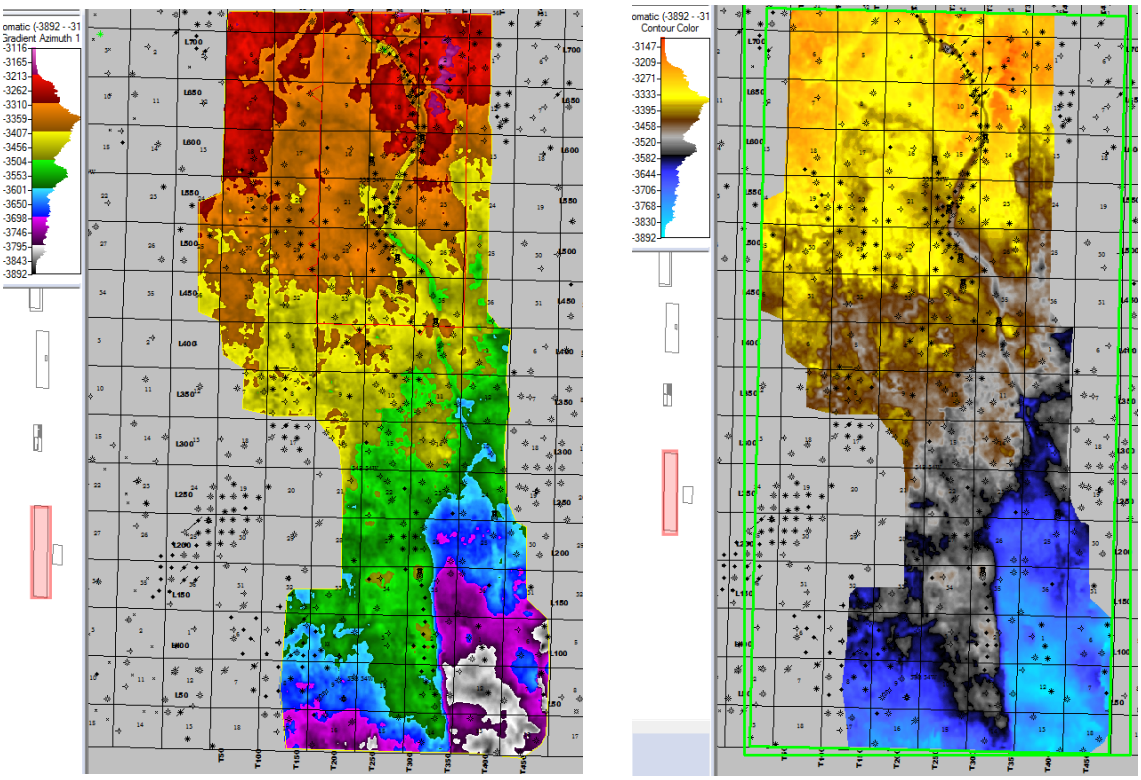

Figure 86. Meramec Depth – Dynamic Range Comparisons.

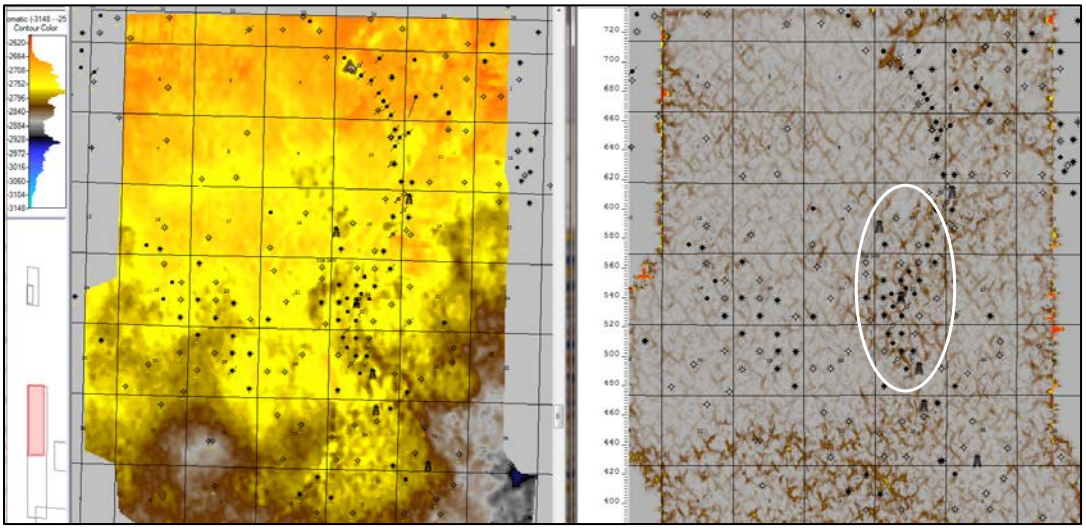

Figure 87. Shuck Area - Morrow Depth Structure w/ Most Negative Curvature 996 ms. Note distinct NW-SE Lattice in VC image, and the correlation of the Karst feature in the NW4 section 3, coalescing the intersection of VC lineaments. Note also the increased chaotic, disturbed VC character in the Shuck Field proper.

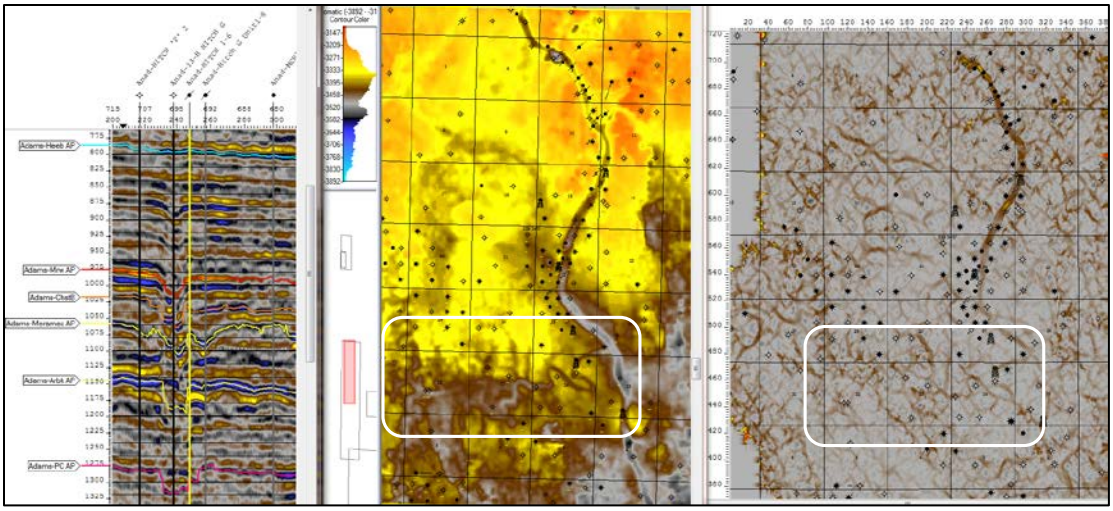

Figure 88. North Shuck Area - Arbitrary Profile Thru Karst Feature w/ VC 1096 ms. Note structural collapse at Anad-13H Hitch G: Top Morrow at 13H (-2884), 1024 ms; that at Hitch 1-6 (-2719), 990 ms. Top Meramec at 13H (-3472), 1095 ms; that at 1-6 (-3398), 1073 ms. Locally, North end trap in IVF occurs at the Karst feature. Lattice structure in VC still evident. Southern meander belt also expressed in VC.

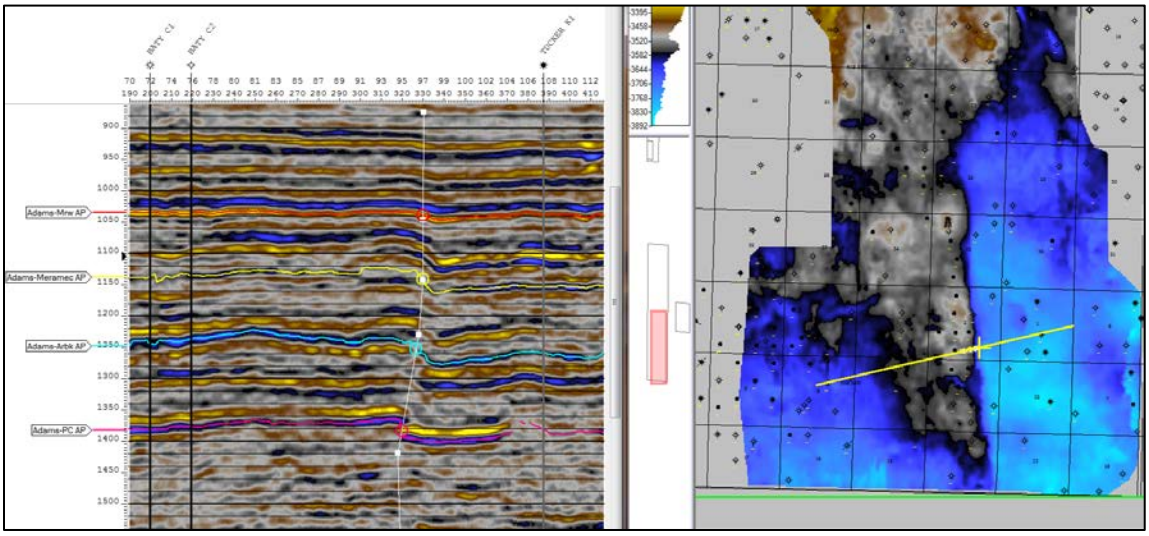

Figure 89. Archer – Liberal West Reverse/Strike-slip Fault -- Horizontal offset from trace 330 (fault tip) to trace 319 (below Precambrian) is approximately 1200 ft. Meramec datum at Baty C1 (-3648), that at Tucker K1 (-3809); Vertical relief 161 ft.

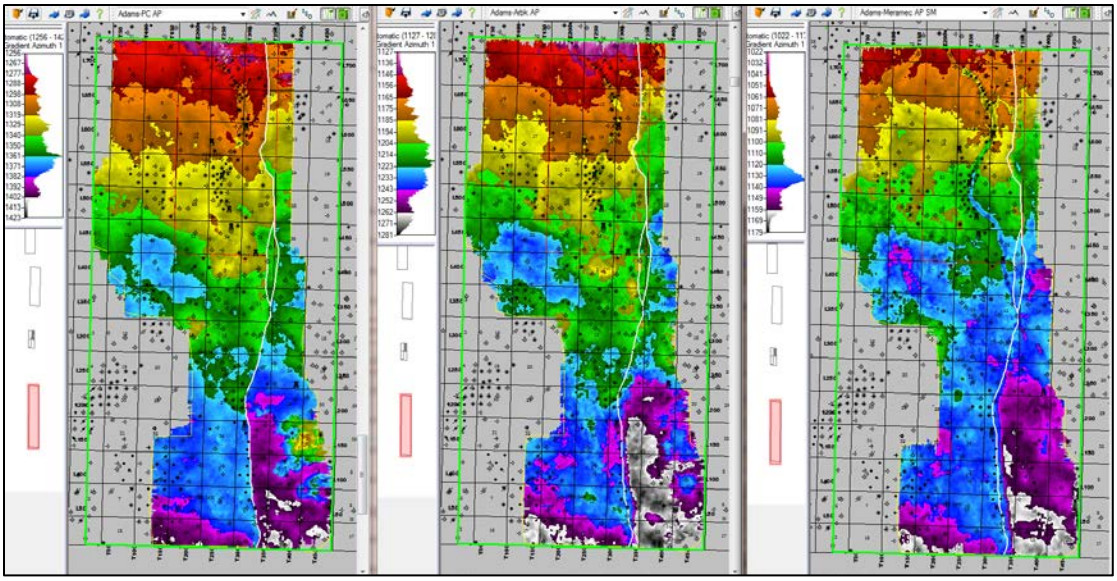

Figure 90. Primary East Bounding Fault - Shuck to Liberal West. Leftmost image is Basement Time, illustrating approximately 2 miles of northward movement of right block relative to left. Lower segment is thrust related, middle region exhibits primarily vertical to normal faulting, northern region returns to slight high angle reverse displacement. Arbuckle Time illustrates the overhang in southern region; Meramec Time illustrates overhang in northern region.

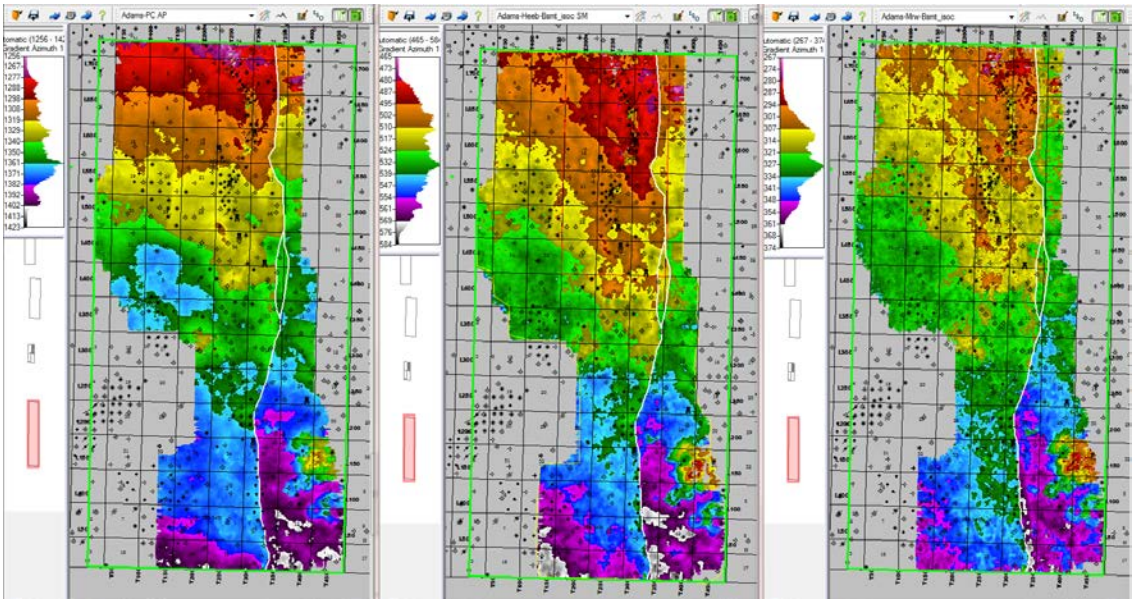

Figure 91. Shuck –West Liberal High-Angle Reverse/Strike-Slip Evidence in Isochrons. Left Image Basement Time, Middle Image Heebner-Basement Isochron, Right Image Morrow-Basement Isochron. It would appear that the corroboration of strike slip movement is evidenced in each of these isochrons, probably more so in the Heebner to Basement.

The structural activity north of Shuck 3D seismic area includes Pleasant Prairie, Eubanks, and Cutter Fields. While the evidence of strike-slip deformation are not proven with clear evidence of lateral movement, the observations from the seismic clearly point to this indicating that tectonic stress was transmitted considerable distances onto the shelf.

Figures 92-117 provide snapshots of the other 3D seismic surveys in the three fields north of Shuck area.

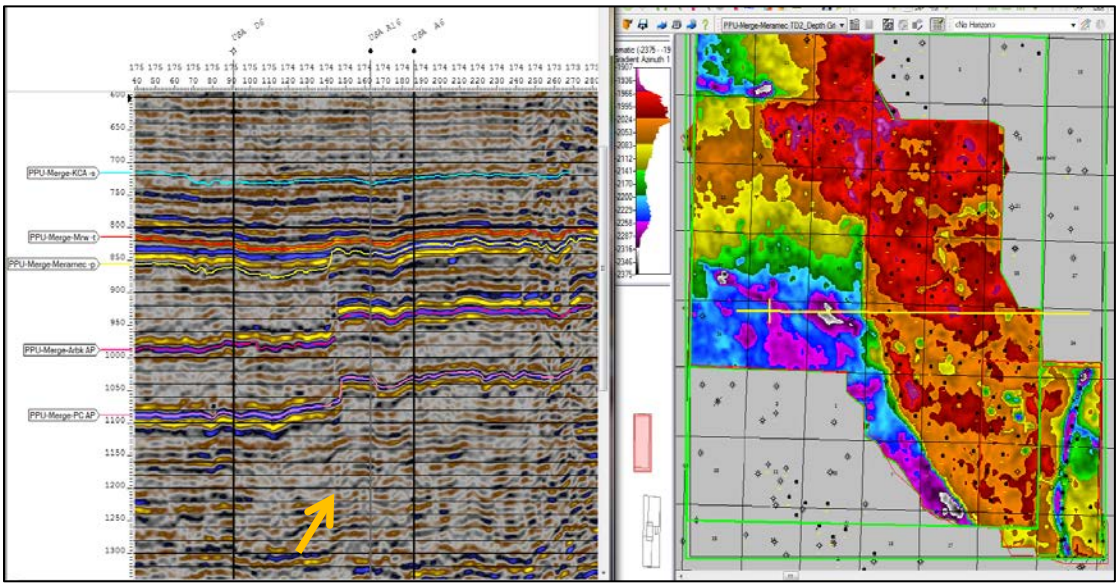

Figure 92. Pleasant Prairie Seismic -- Profile illustrating structure in vicinity of west bounding reverse fault (orange arrow at fault cutting Proterozoic rock. Top Meramec at USA D6 (-2237), at A16 (-2043), at A6 (1999). Note that bounding fault (sta 142 at Meramec, drifts east to sta 147 at PC, implying 550 ft offset. Also, not the increase in the Meramec-Arbuckle isochron west of the bounding fault. Smaller fault immediately east of the bounding fault affects Arbuckle, but not the top of Meramec suggesting an earlier, pre-top Meramec movement.

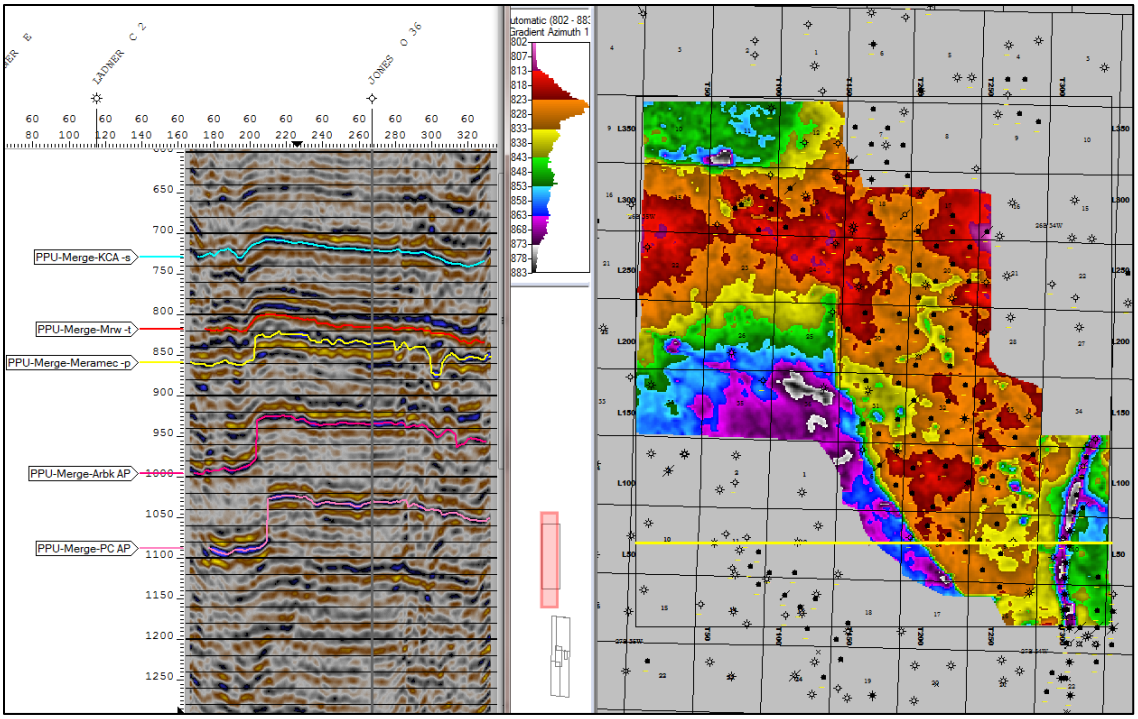

Figure 93. Pleasant Prairie -- West Bounding High Angle Reverse Fault. Fault tip at 650 ms (above KCA horizon) occurs at Crossline 196, tip at Basement at 1028 ms occurs at Crossline 209. West-east offset is 1430 ft. Heart of IVF is seen at Crossline 302. Map is Meramec Time. IVF along west flank of an apparent horst block bounded by high-angle reverse faults. Eastern edge of horst is broken by discontinuous reflectors and staggered offsets indicative of a fracture zone along which the IVF apparently followed due to structurally compromised strata. Note again that the Meramec-Arbuckle isochron thickens across the western bounding fault. Internal reflectors suggest thickening of the Mississippian strata in this interval on the downthrown side, i.e., evidence for concurrent growth of the structure during sedimentation.

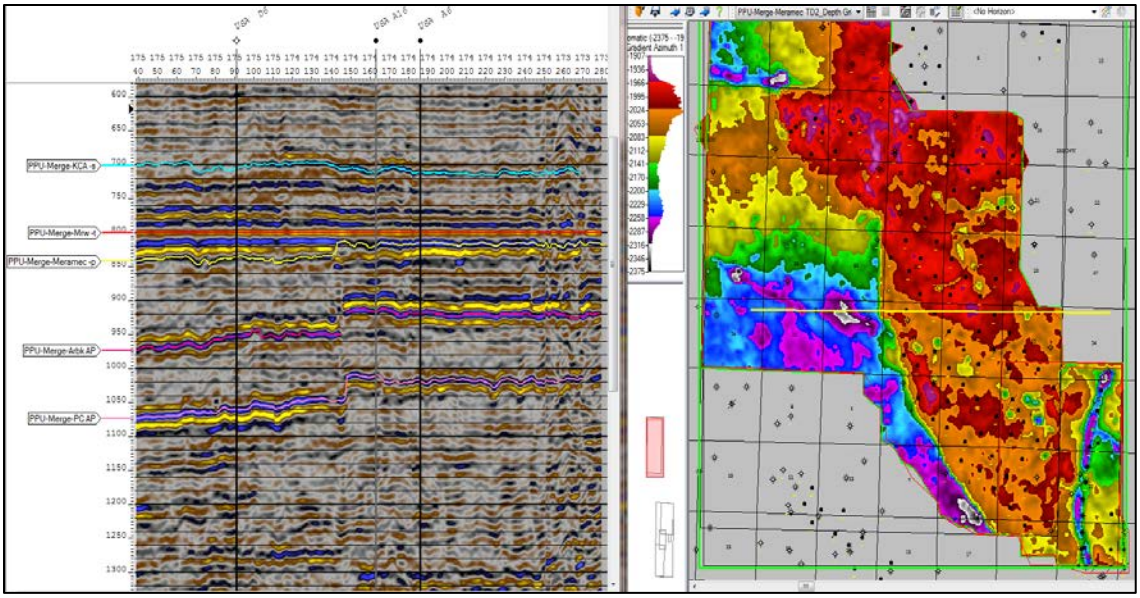

Figure 94. Pleasant Prairie Stratigraphy. West-East Profile Flattened @ Morrow = 800 ms. Note that Meramec – Arbuckle thickens ~ 15 – 30 ms on downthrown side. Arbuckle-PreCambrian also thickens ~ 15 ms on downthrown side. Note also that KCA – Morrow thickens ~ 8 ms on downthrown side. The core of the horst block is intact while the east side again shows discontinuous seismic reflectors.

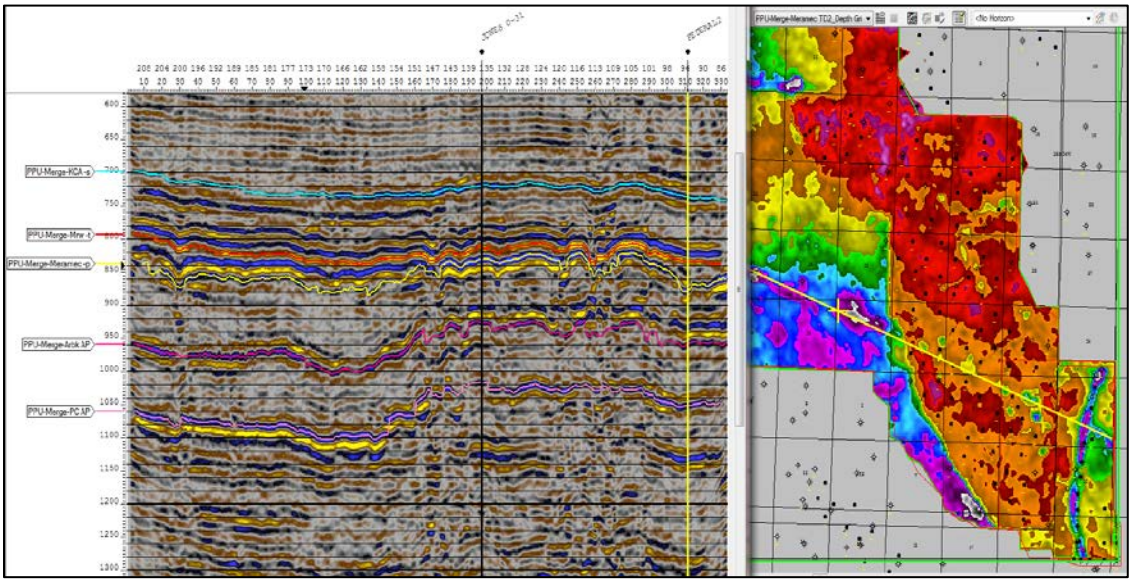

Figure 95. Pleasant Prairie Karst. Arbitrary profile illustrating multiple karst features. In most cases, 'pipes' extend well below Meramec, into Arbuckle/ Prominent features noted at stations 30, 170, 242, 260. IVF system at sta 310, note that profile continues SE of Federal 2 to the IVF tributary. The karst appears to be linked to fragmentation of the horst block especially on the edges. The radiating patterns are also suggestive of a flower structure suggesting strike-slip deformation perpendicular to the plane of the seismic section.

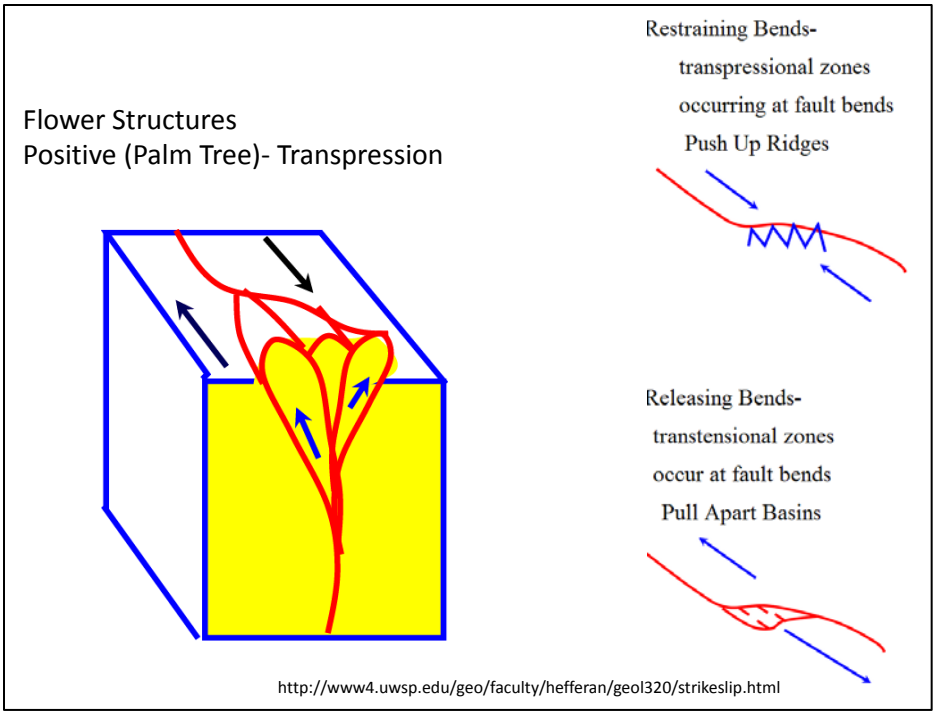

Figure 96. The flower structure results from the accommodation of a change in the direction along a strike-slip fault system, the one shown on the left being a right-lateral fault. A bend in the fault can lead to a push up ridge as illustrated in the upper right. The horst block at Pleasant Prairie with flower structures suggests that it is developed along a restraining bend. The deformation is long lived from the Arbuckle well into the Upper Pennsylvanian.

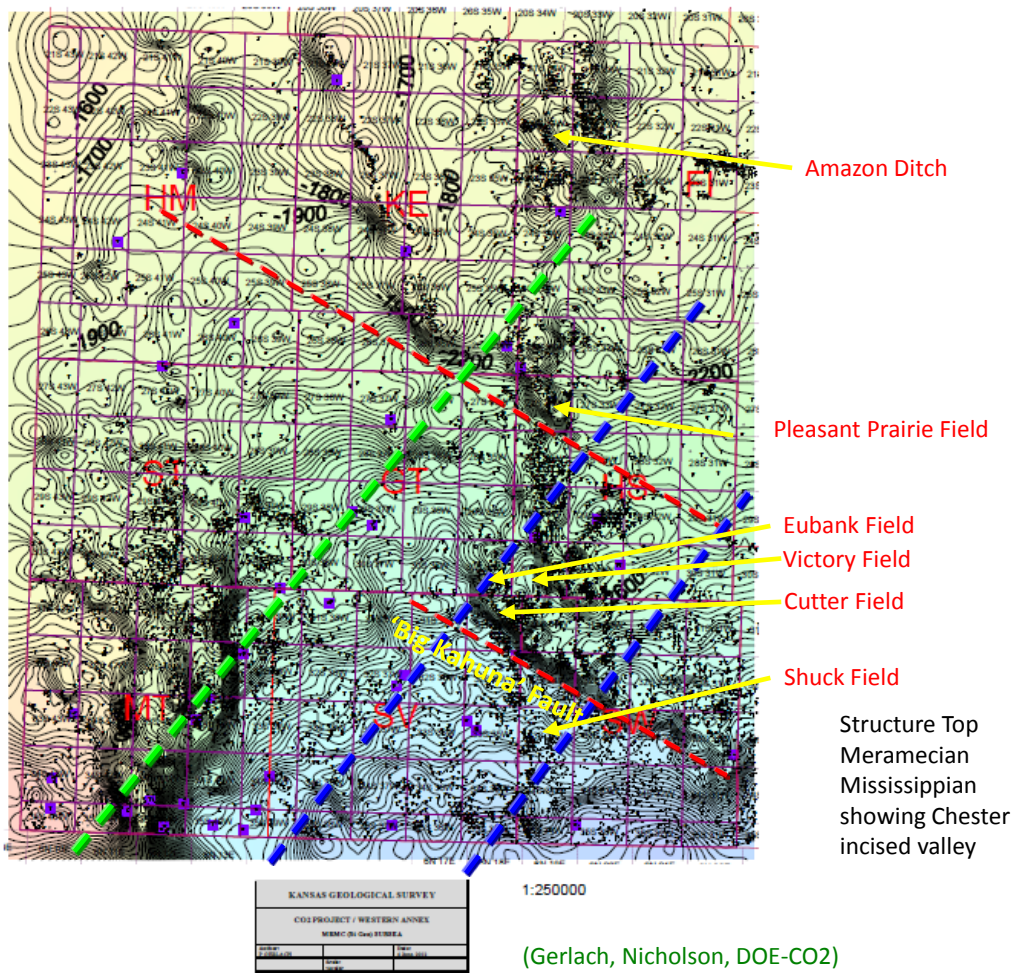

Figure 97. Top of Meramec structure in southwest Kansas with the location of Shuck and Pleasant Prairie fields discussed thus far in this section. Shuck and Pleasant Prairie fields lie along the interaction of lineaments that are long lasting. Shear stress transferred to the shelf from the basin appears to have interacted with these lineaments transferring the stress to inherit weaknesses leading to bending of the faults.

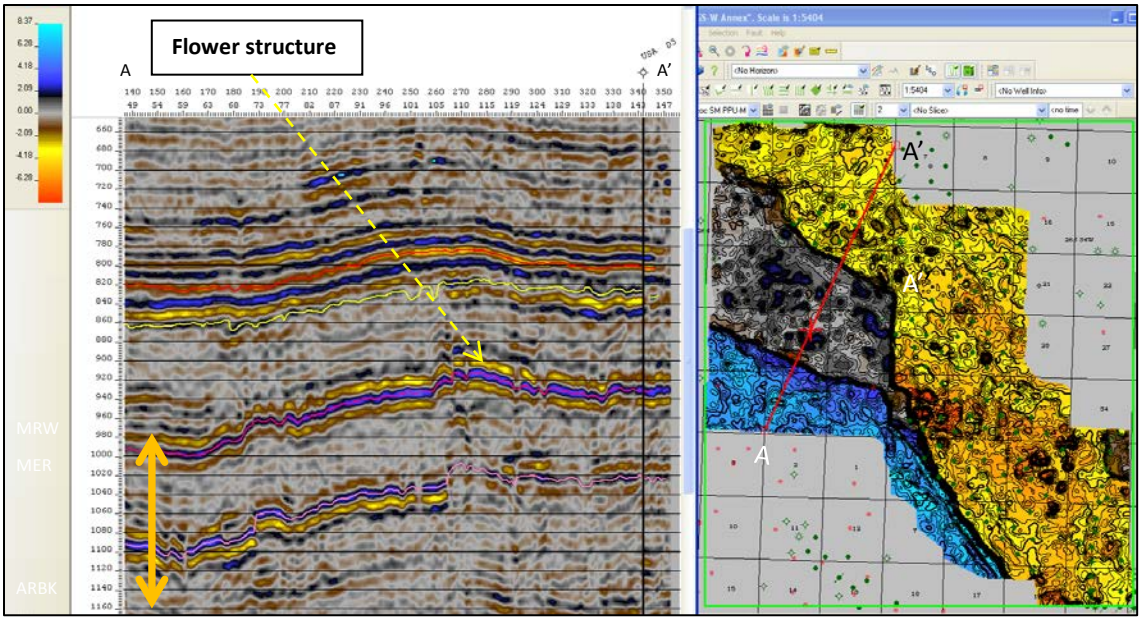

Figure 98. Pleasant Prairie – Morrow - PC Isochron -- Note that while structural arch is clearly exhibited, isochronal thickening occurs in discrete step changes at two fault zones. Radiating fault pattern clearly identify a flower structure along the inner fault zone, not the leading fault. The leading fault zone is comprised of a number of faults, but they are not developed in as clear a radiating pattern. The IVF is not expressed in this isochron. Multiple karst intervals are present including 1) concentration covering the structural terrace between the bounding and inner fault on the northwest, 2) the NW-SE trend in the SE portion of the map that extends east of where the bounding fault would project rather than the bend to the south.

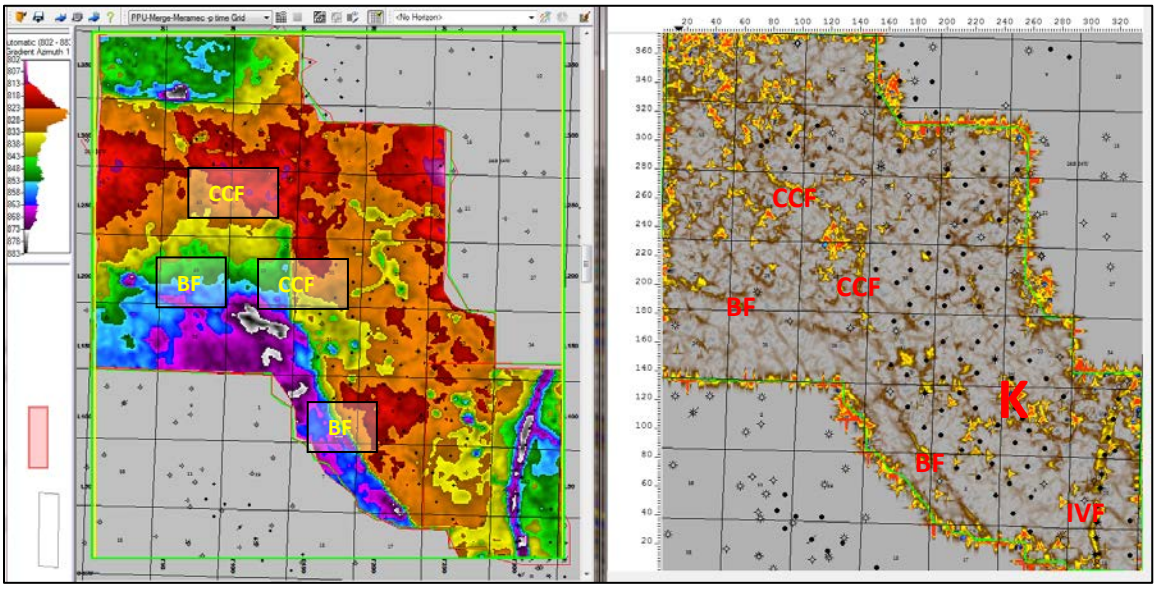

Figure 99. Pleasant Prairie Meramec -- Meramec Time Structure (left) and Most Negative Curvature at 860 ms (right). West bounding fault (BF), cross cutting fault (CCF), karst (K), and IVF are all well expressed.

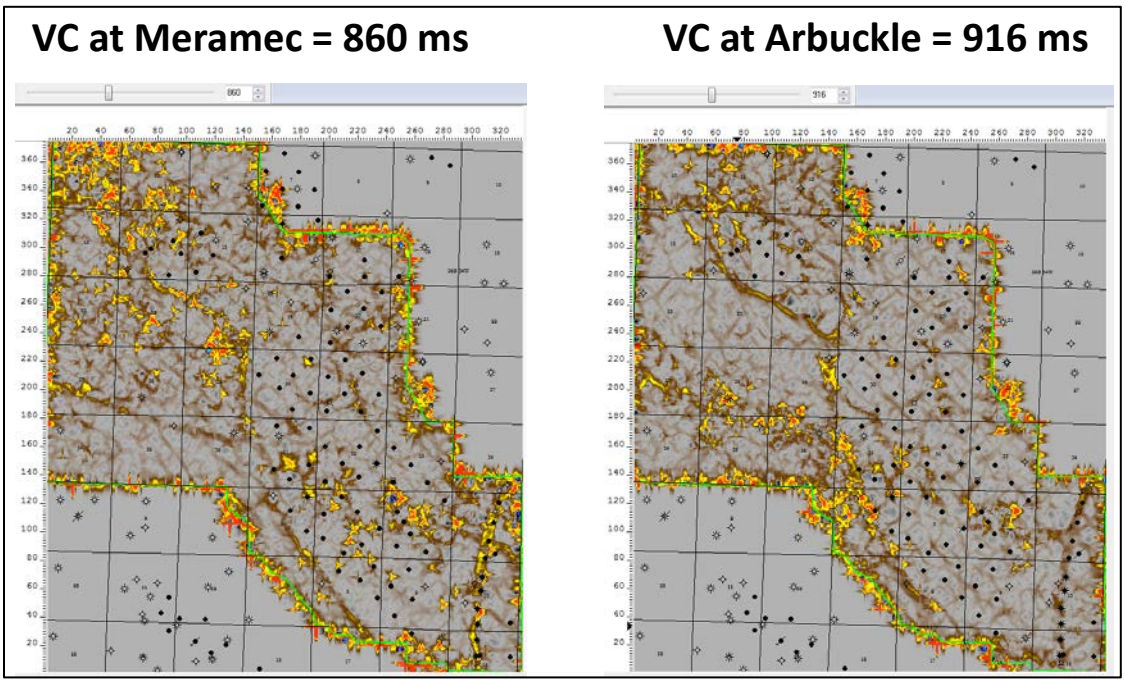

Figure 100. Volumetric curvature at the Meramec and the Arbuckle are very similar reflective of the scale of faulting affecting both horizons. The NW-SE trending karst in the southeast is also similar.

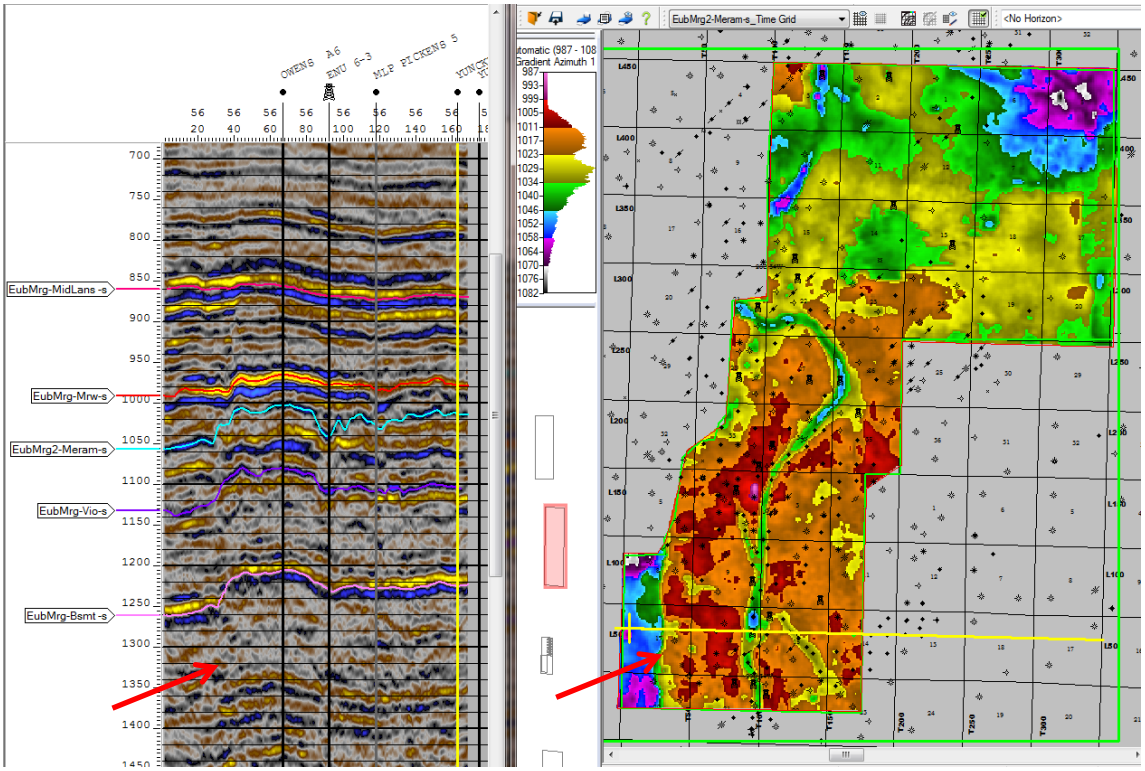

Figure 101. Eubank Seismic Expression – Note west bounding normal fault (red arrows) at approximately crossline 40. Profile crosses elevated structure, IVF and

tributary to IVF. IVF cut (Crossline 92) is not as deep as downthrown block at Meramec. Tributary shallower yet at Crossline 120. Top Meramec at ENU 6-3 (-2563), at Pickens 5 (-2438). Pickens 5 not drilled in deepest Meramec cut in tributary. IVF similar to Shuck and Pleasant Prairie where IVF is on the east edge of the current day structural high. Isocore thinning over the structural highs suggests concurrent structural deformation during sedimentation and probably during the formation of the IVF.

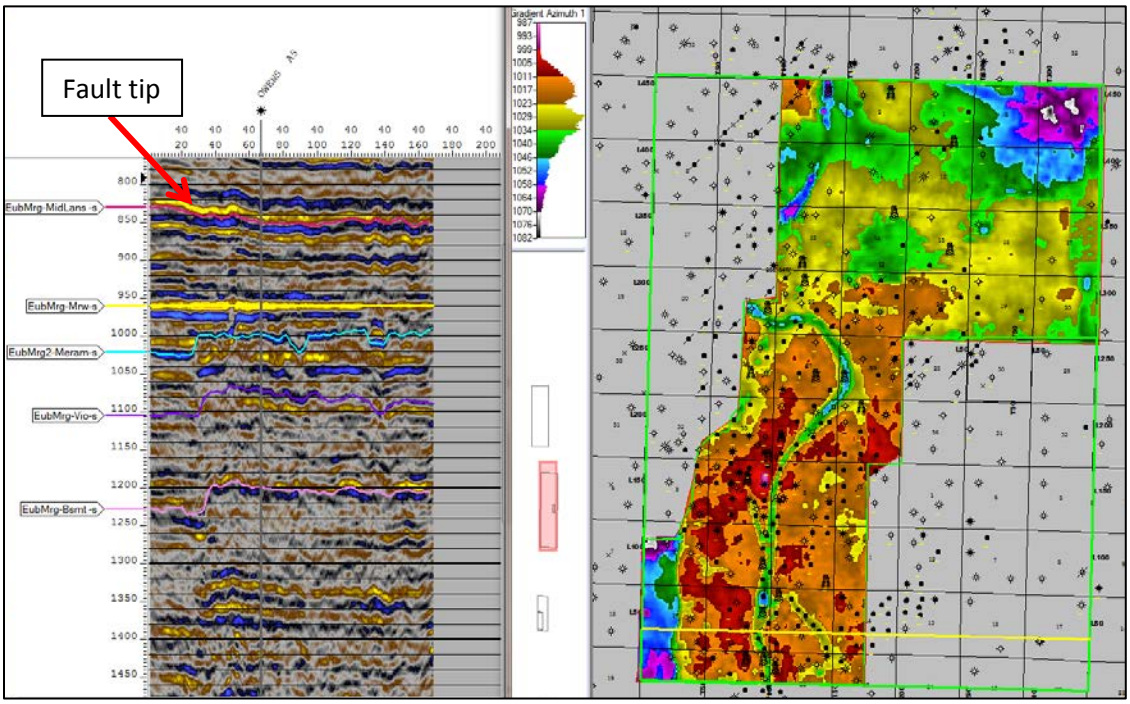

Figure 102. Eubank Seismic Flatten Profile @ Morrow = 960 ms -- Downthrown block thickens at Meramec, but isochron intervals from Meramec to Viola and Meramec to Basement are generally consistent on upthrown and downthrown blocks, although the offset on the basement is greater than at the Meramec. This implies most movement occurred post-Meramec. Note that fault tip (red arrow) at Mid Lansing occurs at Trace 26, tip at Basement occurs at Trace 36, yielding a west-east drift of 1100 ft, a high angle reverse fault. Block on east is extends over block on west. The both the IVF incisions cross the line of section downdip relative to current structure and overlie zones of truncation of seismic horizons, albeit more subtle than in Pleasant Prairie and Shuck.

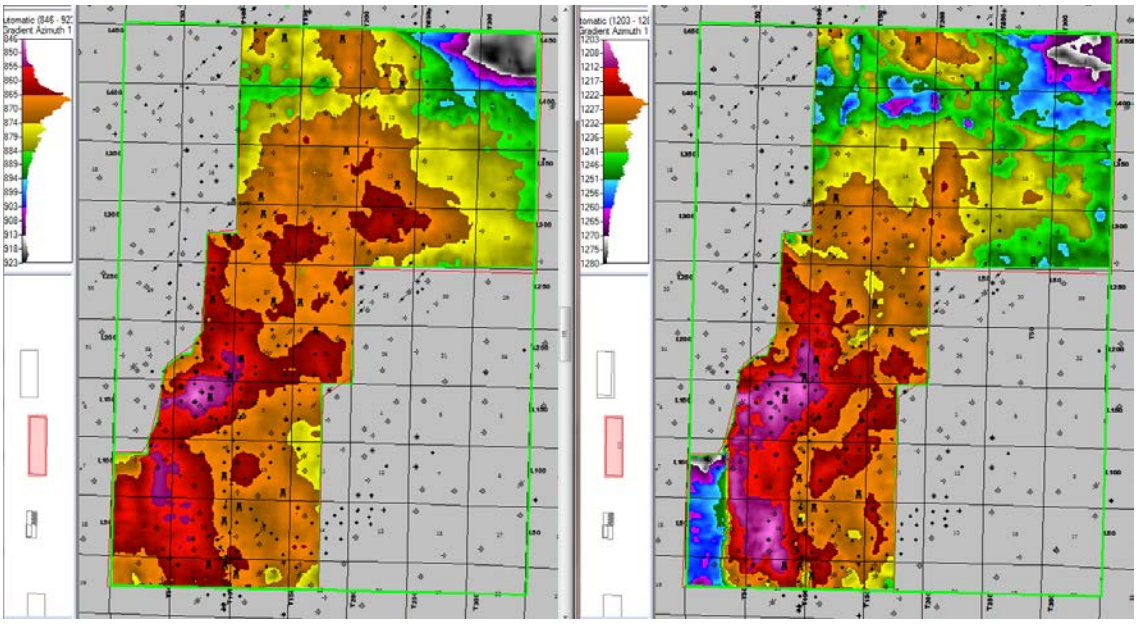

Figure 103. Eubank Structural -- Mid Lansing Time (left), Basement Time (right). Note the persistent expression of the structure deep and shallow even though the major tectonism precedes the Mid Lansing horizon. Also note that the trace of the IVF wraps around the eastern and northern edges of the current day structure strongly suggesting the structural deformation is to some degree through going and episodic. The structure also creates a rectangular block with N-NW and NE-trending edges. These trends parallel the regional lineament trends (Figure 97). The Eubank structure may be another restraining bend with a reverse fault on the west and smaller scale faults and fractures on the east suggesting tensional stress on that side. The would support a right-lateral strike-slip deformation.

Meramec Time Structure **Meramec Depth Structure**

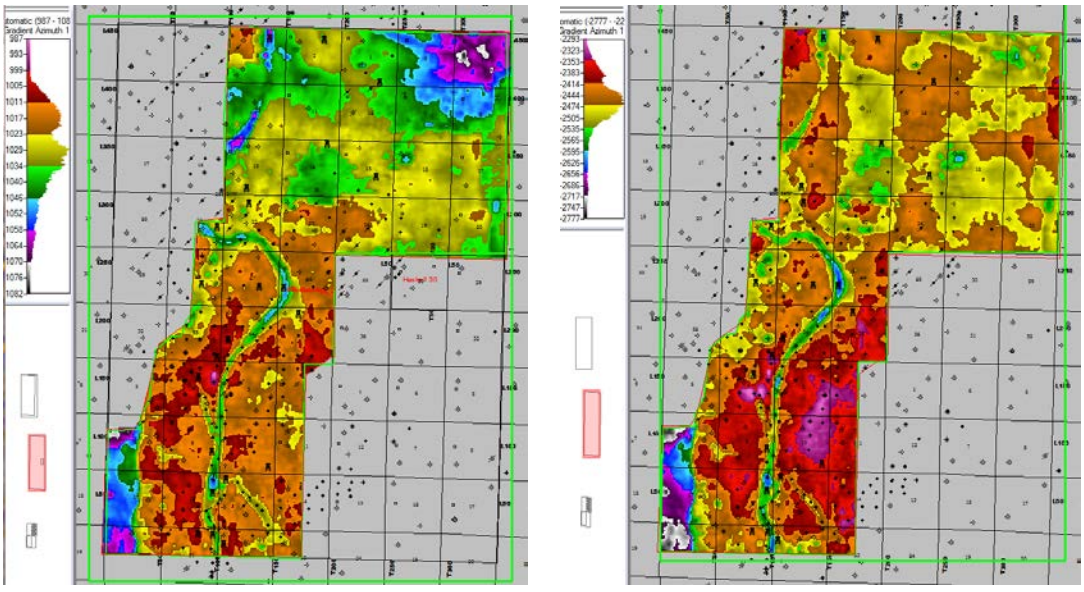

Figure 104. Meramec Time Structure (left) and Meramec Depth Structure (right) – The depth structure places the structural high to the east of the IVF with the IVF bisecting the current day structure.

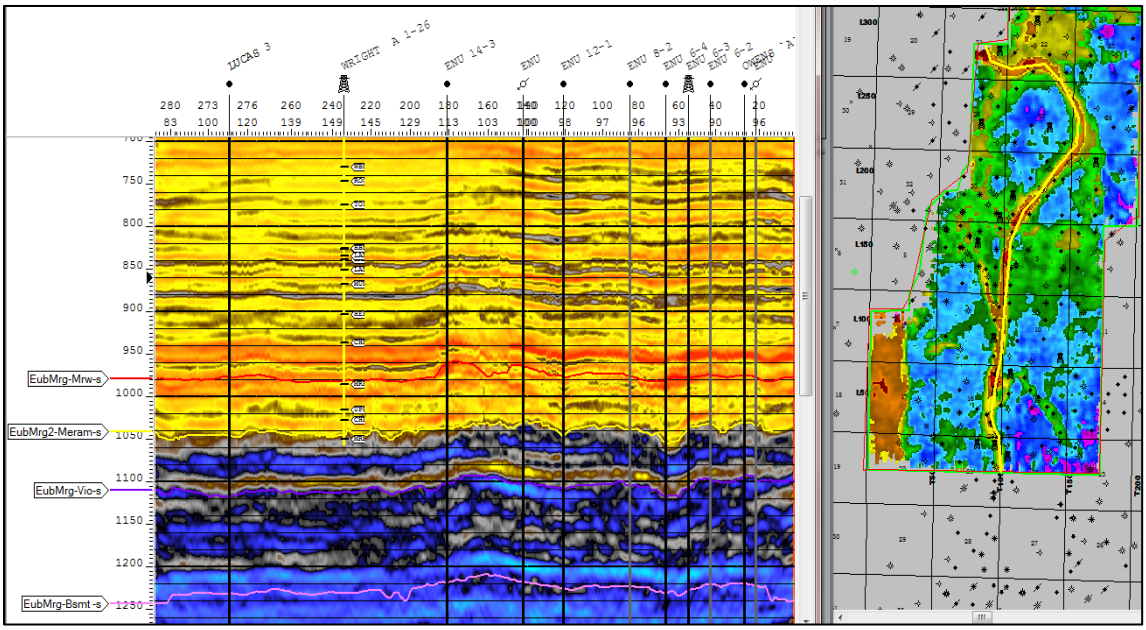

Figure 105. Eubanks Velocity from Impedance Inversion -- Arbitrary Profile thru thalweg (deepest portion) of the IVF, left is north. Map is Morrow – Meramec Isochron (purple and blue areas suggest thining and brown and yellow areas are thicker). Max velocity (light blue) ~25,000 fps; Min velocity (yellow) ~12,500 fps. Morrow & Chester Sands populate lower half of interval between Morrow/Meramec. The IVF crosses two areas of thinning with seeming disregard for the interval thickness. Also, the beds in the Ordovician interval lack continuity compared to shallower intervals, consistent with earlier amplitude profiles and observations from Shuck and Pleasant Prairie fields.

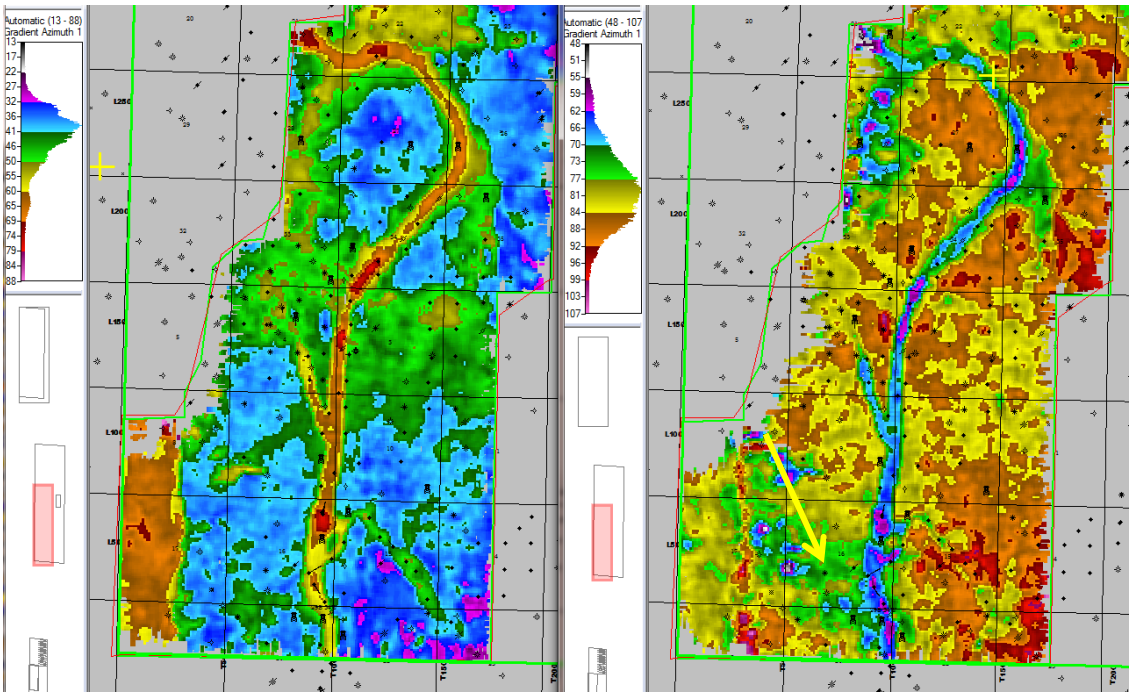

Figure 106. Morrow – Ordovician Stratigraphic Context -- Leftmost map is Morrow-Meramec Isochron. Rightmost map is Meramec-Ordovician Isochron. Both color schemes have blues as thin, yellow-brown as thick. Where IVF occurs thick Morrow-Meramec overlies thin Meramec-Ordovician. West bounding fault not so noticeable on Meramec – Ordovician isochron. The areas of thickening and thinning run are consistent except 1) thickening west of the bounding fault is greater in shallow isochron, the interval encompassing concurrent and maximum structural activity and 2) the SW mapped area between the bounding fault and the IVF on the deeper Meramec-Ordovician isochron (yellow arrow). This rectangular-shaped feature thins in this lower interval suggesting local uplift just prior to or near the time the IFV was formed that is consistent with the regional lineaments (Figure 97). This thinning may be a local structural block as part of a restraining bend, with reverse faulting on the west and more tensional on the east – suggesting right lateral sense to the fault.

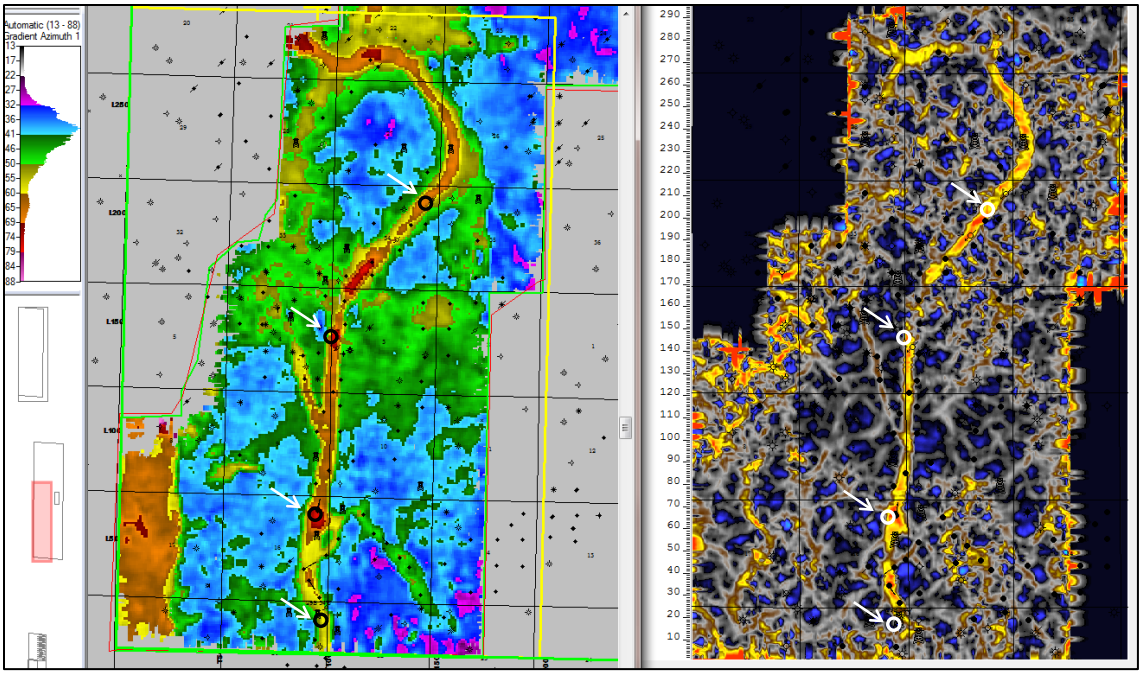

Figure 107. Morrow – Meramec Isochron (as shown previously) -- Most Negative Curvature Near Base IVF Time. NW- and NE-trending lattice fabric of curvature elements in background are generally independent of IVF orientation in south half of map, but are subparallel to the IVF on the north. West bounding fault somewhat expressed W2 section 17. Suggested sinkholes and possible leak points for inferred fluid loss in the IVF sandstone reservoir during waterflood indicated with white arrows. The inferred sinkholes correspond to boundaries where overall VC fabric undergoes change in density and frequency of change. These larger boundaries are also NW- and NE-trending.

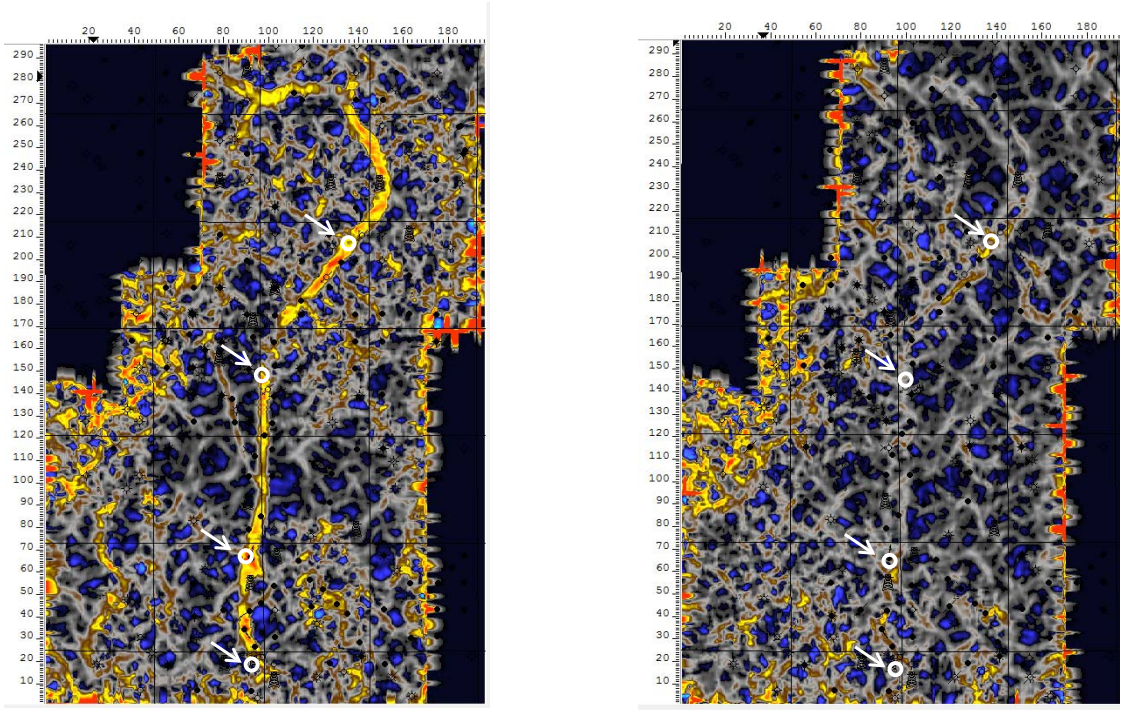

Figure 108. Eubanks Most Negative Curvature -- Basement Lattice Pattern Influences IVF. At the locations indicated by arrows, it would appear that in each instance significant intersections of lattice systems occur. This is evident in both Ordovician as well as Basement VC slices. It would be appropriate to expect that leakage out of IVF into surrounding rock systems could occur if these inferred basement fractures propagated upward, and thereby providing an explanation for volumetric requirements in accounting for 'lost injected fluids'. This leakage could occur either laterally or vertically downward.

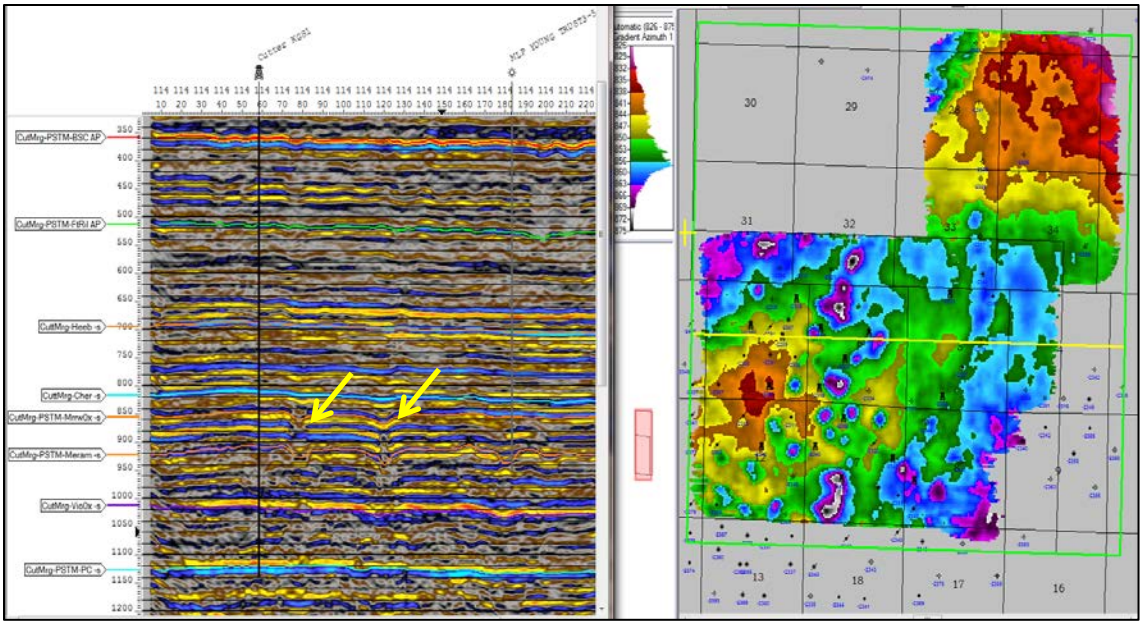

Figure 109. Cutter Amplitude & Morrow Time Structure -- Morrow Time Structure illustrates Karst, which is exemplified in the profile. At traces 80 and 120, apparent collapse well into Mississippian (yellow arrows), and vertical discontinuities appearing to continue up to and above the Stone Corral. IVF at 180.

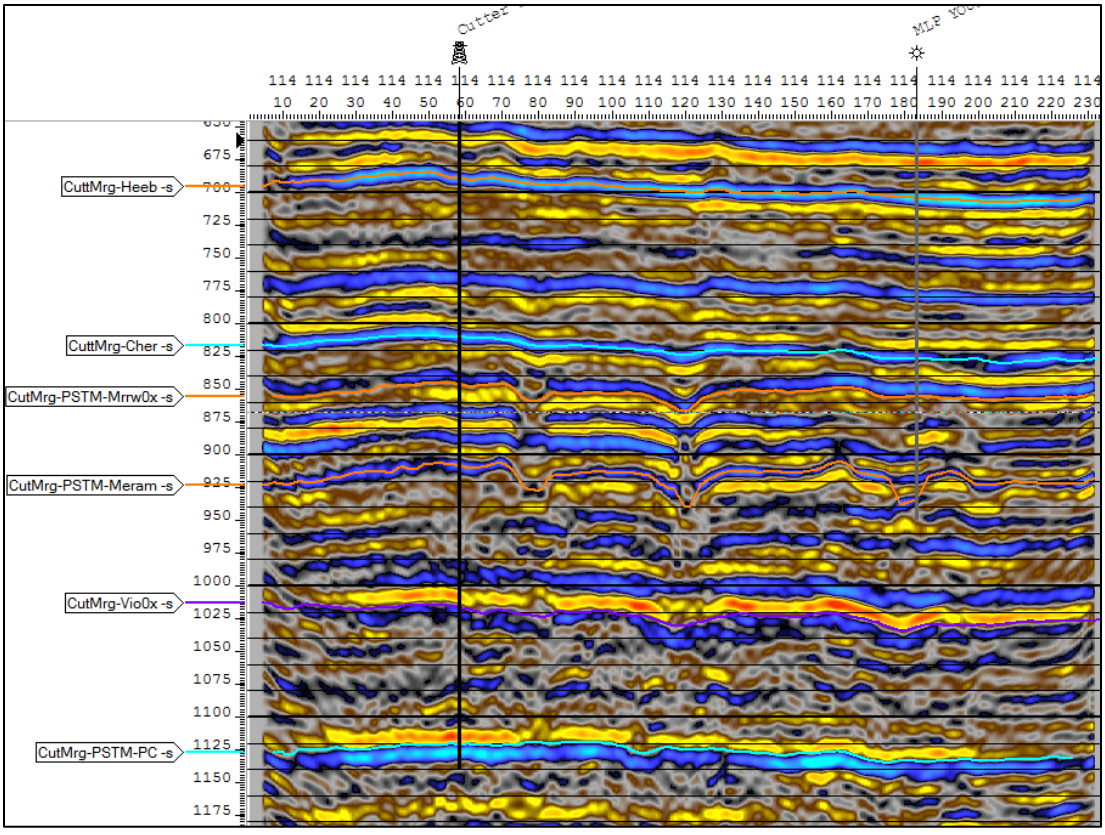

Figure 110. Cutter Amplitude, Inline 114 -- Note the signal disruption at the top of the Viola in two places extending upward to the Top Morrow datum. These features

do not extend further upward and suggest the karst is linked to the uplift and tectonism at in the early Pennsylvanian. These disruptions are circular features (Figure 109, rightside map) that are probable karst pipes. As suggested in the map, a pattern of karst-like features extend along a N-NE trend just east of the Cutter KGS #1 well. Upper Morrow productive sand occurs in the yellow amplitude interval immediately below Morrow Time surface. Morrow datum at KGS 1 (-2268), at MLP Young Trust 3-5 (-2315). Meramec datum at KGS 1 (-2701), at MLP (-2821). Interval at KGS 1 = 433 ft, that at MLP = 506 ft.

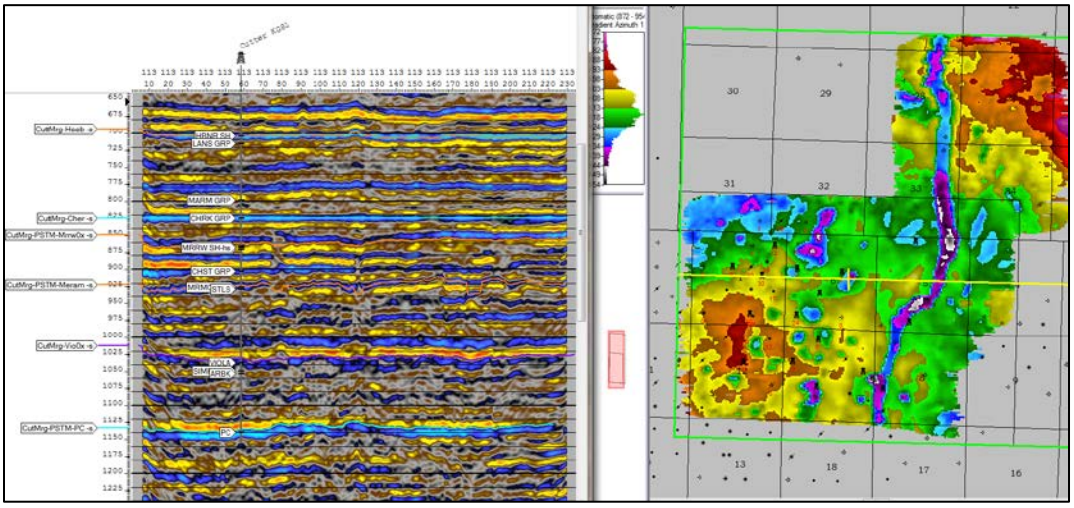

Figure 111. Cutter Seismic, Flattened at Cherokee = 825 ms -- Illustrates very little, if any Pre-Cherokee stratigraphic change in deeper systems. Mississippian-aged karst features had been established much earlier. Note lack of general bed continuity again in Lower Ordovician Arbuckle, as compared to generally consistent bedding in Mississippian beds in most of Lower Mississippian.

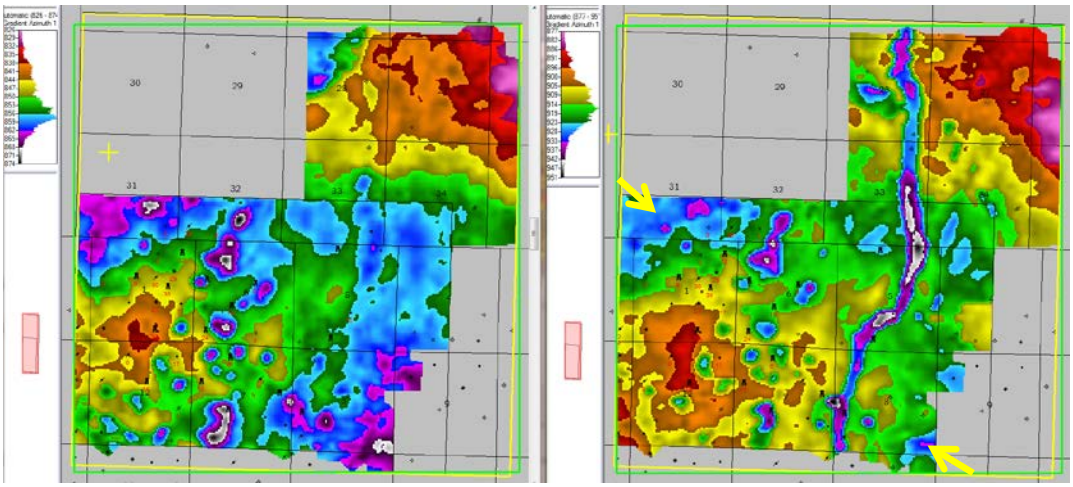

Figure 112. Cutter Morrow Time (left) & Meramec Time Structure (right) -- A dominating karst trends NNE – SSW bisects the Cutter Field Structure. At the Meramec horizon an additional WNW – ESE trend to karst features runs at north end of Cutter, through the IVF (between yellow arrows in map on right).

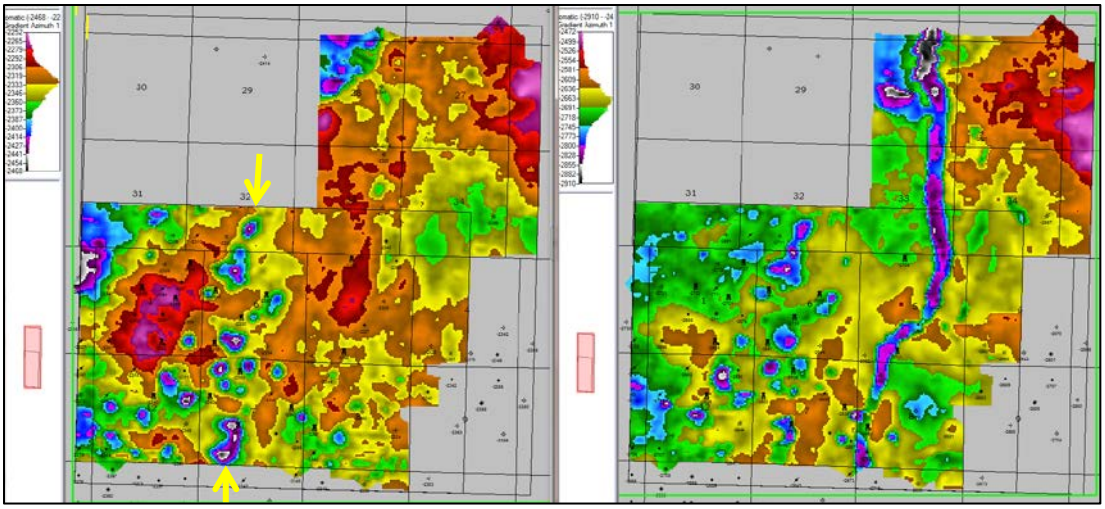

Figure 113. Cutter Morrow Depth & Meramec Depth -- Well defined east edge of Cutter Morrow structure, where karst features are clearly aligned (between yellow arrows). This same dominant lineament persists through Meramec. In a broader context, it would appear that the Cutter Field (Morrow) is separated by this N-S trending karst plain, from another feature to the east that culminates in a structural high in section 5.

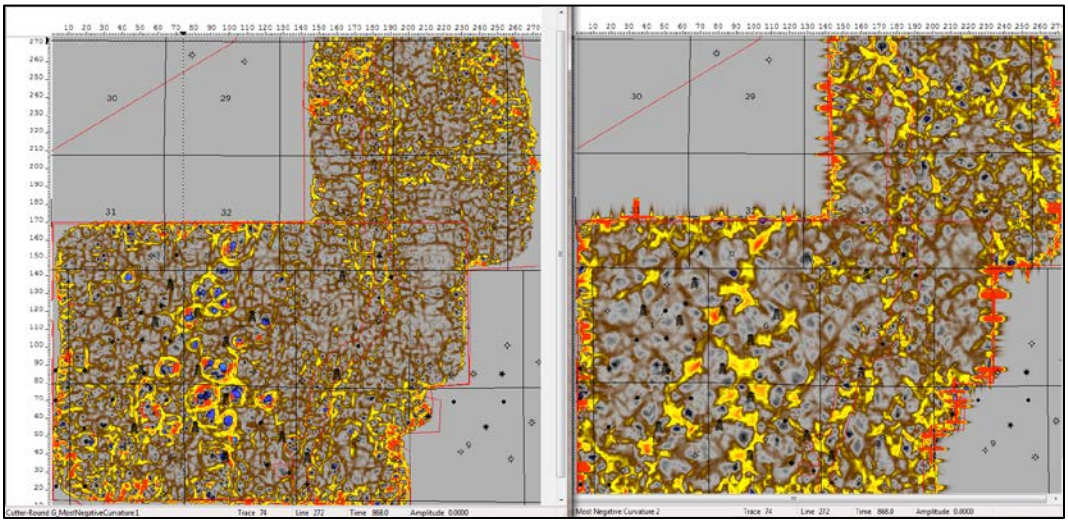

Figure 114. Cutter – Most Negative Curvature. Upper Morrow (868 ms) -- Higher resolution curvature (left) compared to lower resolution (right). Higher resolution manifests the N-S trending sinkholes, while lower resolution manifests apparent underlying fracture systems that trend NW- and NE. Light red outline in eastern image area outlines IVF, includes both Morrow and Chester production.

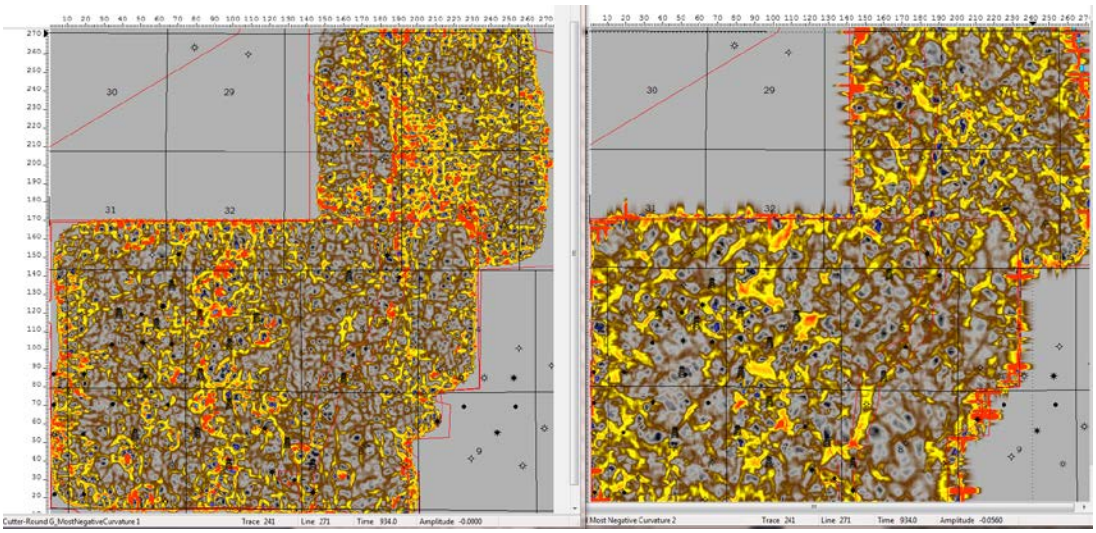

Figure 115. Cutter – Most Negative Curvature Meramec (934 ms) -- Higher resolution image illustrates coalescing of N-S oriented sinkholes expressed higher in stratigraphic section. Lower resolution image continues to express similar trends to those higher in stratigraphic section.

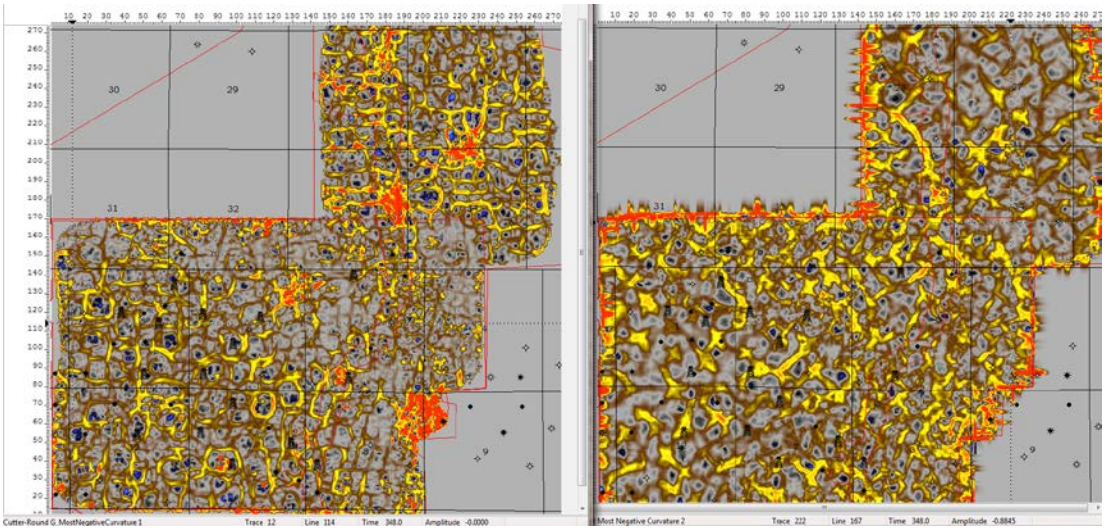

Figure 116. Cutter – Most Negative Curvature Stone Corral (348 ms) -- While the pattern is generally more rectilinear, the expression of NNE – SSW trends persist in the eastern reaches of the higher resolution image. Apparent widespread karst related sinkholes fill the southern portion of the higher resolution image (left), while the lower resolution character expresses much more linearity, consistent with deeper zones.

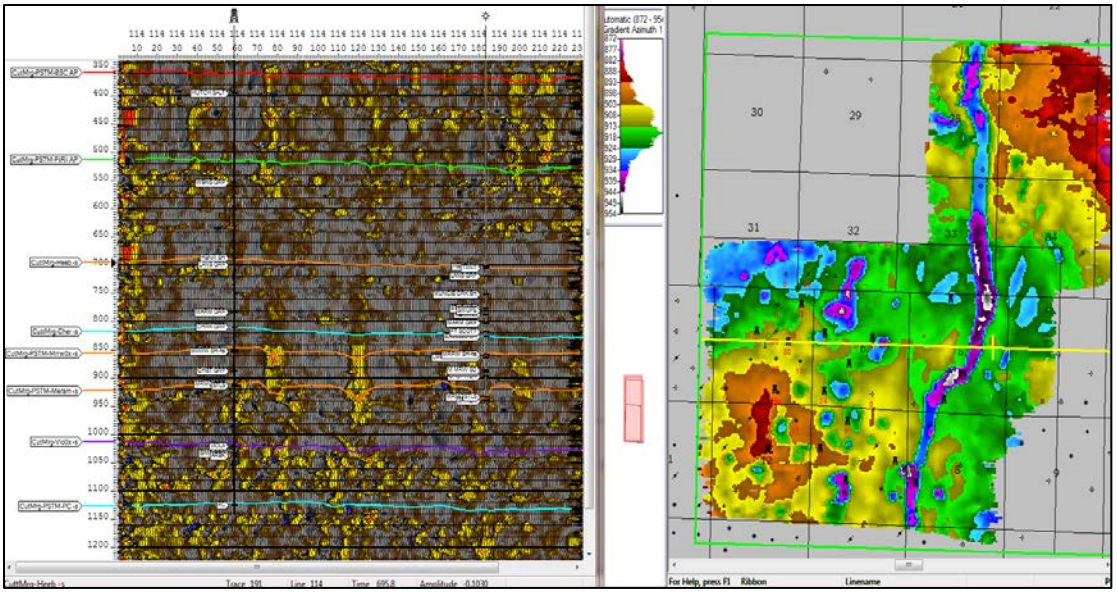

Figure 117. Cutter – Most Negative Curvature Vertical Profile West-East thru Cutter KGS1 -- Image Stretched vertically, covers stratigraphic section from Stone Corral to Basement. Map is Morrow Time with profile location that includes the two karst features that are part of the N-S karst trend. Vertical anomalies are abundant in the pre-Viola interval and into the basement. Less numerous features extend up through the top Morrow horizon. more or less continuo vertical features dim to above the Lower Permian Ft. Riley Limestone and then increase again above that horizon.

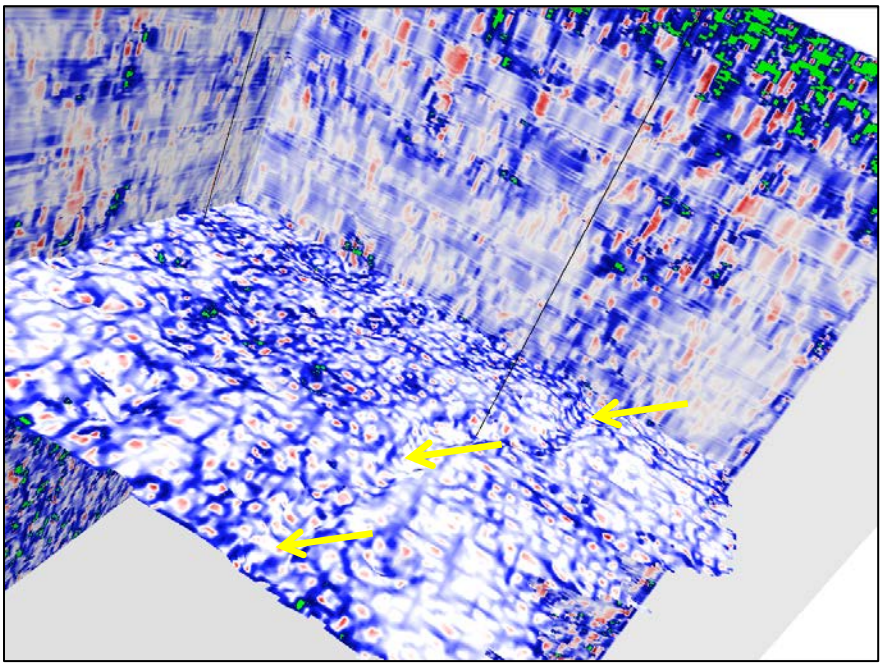

Figure 118. 3D Visualization Most Negative Curvature – Meramec Time surface draped with MNC amplitude overlay. IVF with penetration of MLP Young 1-5; KGS Cutter 1 near west vertical profile; multiple Karst sinks. Note broad disturbed zone north wall profile above IVF (delimited with three yellow arrows).

Conclusions Regarding Risk of Leakage of CO2 as Evidenced in Regional Seismic and Associated Mapping – Contributed by Dennis Hedke and Lynn Watney

1. Based on results from multiple seismic surveys throughout the Western Annex, as well as that at Wellington Field in Sumner County, KS, it is highly improbable that containment of CO2 within any given reservoir or injection zone can be assumed without the due diligence of system characterization to establish evidence for the integrity and continuity caprock/seals suited to the size of injection.

2. Apriori evidence of seals such as oil and gas accumulations, e.g. experience of CO2 use and storage in West Texas, can serve as an initial means to indicate integrity of caprock/seals for containment of stored CO2. However, the detailed analysis of the 3D seismic in the five fields examined in this study also reveal potential breaches in seals along the same structures without hydrocarbon accumulation and warrant the use of 3D seismic to establish why hydrocarbon is not present. Many dry structures with hydrocarbon show or limited fillup suggest breaches to seals that have allowed remigration, e.g., the increasing GOR toward the Anadarko Basin indicating remigration of fluids from the basin.

3. The systematic characterization of the structural framework from a kinematics perspective to ascertain stress-strain history in the context of modern stresses is strongly encouraged. Based on current seismicity, faults appear to be reactivated by large volume brine injection. Size and orientation of faults, basement heterogeneity (size and length of features), maximum and minimum stress direction and magnitudes and critical stress and orientation of larger faults, and an understanding of fluid levels and pore pressure are critical to the characterization.

4. Conventional amplitude data, coupled with processed volumetric curvature data demonstrate probable vertical connectivity from Basement to stratigraphic horizons considerably higher in the section. The distinction of fractures, flexure, and brittle faulting is needed using multiple techniques including geomechanical analytical methods to evaluate the seals and mechanical integrity. The Permian evaporites including halite that lie above most of Kansas reservoirs are a clear indication of the integrity of shallower seals. Oil and gas migration and accumulation over time have been constrained by seals that are both local and regional in extent. Active fracture and fault systems have introduced hydrocarbons into Kansas from both the Anadarko and Arkoma Basins likely during times of strong tectonic forces as well as lessor structural movement and remigration, e.g. the late Tertiary remigration of trillions of feet of natural gas

from the breaching of the Amarillo-Wichita uplift to the updip giant Hugoton oil Field that spans three states and lies above the Western Annex.

5. High angle reverse faults occur in both the northernmost and southernmost study areas, and are likely related to additional structural complexity, and fracture system enhancement. The fault geometries in the northern region such as flower structures also suggest that strike-slip motion has affected these faults in the past.

6. 4D seismic programming planned for the future may be able to monitor CO2 plume movement, but is likely to be at such a scale as to lack the certainty required to confirm or deny leakage.

Subtask 18.3. Simulate potential of CO_2 sequestration in Arbuckle Group saline aquifer

Subtask 18.4. Simulate of CO_2 sequestration potential by CO_2-EOR in the selected Chester/Morrow field

CO2 potentially sequestered at the four Chester/Morrow fields including Cutter, Pleasant Prairie, Eubank, and Shuck was estimated through simulation as summarized in **Table 1**. Total sequestered CO2 is 6.1 million metric tons is based on the crossover of maximum oil recover and minimizing CO2 breakthrough. Reports on the characterization and modeling of these fields will be part of the final report. These Morrow/Chester fields located in southwestern Kansas were the focus of study because of their representativeness of other fields and the strategic orientation that could serve as a basis for extending a CO2 pipeline currently ending in NW Oklahoma.

Reservoir	Co2 Sequestered ton	Co2 Sequestered tonne
Cutter Morrow (1/1/1961)	1,400,000	1,272,727
Pleasant Prairie (1/1/2012)	700,000	636,364
Eubank (6/1/2013)	1,600,000	1,454,545
Shuck (1/1/2013)	3,000,000	2,727,273
Total	6,700,000	6,090,909

Table 1. Estimated sequestered CO2 from simulations of four western Kansas fields.

Based on these results, the maximum displacement of oil and natural gas by CO2 could be to 60% and about 80%, respectively. Displacement of the water in these oil fields would be at least the same as the saline aquifer but probably in the 20% range. Thus, the maximum CO2 that could potentially be sequestered in these fields is about *8 million* tonnes.

Task 19: Integrate Results with Larger 17+ County Regional Project in South-central Kansas

Deliverables for the Final Report

1. Reservoir geomodel of Wellington Mississippian Chat reservoir and its CO_2-sequestration and CO_2-EOR potential.
2. Reservoir geomodel of Arbuckle Group saline aquifer underlying Wellington field and its CO_2-sequestration potential
3. Regional geomodel of OPAS covering 17+ counties in south central Kansas and its CO_2-sequestration potential
4. Risk assessment studies related to CO_2 sequestration including characterization of leakage pathways, vertical communication within the Arbuckle Group, and well abandonment histories in the 17+ county study area and the Western Annex.
5. Geomodel and simulations of CO_2 sequestration potential of the Arbuckle Group saline aquifer and of CO_2-EOR in a select Chester/Morrow incised valley sandstone oil reservoir in the Western Annex – a new addition of ~5,000 mi^2 to the regional study.
6. Results and interpretation of the seismic surveys, and interpretation of all laboratory analysis performed in the 17+ county study area and the Western Annex.

PRESENTATIONS AND PUBLICATIONS

Tandis S. Bidgoli, W. Lynn Watney, Paul Gerlach, Minh C. Nguyen, 2014, Episodic reactivation of critically-stressed basement faults in southern Kansas: Implications for waste-water disposal and long-term storage of CO_2 (for GSA 2014 annual meeting), **https://gsa.confex.com/gsa/2014AM/webprogram/Paper249152.html**

Tiraz Birdie, Lynn Watney, Paul Gerlach, Michael Killion, Eugene Holubnyak, Jennifer Raney, Tandis Banjoli, Gene Williams, Minh Nguyen, and Brownie Wilson, 2014, The Impacts of Carbon Dioxide Storage in the Saline Arbuckle Aquifer on Freshwater Aquifers in Kansas:

Yevhen Holubnyak, Willard Watney, Jason Rush, and Fatemeh Fazelalavi, 2014, Reservoir Engineering Aspects of Pilot Scale CO2 EOR Project in Upper Mississippian Formation at Wellington Field in Southern Kansas, Energy Procedia 00 (2013) 000–000, 9 p.

Watney, W.L., 2014, "Carbon Storage and Utilization in Kansas – Are We Ready?" at Annual Oil and Gas Seminar, Kansas NextStep, Hays, Kansas,

W. Lynn Watney & Jason Rush (Joint PIs), Jennifer Raney*, Modeling CO2 Sequestration in Saline Aquifer and Depleted Oil Reservoir to Evaluate Regional CO2 Sequestration Potential of Ozark Plateau Aquifer System, South-Central Kansas Project Number (DE-FE0002056), U.S. Department of Energy, National Energy Technology Laboratory, Carbon Storage R&D Project Review Meeting, Developing the Technologies and Infrastructure for CCS, August 12-14, 2014.

*presenter

KEY FINDINGS

1. Type logs have been verified.
2. Interactive mapper functioning has been optimized and layers updated for state of Kansas including horizontal wells, earthquakes.
3. "Blind" faults are being verified by induced seismicity resulting from increased brine disposal associated with oil drilling in south-central Kansas.
4. Concerns expressed by regulatory community in Kansas on business as usual regarding permitting of deep fluid disposal.
5. Assessment of CO2 disposal has provided basis to address key parameters associated with fluid disposal including characterization of reservoir/aquifer matrix properties, fractures and faults, data and methodology to assess flow units, aquitards, injectivity, storativity, anisotropy, dual and triple porosity systems that comprise carbonates, seismic calibration and seismic imaging and attribute analysis focused on recognition of faults and karst, geomechanical properties and regional and local stress conditions, critical orientations of faults, 3D geocellular network integrating subsurface information, analysis of pressure and fluid distribution during injection using compositional simulator, and recognition limits to pressure relative to closure pressure.
6. Use of multicomponent seismic has proven the merits of examining anisotropy and reservoir properties via seismic inversion.
7. Regional seismic and regional mapping has clearly shown faults and lineaments of suspected faults that require evaluation prior to considering CO2 storage.
8. Regional simulation of commercial scale CO2 storage using 3D geocellular modeling of conventional petroleum reservoir evaluation will serve as the basis for future discussion and evaluation of CO2 storage and even brine disposal as the nexus of these two technologies converge in Kansas.

PLANS

1. Complete the final report.

SPENDING PLAN

COST PLAN/STATUS											
	BP 1 Starts: 12/8/09	Ends: 2/7/11					BP2 Starts 2/8/11	Ends 8/7/12			
Baseline Reporting Quarter	12/8/09-12/31/09 Q1	1/1/10-3/31/10 Q2	4/1/10-6/30/10 Q3	7/1/10-9/30/10 Q4	10/1 - 12/31/10 Q5	1/1/11 - 3/31/11 Q6	4/1/11 - 6/30/11 Q7	7/1/11-9/30/11 Q8	10/1/11 - 12/31/11 Q9	1/1/12 - 3/31/12 Q10
Baseline Cost Plan (from SF-424A)	(from 424A, Sec. D)									
Federal Share	$1,007,622.75	$1,007,622.75	$1,007,622.75	$1,007,622.75	$0.00	$0.00	$0.00	$1,169,543.00	$1,169,543.00	$1,169,543.00
Non-Federal Share	$277,260.75	$277,260.75	$277,260.75	$277,260.75	$0.00	$0.00	$0.00	$303,182.75	$303,182.75	$303,182.75
Total Planned (Federal and Non-Federal)	$1,284,883.50	$1,284,883.50	$1,284,883.50	$1,284,883.50	$0.00	$0.00	$0.00	$1,472,725.75	$1,472,725.75	$1,472,725.75
Cumulative Baseline Cost	$1,284,883.50	$2,569,767.00	$3,854,650.50	$5,139,534.00	$5,139,534.00	$5,139,534.00	$5,139,534.00	$6,612,259.75	$8,084,985.50	$9,557,711.25
Actual Incurred Costs										
Federal Share	$4,019.93	$84,603.97	$494,428.37	$111,405.52	$238,675.97	$1,902,936.55	$625,853.17	$275,754.50	$523,196.12	$453,026.11
Non-Federal Share	$0.00	$43,980.04	$40,584.78	$13,195.88	$526,210.30	$35,887.34	$414,511.02	$20,247.24	$16,687.00	$61,683.20
Total Incurred Costs-Quarterly (Federal and Non-Federal)	$4,019.93	$84,603.97	$535,013.15	$124,601.40	$764,886.27	$1,938,823.89	$1,040,364.19	$296,001.74	$539,883.12	$514,709.31
Cumulative Incurred Costs	$4,019.93	$88,623.90	$623,637.05	$748,238.45	$1,513,124.72	$3,451,948.61	$4,492,312.80	$4,788,314.54	$5,328,197.66	$5,842,906.97
Variance										
Federal Share	$1,003,602.82	$923,018.78	$513,194.38	$896,217.23	-$238,675.97	-$1,902,936.55	-$625,853.17	$893,788.50	$646,346.88	$716,516.89
Non-Federal Share	$277,260.75	$233,280.71	$236,675.97	$264,064.87	-$526,210.30	-$35,887.34	-$414,511.02	$282,935.51	$286,495.75	$241,499.55
Total Variance-Quarterly Federal and Non-Federal)	$1,280,863.57	$1,156,299.49	$749,870.35	$1,160,282.10	-$764,886.27	-$1,938,823.89	-$1,040,364.19	$1,176,724.01	$932,842.63	$958,016.44
Cumulative Variance	**$1,280,863.57**	**$2,437,163.06**	**$3,187,033.41**	**$4,347,315.51**	**$3,582,429.24**	**$1,643,605.35**	**$603,241.16**	**$1,779,965.17**	**$2,712,807.80**	**$3,670,824.24**

	BP3 Starts 8/8/12	Ends 9/30/14							
4/1/12 - 6/30/12 Q11	7/1/12 - 9/30/12 Q12	10/1/12 - 12/31/12 Q13	1/1/13 - 3/31/13 Q14	4/1/13 - 6/30/13 Q15	7/1/13 - 9/30/13 Q16	10/1/13 - 12/31/13 Q17	1/1/14 - 3/31/14 Q18	4/1/14 - 6/30/14 Q19	7/1/14 - 9/30/14 Q20
$1,169,543.00	$316,409.00	$316,409.00	$316,409.00	$316,409.00	$0.00	$0.00	$0.00	$0.00	$0.00
$303,182.75	$81,854.50	$81,854.50	$81,854.50	$81,854.50	$0.00	$0.00	$0.00	$0.00	$0.00
$1,472,725.75	$398,263.50	$398,263.50	$398,263.50	$398,263.50	$0.00	$0.00	$0.00	$0.00	$0.00
$11,030,437.00	$11,428,700.50	$11,826,964.00	$12,225,227.50	$12,623,491.00	$12,623,491.00	$12,623,491.00	$12,623,491.00	$12,623,491.00	$12,623,491.00
$238,793.52	$1,282,545.00	$1,314,156.54	$395,319.33	$299,454.96	$465,714.15	$190,945.64	$234,848.28	$214,216.79	$418,577.50
$150,646.51	$221,053.41	$121,637.40	-$65,989.76	$23,362.67	$34,263.50	$915,863.95	$32,999.36	$23,638.80	$31,847.40
$389,440.03	$1,503,598.41	$1,435,793.94	$329,329.57	$322,817.63	$499,977.65	$1,106,809.59	$267,847.64	$237,855.59	$450,424.90
$6,232,347.00	$7,735,945.41	$9,171,739.35	$9,501,068.92	$9,823,886.55	$10,323,864.20	$11,430,673.79	$11,698,521.43	$11,936,377.02	$12,386,801.92
$930,749.48	-$966,136.00	-$997,747.54	-$78,910.33	$16,954.04	-$465,714.15	-$190,945.64	-$234,848.28	-$214,216.79	-$418,577.50
$152,536.24	-$139,198.91	-$39,782.90	$147,844.26	$58,491.83	-$34,263.50	-$915,863.95	-$32,999.36	-$23,638.80	-$31,847.40
$1,083,285.72	-$1,105,334.91	-$1,037,530.44	$68,933.93	$75,445.87	-$499,977.65	-$1,106,809.59	-$267,847.64	-$237,855.59	-$450,424.90
$4,754,109.96	**$3,648,775.05**	**$2,611,244.61**	**$2,680,178.54**	**$2,755,624.41**	**$2,255,646.76**	**$1,148,837.17**	**$880,989.53**	**$643,133.94**	**$192,709.04**